

Synthesis and Characterization of Liposomes with Controlled Surface Design for Analytical Applications

Dissertation zur Erlangung des Doktorgrades der Naturwissenschaften

(Dr. rer. nat.)

an der Fakultät Chemie und Pharmazie

der Universität Regensburg

Deutschland



vorgelegt von

Carola Hofmann

aus München

im Jahr **2019**

Die vorliegende Dissertation entstand in der Zeit von März 2015 bis Juli 2019 am Institut für Analytische Chemie, Chemo- und Biosensorik der Universität Regensburg.

Die Arbeit wurde angeleitet von Prof. Dr. Antje J. Bäumner.

Promotionsgesuch eingereicht am: 24. Juli 2019

Kolloquiumstermin: 09. September 2019

Prüfungsausschuss:

Vorsitzender: Prof. Dr. Arno Pfitzner

Erstgutachterin: Prof. Dr. Antje J. Bäumner

Zweitgutachter: PD Dr. Hans-Heiner Gorris

Drittprüfer: Apl. Prof. Dr. Rainer Müller

Für meine Söhne

Danksagung

Zu allererst möchte ich mich bei Prof. Dr. Antje J. Bäumner für die Möglichkeit zur Bearbeitung dieses spannenden Themas, für die ausgezeichnete Betreuung und Unterstützung während der gesamten Arbeit bedanken. Vielen Dank für die zahlreichen und hilfreichen Anregungen während der vielen, wissenschaftlichen Diskussionen.

Vielen Dank an PD Dr. Hans-Heiner Gorris für die Übernahme des Zweitgutachtens, Apl. Prof. Dr. Rainer Müller für die Übernahme der Aufgabe des Drittprüfers und Prof. Dr. Arno Pfitzner für die Übernahme der Funktion des Prüfungsvorsitzenden.

Darüber hinaus geht mein Dank auch an Joachim Rewitzer für die Unterstützung bei den ICP-OES- und ICP-MS Messungen meiner Proben.

Vielen Dank auch an Vanessa Tomanek für die Unterstützung bei den ICP-OES-Messungen meiner Proben, den Zeichnungen für meine Publikationen und für die Wiederholung und Optimierung einiger Messungen für das DNA Preconcentration-Projekt. Besonders bedanken möchte ich mich außerdem für ihre Unterstützung während des gesamten Bakterien-Projekts.

Darüber hinaus gilt mein Dank Susanne Dechantsreiter, Barbara Kaiser, Susanne Märkl und Clemens Spitzenberg für ihre Hilfe während ihrer Bachelorarbeit, Praktika oder WHK-Zeit.

Ebenfalls bedanken möchte ich mich bei meiner Arbeitsgruppe im „4.Stock“ für die tolle Zeit, Unterstützung und auch für die schönen Abende außerhalb der Arbeitszeit. Ich bedanke mich außerdem bei allen Kollegen und Kolleginnen des Instituts für die angenehme Arbeitsatmosphäre.

Außerdem möchte ich mich bei meinen Eltern, Helmut und Claudia, bei meinen zwei kleinen Schwestern, Christina und Iris, und bei meinem Mann, Joachim, dafür bedanken, dass sie zu jedem Zeitpunkt an mich geglaubt haben und mich immer mit unendlicher Geduld und liebevoller Fürsorge unterstützt haben.

Declaration of Collaborations

Most of the theoretical and experimental work presented in this thesis was conducted solely by the author. However, parts of the results were gained in collaboration with other researchers, which are stated in this section in accordance with §8 Abs. 1 Satz 2 Punkt 7 of the “Ordnung zum Erwerb des akademischen Grades eines Doktors der Naturwissenschaften (Dr. rer. nat.) an der Universität Regensburg vom 18. Juni 2009“.

Nanocontainers for Analytical Applications (Chapter 1)

The literature search and writing of the manuscript was done by the author. Axel Duerkop and Antje J. Baeumner revised the manuscript. AJB is corresponding author.

Tethering Functionality to Lipid Interfaces by a Fast, Simple and Controllable Post Synthesis Method (Chapter 3)

The experimental work was carried out by the author. Guenter Roth provided the lipopeptide-biotin. Thomas Hirsch, Axel Duerkop and Antje J. Baeumner contributed with strategic discussions. The manuscript was written by the author and revised by GR, TH, AD and AJB. AJB is corresponding author.

Optical Characterization of DNA-tagged Fluorescent Liposomes (Chapter 4)

Most of the experimental work was solely done by the author. The author also wrote this chapter. The experimental work was partly done at Abbott Diagnostics in Lake Forest, IL in cooperation with Qiaoqiao Ruan. Sergey Tetin, Thomas Hirsch, Axel Duerkop and Antje J. Baeumner contributed with strategic discussions. Antje J. Baeumner was the leader of this project.

Electrostatic Interactions of Cationic liposomes for Pathogen Detection (Chapter 5)

The author did most of the experimental work and wrote this chapter. Barbara Kaiser contributed with ζ -potential measurements of the *E.coli* cells and the fluorescence microtiter plate assay in different buffers as part of a research internship under the supervision of the author. Susanne Märkl contributed with measurements of the interaction of cationic liposomes and magnetic beads. Thomas Hirsch, Axel

Duerkop and Antje J. Baeumner contributed with strategic discussions. Antje J. Baeumner was the leader of this project.

Cationic Liposomes for DNA Preconcentration (Chapter 6)

The author did most of the experimental work and wrote this chapter. Cornelia Hermann contributed with the synthesis and characterization of one of the liposome batches. Vanessa Tomanek and Clemens Spitzenberg repeated and optimized some of the experiments under the supervision of the author. Antje J. Baeumner contributed with strategic discussions and was the leader of this project.

Table of Contents

Summary	1
Zusammenfassung.....	5
1 Nanocontainers for Analytical Applications	9
1.1. Introduction: General Information on Nanocontainers and Possible Applications	10
1.2. Synthesis and Surface Functionalization.....	10
1.2.1. Materials for Nanocontainers in (Bio)analysis – Synthesis and Characterization.....	11
1.2.2. Surface Chemistry	13
1.3. Relevant Features Supporting Nanocontainer Applications in (Bio)analysis.....	15
1.3.2. Signal Generation Through Controlled Release of Entrapped Molecules.....	21
1.3.3. Release-Independent Signal Generation Strategies.....	21
1.4. Analytical Applications of Nanocontainers	22
1.4.1. Bioassays	22
1.4.2. Chemosensors	32
1.4.3. Bioimaging and <i>in vivo</i> Applications.....	38
1.5. Conclusion, Future Perspectives and Challenges.....	40
Acknowledgements.....	42
References.....	42
2 Introduction and Structure of the Thesis	49
3 Tethering Functionality to Lipid Interfaces by a Fast, Simple and Controllable Post	
Synthesis Method.....	55
3.1. Introduction	56
3.2. Experimental	59
3.2.1. Materials	59
3.2.2. Methods	60
3.3. Results and Discussion	62
3.3.1. Insertion Method – Preparation and Characterization.....	62

3.3.2. Optimization of Insertion Conditions	64
3.3.3. Binding Behaviour of Functionalized Liposomes	65
3.3.4. Comparison of Lipopeptide-Insertion and Standard Modification	68
3.4. Conclusions.....	73
Acknowledgements	73
References	73
4 Optical Characterization of DNA-tagged Fluorescent Liposomes.....	77
4.1. Introduction.....	78
4.2. Experimental.....	79
4.2.1. Materials.....	79
4.2.2. Methods	80
4.3. Results and Discussion.....	83
4.3.1. Liposome Preparation and General Characterization	83
4.3.2. Theoretical Calculations	85
4.3.3. Control Experiments and Imaging	86
4.3.4. Fluorescence Correlation Spectroscopy of Liposomes.....	89
4.3.5. Imaging of DNA-Tagged SRB Liposomes.....	91
4.4. Conclusions.....	96
References	96
5 Electrostatic Interactions of Cationic Liposomes for Pathogen Detection	99
5.1. Introduction.....	100
5.2. Experimental.....	101
5.2.1. Materials.....	101
5.2.2. Methods	102
5.3. Results and Discussion.....	105
5.3.1. Liposome Preparation and Characterization	105
5.3.2. Electrostatic Interaction with Magnetic Beads	106
5.3.3. Bacteria Quantification via Fluorescence Readout	108

5.3.4. Bacteria Quantification via Chemiluminescence Readout	114
5.4. Conclusions	117
References.....	117
6 Cationic Liposomes for DNA Preconcentration	119
6.1. Introduction	120
6.2. Experimental	121
6.2.1. Materials	121
6.2.2. Methods	122
6.3. Results and Discussion	125
6.3.1. Liposome Preparation and DNA Extraction.....	125
6.3.2. Concepts for DNA Preconcentration with Cationic Liposomes.....	126
6.3.3. Optimization of DNA Preconcentration Using Centrifugation	129
6.4. Conclusions	132
References.....	133
7 Conclusions and Future Perspectives	135
Curriculum Vitae.....	143
Publications	145
Presentations	147

Summary

Nanocontainers are being applied for many bioanalytical strategies, *e.g.* in bioassays, in chemosensors or for bioimaging and *in vivo* applications. They vary with respect to the materials used (such as mesoporous silica, polymers or proteins). These enable different unique characteristics mainly through their cavities or pores for the entrapment of numerous signaling molecules and their large surface area for the attachment of various surface tags. Of special interest is their signal amplification capability where the surface tags enable a specific analyte recognition as well as a controlled pore permeability. Among all the different types of nanocontainers, liposomes excel by their relatively simple preparation and surface functionalization, their large inner cavity and variety of possible entrapped molecules, short assay response times due to an efficient lysis of the membrane, promising multimodal approaches for clinical diagnosis and therapy as well as by their natural biocompatibility and are thus of major interest in the field of (bio)analysis (Chapter 1).

For all applications in this area a careful control of the vesicle surface is necessary as it not only provides colloidal stability in complex aqueous solutions but also enables a specific binding to surfaces or the recognition of the analyte of interest. Therefore, the surface charge as well as methods for the introduction of specific functionalities were studied in detail in this thesis and the developed liposomes characterized and investigated towards their applicability as signal enhancers for the detection of bacteria or the preconcentration of DNA.

Standard methods for the surface functionalization of liposomes via covalent coupling post synthesis or modification directly during synthesis using functionalized lipids result in the production of numerous functionalized liposomes suitable for many applications. However, due to the need for elevated temperatures and organic solvents, time-consuming preparation and purification steps, low coupling yields, crosslinking or the decoration of the inner and outer leaflet of the bilayer, these methods are accompanied by a comparatively high loss of functionalities and are often unsuitable for fragile moieties. Moreover, large variations in the insertion efficiency, high batch-to-batch differences, and an incorporation limit of 4 mol% in case of direct modification with DPPE-biotin during synthesis were observed. Therefore, an alternative strategy for the insertion of different anchor molecules into dye-loaded liposomes composed of DPPC, DPPG and cholesterol was developed, and the tested molecules studied for their ability to effectively insert into the lipid bilayer and their binding functionality. The best system (lipopeptide-biotin) provided a fast, concentration-controlled functionalization up to 10 mol% in aqueous solution at room temperature and a reliable and quantitative binding to streptavidin with no effect on the analytical properties of the vesicles. Thus,

the vesicles only differ by the type or concentration of the functional moiety on the liposome surface which provides a huge potential for applications in the development of bioanalytical assays or for multi-analyte detection but can also be extended to other lipid-based nanomaterials and general analytical or pharmaceutical applications (Chapter 3).

Standard characterization of liposomes includes the determination of the vesicle size, ζ -potential and phospholipid concentration. However, there are several other parameters that can be investigated, such as the number of particles and surface tags or the specific binding of the vesicles to particles or surfaces. Therefore, ssDNA-tagged liposomes were prepared and characterized in detail using the standardly applied methods like DLS or ICP-OES as well as other optical methods. The number of liposomes was *e.g.* successfully determined via fluorescence correlation spectroscopy. Moreover, a hybridization assay with a fluorophore-tagged complementary oligonucleotide strand was developed to determine the number of ligands on the vesicle surface. In addition, fluorescence microscopy confirmed *e.g.* a successful purification, the specific binding of the functionalized vesicles to magnetic microparticles and enabled the imaging of the ideal lysis conditions for the applied liposomes (22 mM OG). Also the superior performance of liposomes over simple fluorophore-tagged oligonucleotides with respect to signal amplification was successfully demonstrated (Chapter 4).

The ability of liposomes to strongly enhance signals has already been exploited for many different bioanalytical assays. Here, mainly anionic lipid vesicles are applied as they prevent non-specific binding to most biological molecules or surfaces. The use of cationic liposomes is mainly restricted to pharmaceutical applications, such as in gene delivery. Therefore, a different approach for the use of dye-loaded cationic liposomes has been developed which is based on their electrostatic binding to the negatively charged surface of the model bacterium *E.coli*. Two different assay concepts were investigated and optimized to exploit this interaction for the detection of *E.coli*. The first concept is based on centrifugation and the second one on the immobilization of the bacteria to Poly-L-Lysin-coated microtiter plates. Sulforhodamine B-loaded liposomes enabled the analysis via fluorescence and yielded detection limits between 10^6 and 10^7 cfu ml⁻¹. This was further improved by the entrapment of the chemiluminescent marker m-carboxy-luminol. Here, detection limits of $\sim 10^5$ cfu ml⁻¹ were achieved using the centrifugation-based assay. As most bacteria provide a negative surface charge, this method offers the possibility for a simple and universal detection of gram-positive and gram-negative bacteria. However, further optimizations will be necessary to achieve lower limits of detection (Chapter 5).

Besides their use for bacteria detection, preliminary studies also revealed the suitability of cationic liposomes for the preconcentration of genomic DNA. Preconcentration of analytes is a common tool in analytical chemistry and often described for DNA samples. Here, PCR, alcohol precipitation and

Summary

magnetic beads belong to the most common methods. As in case of bacteria also DNA is negatively charged due to its phosphate backbone. This enables the electrostatic attachment to the cationic vesicle surface. For separation two concepts were investigated. The first concept based on the separation via magnetic beads resulted in only low enrichment factors of ~2. The second concept was based on centrifugation. Here, an incubation time of only 5 min followed by centrifugation for 15 min at 15.000 g resulted in an efficient preconcentration of genomic DNA with enrichment factors up to 75. Thus, these preliminary studies show that cationic liposomes are a promising material in the field of DNA preconcentration and may be able to overcome some of the disadvantages of other methods, such as the need for organic solvents or chaotropic salts (Chapter 6).

Zusammenfassung

Nanocontainer werden für zahlreiche bioanalytische Strategien eingesetzt, z.B. in Bioassays, in Chemosensoren oder für die Bildgebung und *in vivo* Anwendungen. Sie variieren in Bezug auf die verwendeten Materialien (wie z.B. mesoporöses Siliziumdioxid, Polymere oder Proteine). Diese bestimmen die spezifischen Eigenschaften vor allem durch ihre Hohlräume und Poren für den Einschluss zahlreicher Signalmoleküle und ihre große Oberfläche für das Anbringen von Oberflächenfunktionalitäten. Ihre Fähigkeit zur Signalverstärkung ist hierbei von besonderem Interesse, wobei funktionelle Gruppen an der Oberfläche sowohl eine spezifische Erkennung des Analyten als auch eine kontrollierte Porendurchlässigkeit ermöglichen. Unter all den verschiedenen Arten von Nanocontainern stehen Liposomen durch ihre relative leichte Herstellung und Oberflächenmodifizierung, ihren großen inneren Hohlraum und die Vielzahl an einschließbaren Molekülen, kurze Assay-Antwortzeiten durch effizientes Lysieren der Membran, vielversprechende multimodale Ansätze für die klinische Diagnostik und Therapie, sowie durch ihre natürliche Biokompatibilität heraus. Sie sind daher von großem Interesse für die (Bio)analytik (Kapitel 1).

Für alle Anwendungen auf diesem Gebiet ist eine sorgfältige Kontrolle der Vesikeloberfläche nötig, da sie nicht nur die kolloidale Stabilität in komplexen, wässrigen Lösungen, sondern auch die spezifische Bindung an Oberflächen oder die Erkennung des Ziel-Analyten ermöglicht. Daher wurde in dieser Arbeit sowohl die Ladung der Liposomoberfläche als auch das Einführen spezifischer Funktionalitäten im Detail untersucht, die entwickelten Liposomen charakterisiert und in Bezug auf ihre Anwendbarkeit als Signalverstärker für die Detektion von Bakterien oder für das Aufkonzentrieren von DNA analysiert.

Standardmethoden für die Oberflächenfunktionalisierung über kovalente Kopplung nach der Synthese oder über direkte Modifizierung während der Synthese mit Hilfe von funktionalisierten Lipiden führt zur Herstellung von zahlreichen, funktionalisierten Liposomen, die für verschiedenste Anwendungen geeignet sind. Allerdings kommt es bei diesen Methoden durch die Notwendigkeit für erhöhte Temperaturen und organische Lösungsmittel, die zeitaufwendige Herstellung und Aufreinigung, niedrige Kopplungsraten, Quervernetzungen oder die Dekoration der äußeren und inneren Membranschicht zu einem verhältnismäßig großen Verlust an Funktionalitäten. Außerdem sind sie dadurch oft nicht für fragile Moleküle geeignet. Darüber hinaus wurden im Fall der direkten Modifizierung mit DPPE-biotin während der Synthese große Variationen in der Einbaueffizienz, hohe Unterschiede zwischen verschiedenen Ansätzen und eine Einbaugrenze von 4 mol% beobachtet. Daher wurde eine alternative Strategie für den Einbau unterschiedlicher Ankermoleküle in Farbstoff-beladene Liposomen aus DPPC, DPPG und Cholesterol entwickelt und die untersuchten Moleküle in

Hinblick auf ihre Fähigkeit effektiv in die Lipiddoppelschicht zu insertieren und auf ihre Bindungsfunktionalität hin analysiert. Das beste System (Lipopeptid-biotin) ermöglichte eine schnelle, konzentrations-kontrollierte Funktionalisierung bis zu 10 mol% bei Raumtemperatur in wässriger Lösung und eine zuverlässige, quantitative Bindung an Streptavidin, ohne dabei die analytischen Eigenschaften der Vesikel zu beeinflussen. Daher unterscheiden sich die Vesikel ausschließlich durch die Art oder Konzentration des funktionellen Restes an der Liposomoberfläche, was ein großes Potential für Anwendungen im Bereich der Entwicklung von bioanalytischen Assays oder der Multi-Analyt-Detektion ermöglicht. Darüber hinaus kann diese Methode auch auf andere Lipid-basierte Nanomaterialien oder auf allgemeine analytische oder pharmazeutische Anwendungen ausgeweitet werden (Kapitel 3).

Die standardmäßige Charakterisierung von Liposomen beinhaltet die Bestimmung der Vesikelgröße, ihres ζ -Potentials und ihrer Phospholipidkonzentration. Es gibt allerdings zahlreiche andere Parameter, die ebenfalls untersucht werden können, sowie die Anzahl an Partikeln und Oberflächenfunktionalitäten oder die spezifische Bindung der Vesikel an Partikel oder Oberflächen. Dazu wurden ssDNA-markierte Liposomen hergestellt und im Detail charakterisiert, wobei sowohl Standardmethoden wie DLS oder ICP-OES zum Einsatz kamen als auch andere optische Methoden. Die Anzahl an Liposomen wurde beispielsweise erfolgreich über Fluoreszenzkorrelationsspektroskopie ermittelt. Darüber hinaus wurde ein Hybridisierungsassay mit einem Fluorophor-markierten, komplementären Oligonukleotidstrang entwickelt, um die Anzahl an Liganden auf der Vesikeloberfläche zu bestimmen. Außerdem bestätigte die Fluoreszenzmikroskopie beispielsweise eine erfolgreiche Aufreinigung, die spezifische Bindung der funktionalisierten Liposomen an magnetische Mikropartikel und ermöglichte die Bildgebung der idealen Lyse-Bedingungen für die angewendeten Liposomen (22 mM OG). Die überlegene Performance der Liposomen im Vergleich zu einfachen Fluorophor-markierten Oligonukleotiden in Bezug auf eine Signalverstärkung wurde ebenfalls erfolgreich gezeigt. (Kapitel 4).

Die Fähigkeit von Liposomen, Signale kräftig zu verstärken, wurde bereits für eine Vielzahl an bioanalytischen Assays genutzt. Dazu wurden hauptsächlich anionische Lipidvesikel verwendet, da sie eine unspezifische Bindung an die meisten biologischen Moleküle und Oberflächen verhindern. Der Einsatz von kationischen Liposomen ist hauptsächlich auf pharmazeutische Anwendungen beschränkt, wie z.B. für den Gentransfer. Daher wurde ein anderer Ansatz für den Einsatz von Farbstoff-beladenen, kationischen Liposomen entwickelt, welcher auf der elektrostatischen Bindung an die negativ geladene Oberfläche des Modell-Bakteriums *E.coli* beruht. Es wurden zwei verschiedene Assay-Konzepte untersucht und optimiert, um diese Wechselwirkung für den Nachweis von *E.coli* zu verwenden. Das erste Konzept basiert auf Zentrifugation und das zweite auf der Immobilisierung der Bakterien an Poly-

L-Lysin-überzogene Mikrotiterplatten. Sulforhodamin B-beladene Liposomen ermöglichten die Analyse über Fluoreszenz und erzielten Detektionsgrenzen zwischen 10^6 und 10^7 cfu ml⁻¹. Das wurde weiter verbessert durch den Einschluss des chemilumineszenten Markers *m*-Carboxyluminol. Damit wurde mit Hilfe des Zentrifugation-basierten Assays eine Detektionsgrenze von $\sim 10^5$ cfu ml⁻¹ erreicht. Da die meisten Bakterien eine negative geladene Oberfläche besitzen, bietet diese Methode die Möglichkeit für eine einfache und universelle Detektion sowohl von gram-positiven als auch von gram-negativen Bakterien. Allerdings werden weitere Optimierungen nötig sein, um noch niedrigere Detektionsgrenzen zu erreichen (Kapitel 5).

Neben ihrer Verwendung für die Bakteriendetektion, zeigen erste Studien auch die Eignung von kationischen Liposomen für die Aufkonzentrierung von genomischer DNA. Das Aufkonzentrieren von Analyten ist ein weit verbreitetes Mittel in der analytischen Chemie und wird häufig für DNA-Proben beschrieben. Dabei gehören die PCR, die alkoholische Fällung und die Verwendung magnetischer Beads zu den bekanntesten Methoden. Wie im Fall von Bakterien ist auch DNA aufgrund ihres Phosphat-Rückgrats negativ geladen. Dies ermöglicht eine elektrostatische Bindung an die Oberfläche der kationischen Vesikel. Für die Abtrennung ungebundener DNA wurden zwei Konzepte untersucht. Das erste Konzept, welches auf der Abtrennung über magnetische Beads basiert, erzielte nur geringe Aufkonzentrierungsfaktoren von ~ 2 . Das zweite Konzept basiert auf Zentrifugation. Dabei resultierten eine Inkubationszeit von nur 5 min, gefolgt von Zentrifugation für 15 min bei 15.000 g in einer effizienten Aufkonzentrierung genomischer DNA mit Aufkonzentrierungsfaktoren bis zu 75. Diese ersten Studien zeigen daher, dass kationische Liposomen ein vielversprechendes Material im Bereich der DNA-Aufkonzentrierung sind und möglicherweise einige Nachteile der anderen Methoden, wie z.B. die Notwendigkeit für organische Lösungsmittel oder chaotrope Salze, beseitigen können (Kapitel 6).

1 Nanocontainers for Analytical Applications

Abstract

Nanocontainers such as mesoporous silica particles and polymersomes are versatile structures containing holes or pores used for the entrapment of small molecules and the introduction of specific functionalities. They are widely applied in drug delivery, biomedicine, bioreactors and analytical applications. In the latter, nanocontainers usually serve as amplification system. They are hence synthesized to entrap signaling molecules and to bear functional moieties at the outer surface, which in turn enable specific analyte recognition and control of the nanocontainer pore permeability. This review outlines the most important nanocontainer materials, discussing their synthesis, surface chemistry modifications and strategies for molecule entrapment. Their advantages, challenges and limitations in light of (bio)analytical applications are critically discussed in view of other common signal amplification strategies for different assay formats and various detection methods.

This chapter has been published.

C. Hofmann, A. Duerkop, A. J. Baeumner, *Angew. Chem. Int. Ed.* **2019**, 10.1002/anie.201811821.

Author contributions:

The literature search and writing of the manuscript was done by CH. AD and AJB revised the manuscript. AJB is corresponding author.

1.1. Introduction: General Information on Nanocontainers and Possible Applications

Nanomaterials consisting of hollow structures, *i.e.* cavities or pores that are able to entrap small molecules are called nanocontainers. Liposomes are probably the most established type of nanocontainer to find successful application in analytical assays, drug delivery and skin care products.^[1–5] Over the last couple of years, new concepts of nanocontainers have been proposed and successfully demonstrated in similar applications. These are made from a variety of materials such as mesoporous silica, polymers,^[6] proteins,^[7] DNA,^[8] gold,^[9] metal oxide^[10] or carbon.^[11] Common to all of these structures is their large surface area and inner volume, and their resulting superior ability to entrap molecules and enable various chemical surface functionalities. The pores and cavities enable the inclusion of molecules such as dyes, drugs, or nanoparticles but can also serve as confined environment for biological and chemical reactions. These unique features drive their application as nanoreactors,^[12–15] nanostorage containers in batteries,^[16] for environmental remediation^[17] or waste water treatment,^[18] as biomimetic structures,^[19] for drug delivery,^[6,20,21] bioimaging,^[22,23] theranostics^[9] and in analytical assays^[11,24,25] and sensors.^[26,27]

Reviews on nanocontainers for sensor applications in the last 5 years are either specialized on one material ^[1,28] or cover only biomedical or nanoreactor applications, whereas a focus on analytical applications is either missing or kept to a minimum.^[7,29] Earlier, in 2012, a more general overview on nanoporous materials for bioanalysis was published by Dai *et al.*^[30] In general, for analytical applications, the cavities and pores are exploited for the entrapment of signaling molecules and the available large surface is functionalized for specific targeting toward the analyte of interest.

This review discusses the applied materials, their syntheses, advantages provided in analytical assays and provides an overview of nanocontainers published between 2013 and 2018 within this topic. The reader is directed to other reviews for specialized overviews on liposomes,^[1,4] hollow or mesoporous structures,^[29,31] preparation or functionalization of specific nanocontainers^[6,14,32] or on applications such as drug delivery,^[20,33,34] theranostics,^[9] biomimetics,^[35] in biomedicine^[7,36] and nanoreactors.^[12,13,15]

1.2. Synthesis and Surface Functionalization

Analytically relevant nanocontainers and nanocages are discussed in this review and cover mesoporous silica particles, liposomes, and polymer, gold, carbon, protein and metal oxide nanocontainers, respectively. Each material requires specific synthesis, purification and characterization methods. Common to all are strategies for surface chemistry and functionalization to obtain biocompatibility and render the surfaces suitable for analytical applications.

1.2.1. Materials for Nanocontainers in (Bio)analysis – Synthesis and Characterization

1.2.1.1. Liposomes

Liposomes are prepared by various methods.^[2] The most common techniques are thin film hydration and reverse phase evaporation which produce reliably large amounts of liposomes. Lately, also microfluidic based approaches have been described, however, large-scale production is limited.^[4] Purification of liposomes is usually done by size exclusion chromatography or dialysis. For characterization of the vesicle morphology dynamic light scattering (DLS), zeta-potential measurements, transmission electron microscopy (TEM), scanning electron microscopy (SEM) can be applied. NMR, inductively coupled plasma-optical emission spectroscopy (ICP-OES), Bartlett assay or nanoparticle tracking analysis are used to obtain information on their molecular composition and overall concentration.^[25,37–39] The size and lamellarity of liposomes depends on the method used for preparation and can be tuned via extrusion through polycarbonate membranes or sonication. Small lipid vesicles are around 50 nm in size, giant lipid vesicles can be as big as 1 μm .^[3] Similarly, the nature of the lipids can tune the overall functionality and for example render liposomes cationic, anionic or non-ionic; can make them highly stable or include trigger molecules for lysis. Liposomes have been intensively studied as cell membrane models, for drug delivery and as signaling means in bioassays.^[1] In all cases, their large hydrophilic cavity, suitable for entrapment of a large number of signaling molecules, the easy surface functionalization, and their inherent biocompatibility makes them highly useful.

1.2.1.2. Mesoporous Silica Nanocontainers

Mesoporous silica nanocontainers are hollow particles with regular, ordered tunable pores. Diameters of 50-180 nm have been reported, the pore sizes are usually in the range of 2.3 to 3.1 nm.^[40–42] Larger pores of 25 nm can be found for the entrapment of larger compounds like nanoparticles.^[43] Possible synthesis strategies include soft and hard templating routes,^[29,31] but a modified Stöber method is the most reported method. Here, a cationic, quaternary ammonium surfactant like cetyltrimethylammoniumbromid (CTAB) is mixed with a silicate like tetraethylorthosilicate (TEOS) in a mixture of water/ ethanol and ammonia. The surfactant forms positively charged micelles and electrostatically forms assemblies with the negatively charged silicate molecules. For functionalization often (3-aminopropyl)triethoxysilane (APTES) is added to the initial mixture.^[32] Purification of mesoporous silica is accomplished by simple centrifugation or filtration followed by reflux in a mixture of ethanol and ammonium nitrate or HCl for complete CTAB removal. For characterization of the vesicles' morphology and composition DLS, zeta-potential measurements, TEM, SEM, atomic force microscopy (AFM), x-ray diffraction (XRD) and Fourier-transform infrared (FT-IR) spectra are used.

Furthermore, nitrogen adsorption-desorption isotherms are used to obtain information on the surface area, porosity and pore size.^[24,41,42]

1.2.1.3. Polymer Nanocontainers

Polymer nanocontainers are vesicles consisting of an ordered polymer membrane and an aqueous inner cavity. If amphiphilic, non-branched, synthetic block copolymers are applied for the formation the nanocontainers are called polymersomes.^[15] They exist in a broad size range of 30-500 nm^[12] but for analytical applications they are usually below 400 nm.^[44-47] There are several ways to synthesize polymersomes and polymeric capsules.^[15] In the bottom up approach the vesicles are built by self-assembly of block copolymers, which consist of a hydrophilic and a hydrophobic block. In the top down approach a thin polymer film is rehydrated to form the polymersomes. Another approach is based on the formation of vesicles during polymerization, which is often applied for polydiacetylene vesicles. Moreover, phase separation techniques or template-based polymerization have been reported. Purification of polymersomes is mostly done by dialysis, filtration or size exclusion chromatography. For characterization of the vesicles' morphology again DLS, zeta-potential measurements, TEM, SEM or AFM are frequently used.^[23,45,47,48]

1.2.1.4. Protein-Based Nanocontainers

The most interesting material for protein-based nanocontainers for analytical applications is ferritin. Ferritin is a spherically shaped protein with a diameter of 12 nm consisting of 24 subunits, which form an 8 nm big cavity suitable for the entrapment of signaling molecules. Of the two types of ferritin, the iron containing holoferritin and the iron free apoferritin,^[20,49] the latter has been used most often for analytical applications.^[49,50,51,52] Ferritin is commercially available and can be isolated, *e.g.* from horse spleen, some human organs, plants, fungi or bacteria.^[20] Other protein-based nanocontainers or nanocages like heat-shock proteins, encapsulins or virus capsids have only seldomly been reported for analytical applications.^[14] Purification and characterization methods rely heavily on standard biochemical approaches including dialysis, column chromatography, centrifugation, filtration, sodium dodecyl sulfate (SDS) polyacrylamide gel electrophoresis, absorbance measurements, HPLC, Bradford assay or Western blot analysis.^[53]

1.2.1.5. Gold Nanocages

Gold nanocages are mostly cubic structures between 20 and 500 nm in size and consist of hollow interiors and porous walls with thicknesses between 2 and 10 nm. They are formed by galvanic replacement of Ag nanocubes with aqueous HAuCl₄, and their hollow pores are created by dealloying of the Ag atoms.^[9] Purification of gold nanocages is usually done by centrifugation. For characterization of the cage morphology TEM, SEM or energy-dispersive X-ray spectroscopy (EDS), is used as well as UV-vis for investigation of their optical properties.^[26,54,55] In addition to using their entrapment

capabilities, gold nanocages are analytically also employed due to their localized surface plasmon resonance (LSPR) properties, which can be tuned from 600 to 1200 nm. These optical properties are influenced by the degree of HAuCl_4 replacement, and additional incorporation of metals such as Pt or Pd into the walls of the nanocages.^[9,20]

1.2.1.6. Carbon-Based Nanocages

Carbon nanocages can be cubic or spherical hollow structures with sizes up to 20 nm, shell thicknesses of 3-5 nm and pore sizes between 3 and ~14 nm.^[11,56,57] For their synthesis carbon atom deposition, pyrolysis or hard and soft templating techniques have been described.^[20] For example cage type mesoporous silica has been used as hard template and is removed after successful formation.^[56,58] Purification is mostly accomplished using size exclusion chromatography. For characterization of the cage morphology and composition TEM and FT-IR spectra have been reported and absorbance and fluorescence spectra for investigation of the optical properties.^[11]

Also here, nitrogen adsorption-desorption isotherms are used to obtain information on the surface area, porosity and pore size.^[57,59] Carbon nanocages are usually not applied for the entrapment of signaling molecules, instead, changes in the intrinsic fluorescence of the nanocage are exploited for sensing.^[11,58]

1.2.1.7. Metal Oxide Nanocontainers

Metal oxide nanocontainers or nanocages are about 400 nm in size and consist *e.g.* of CuO, ZnO or Co_3O_4 .^[27,60,61] For synthesis the use of metal organic frameworks as template or precursor has been widely applied^[61] mostly starting with zeolite imidazolate frameworks (ZIF).^[60] After formation of the ZIF-templates core shell structures are formed using an etching and deposition method. By thermal annealing at 450 °C the final structures are formed.^[60,62] Purification of metal oxide nanocages is usually done by centrifugation of the template before the final annealing. For characterization of the cage morphology and composition TEM, SEM, XRD, x-ray photoelectron spectroscopy (XPS) or FT-IR spectra are used, and again nitrogen adsorption-desorption isotherms to obtain information on the surface area, porosity and pore size.^[10,27,61,63] Also metal oxide nanocontainers are usually not applied for the entrapment of signaling molecules, however, changes in the nanocontainer resistance are exploited for sensing.

1.2.2. Surface Chemistry

Stabilization under physiological conditions or even in simple aqueous buffer environment is a great challenge for nanoparticles and nanovesicles. In addition, the desirable surface chemistry of nanocontainers must be biocompatible and allow for targeted functionalization with tags or probes.^[64,65] In some instances, such as with gatekeepers (see Chapter 1.2.2 below), modulating

surface tags also have to be added. Table 1.1 provides an overview of common surface functionalization strategies for the different nanocontainer categories.

Table 1.1. Surface functionalization strategies for the different nanocontainer categories.

Nanocontainer	Biocompatibility/ stability in aqueous environment	Introducing functionality	Common functional groups	Common reaction mechanisms	Ref.
Liposomes	Naturally	Functional lipids	-COOH, -NH ₂ , -OH, -SH	Covalent coupling	[66], [22], [4]
		Functional lipids	Biotin, DNA, folic acid	Non-covalent conjugation, e.g. biotin-streptavidin	[37], [4], [67]
Polymeric	Hydrophilic polymers	Functional polymers	-COOH, -NH ₂ , -SH	Covalent coupling	[68]
		Stimuli responsive polymers	-	-	[6], [14]
Protein based	Naturally	Naturally occurring amino acids	-COOH, -NH ₂ , -OH, -SH, -N ₃ , alkyne	Covalent coupling	[34]
Mesoporous silica		Polycondensation with silanes	-COOH, -NH ₂ , -OH, -SH, -N ₃	Covalent coupling	[14], [68]
		Gatekeeper	Aptamers; proteins; enzymes; antibodies; microspheres; NPs	Electrostatic, covalent; Enzyme cofactor; Inhibitor(anchor);	[43], [69] [70], [71], [72], [73]; [42]
Carbon based	Naturally		-COOH, -OH	Covalent coupling	[68]
Gold based	Coating with biocompatible polymers		-SH	Covalent coupling	[9]
		Coating functional polymers with	-COOH, -NH ₂ , -OH, -SH	Covalent coupling	[68]
		Stimuli-responsive polymers	-	-	[20]
		Gatekeeper	Aptamers	Electrostatic	[55]

Active groups on the nanocontainer surface like carboxyl, hydroxyl, sulfhydryl or amino groups can be used for the attachment of biological receptors. Common covalent coupling techniques include 1-ethyl-3-(3-dimethylaminopropyl)-carbodiimide/N-hydroxysuccinimide (EDC/NHS) chemistry for

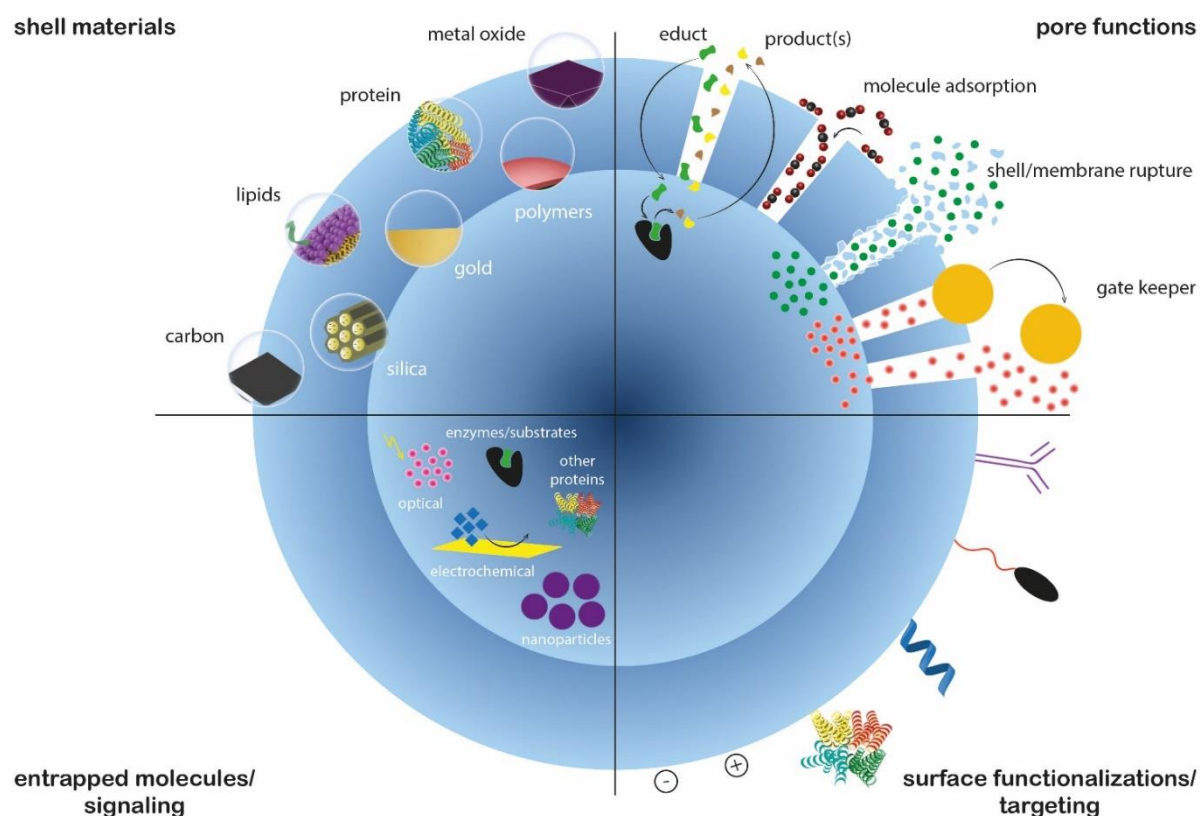
coupling of carboxyl and amino groups, Michael addition for the conjugation of thiol with maleimide groups, copper catalyzed click chemistry for conjugation of azide and alkyne groups or carbinolamine chemistry for the coupling of aldehyde and amine groups. Also, non-covalent conjugation is possible, *e.g.* by simple electrostatic interactions or a biotin-streptavidin system.^[68]

For the conjugation of gatekeepers, reversible attachment is necessary to enable controlled release of entrapped molecules. Therefore, only weak bonding or non-covalent conjugation is applied, which responds to an external stimulus. This can be a change in pH or temperature, an enzymatic reaction or non-covalent interaction, *e.g.* with the analyte of interest. As gatekeepers often aptamers,^[43] proteins,^[70] enzymes^[71] or microspheres^[74] are applied.

1.3. Relevant Features Supporting Nanocontainer Applications in (Bio)analysis

Nanocontainers consist of a hollow interior enabling the entrapment of small molecules and have a large surface area for the introduction of various functionalities. Some nanocontainers also possess pores for controlled mass transport in and out of the nanocontainer and in some instances gatekeepers that control this mass-flow. An overview of the features of nanocontainers can be found in Scheme 1.1.

Scheme 1.1. Schematic overview of nanocontainer features, possible entrapment molecules and signalling techniques and principles.



These features have been exploited and widely applied for analytical applications ranging from bioassays and biosensors to chemosensors and imaging. In bioassays or sensors, the analyte of interest is recognized by a suitable biological recognition element, *e.g.* antibodies, antigens, enzymes, receptors, cells, or DNA. This recognition must be convertible into a measurable, concentration-dependent signal.^[75] Most sensitive bioassays employ hence a signal amplification strategy to obtain favorable signal-to-noise ratios at low analyte concentrations. Enzymes were the first highly successful signal enhancers used in immunoassays leading to the development of enzyme-linked immunosorbent assays (ELISAs) that are now gold standards in clinical diagnostics.^[76] With the advancements in nanotechnology, various nanocontainers have been developed that significantly broadened and improved the possibilities of signal enhancement in bioassays. They have a large surface-to-volume ratio; their cavities or pores can be loaded with a huge amount of signaling molecules, and multiple receptors can be attached to their surface.^[1,70] In contrast to enzymes they provide instantaneous signal amplification, can be more robust and can provide higher signal enhancement. An ideal nanocontainer must hence be stable under physiological conditions, not only during the bioassay but also for long-term storage, enable fast and simple surface functionalization and efficient loading with the desired signaling molecules. These can be *e.g.* small hydrophilic or hydrophobic molecules, proteins, enzymes, DNA probes, or nanoparticles.^[1] For signal generation those molecules can either be released in a controlled manner using external stimuli^[41] or the signal is generated without release of the entrapped molecules, *e.g.* in the case of enzymatic reactions inside the container, where the substrate can enter through permeable pores.^[44] In literature most examples can be found for liposomes^[25,37,66] and mesoporous silica nanocontainers^[24,40,41] but also polymersomes,^[45] protein,^[49] carbon^[11] and gold-based nanocages^[55] have been reported.

For bioimaging similar requirements have to be met. Here, the focus lies on the visualization and investigation of tissues, cells, tumor cells, subcellular structures, cellular processes, and interactions of molecules or quantification of ions or metabolites.^[77] Therefore, the nanocontainers used for bioimaging usually carry contrast agents, which increase the signal in the areas of interest compared to the background.^[78] Those contrast agents like fluorescent dyes, upconverting nanomaterials or magnetic iron oxide, find their applications in simple optical bioimaging, magnetic resonance imaging (MRI), computed chromatography, ultrasound or photoacoustic imaging.^[78] Here, nanocontainers must demonstrate *in vivo* stability, biocompatibility, biodegradability and non-toxic properties,^[33] which has been achieved primarily with liposomes^[22] and polymersomes,^[23] but also with mesoporous silica^[79] and lanthanide-metal organic framework (Ln-MOF) structures.^[80]

Furthermore, the high surface-to-volume ratio of nanocontainers and hollow pores are exploited for gas sensing, mostly using metal oxides.^[27,60,61] Gas diffusion and mass transport to the surfaces are

enhanced over non-porous macro surfaces^[29] hence leading to increased sensitivity. Typically, reducing or oxidizing gases change the resistance of the nanomaterials, which is transduced into a concentration dependent electronic signal. Similarly, nanocontainers can be applied for metal ion sensing. Here the intrinsic properties of the nanocontainer changes upon contact with the analyte.^[81] Most examples in literature can be found for hollow Ln-MOF^[81] structures or gold nanocages.^[82]

1.3.1. Classes of Entrapped Signaling Molecules and Detection Techniques

Nanocontainers can entrap several types of molecules. For analytical applications often signaling molecules like dyes, redox molecules or enzyme substrates are used, but also macromolecules such as proteins and DNA, or nanoparticles can be entrapped. Table 1.2 provides an overview of common entrapment molecules and their associated detection strategies.

Table 1.2. Overview on common entrapment molecules, release mechanisms, and associated detection strategies.

Nanocontainer	Entrapped concentration	molecule/	Release mechanism of entrapped molecules/ duration	Detection technique	Ref.
Liposomes	150 mM SRB (~1.1 million molecules/ liposome)		Detergent lysis, fast	Fluorescence	[38]; [83]; [84]
	Squaraine		no	Fluorescence	[22]
	17 mM <i>m</i> -carboxy luminol		Detergent lysis, complete, fast	ECL[b]	[37]
	0.16 M enediol ligands (~7.09 10 ⁶ ligands/ liposome)		Detergent lysis, complete, fast	Photoelectrochemistry ^[a]	[66]
	~1.48 10 ⁷ Cu nanoclusters/ liposome		Detergent lysis, complete, fast	Photoelectrochemistry ^[a]	[39]
	30 mg mL ⁻¹ UCNPs		no	Luminescence	[85]
	-		no	FRET ^[f] , FCM ^[h]	[86]
	0.1 M dopamine		Detergent lysis, complete, fast	Photoelectrochemistry ^[a]	[87]
	100 mM cysteine		Enzymatic, concentration-dependent, slow (1 h)	Absorbance	[25]
	Polymer dots		no	Fluorescence	[67]
Mesoporous silica	Carboxyfluorescein-C12		no	Fluorescence	[88]
	Cationic polyfluorene	conjugated	no	Fluorescence	[89]
	Rhodamine Fluorescein	6G and	no	CL ^[c]	[40]

	1.2 mM rhodamine B	Gatekeeper, concentration-dependent, (90 min)	slow	Fluorescence	[90]
	0.2 mg mL ⁻¹ rhodamine B	Gatekeeper, concentration-dependent, slow (90 min)		Absorbance	[70]
	1 mM methylene blue; 60 mg mL ⁻¹ methylene blue	Gatekeeper, complete, slow (120 min); Gatekeeper, concentration-dependent, slow (80 min)		SWV ^[d]	[41]; [73]
	80 μM Cy754 (~256 molecules/particle)	no		Fluorescence; Photoacoustic	[91]
	Glucose	Gatekeeper, concentration-dependent, slow (80 min)		Fluorescence	[24]
	1 M glucose; 350 mg mL ⁻¹ glucose	Gatekeeper, concentration-dependent, medium (20 min); Gatekeeper, concentration-dependent, medium (25 min)		Glucometer	[42]; [74]
	150 mM N,N-phenylenebis-(salicylideneimine)dicarboxylic acid	no		Fluorescence	[79]
	50 mM CuSO ₄	Gatekeeper, concentration-dependent, medium (30 min)		Photoelectrochemistry ^[a]	[92]
	0.08 mM [Ru(bpy) ₃] ²⁺	Gatekeeper, concentration-dependent, slow (2 h)		ECL ^[b]	[43]
	0.16-0.5 mmol rhodamine B	Gatekeeper, concentration-dependent, medium (30-35 min)		Fluorescence	[93], [69]
	0.32 mmol rhodamine B	Gatekeeper, concentration-dependent, slow (60 min)		Fluorescence	[94]
	BODIPY	no		Fluorescence	[95]
	Rhodamine 6G	no		Fluorescence	[96]
AuNCs	100 μM rhodamine B	Gatekeeper, concentration-dependent, slow (1 h)		Fluorescence	[55]
	[Ru(bpy) ₃] ²⁺	no		ECL ^[b]	[54]
	-	no		LSPR ^[e]	[82]

Nanocontainers for Analytical Applications

	-	no	Voltammetry	[26]; [97]
Polymer	<i>e.g.</i> 50 mM CF, 50 mM SRB, 100 mM calcein, 330 mM sodium azide, 3 mM nile red	Enzymatic, complete, medium (30 min)	Fluorescence	[45]
	30 μ M conjugated polymer	no	Fluorescence	[44]
	50 μ g mL ⁻¹ nile red; 40 μ g mL ⁻¹ nile red	no; no	FRET ^[f]	[23]; [46]
	0.4-1.5 mg mL ⁻¹ (~2400 UCNPs/ capsule)	no	Luminescence	[47]
	5 mM pyranine	Redox-responsive, slow (2 h)	Fluorescence	[48]
	PDA ^[g] polymer	no	Fluorescence	[98]
	PDA ^[g] polymer	no	Absorbance	[99]
	1,8-naphthalimide-PDA ^[g] -conjugate	no	Fluorescence	[100]
Carbon NCs	52 mg mL ⁻¹ Cresol red	Competitive replacement, fast	Absorbance	[101]
	-	no	Fluorescence quenching	[11]
	-	no	QCM ^[e]	[58]
Apoferitin	10 mM metal phosphates	pH-responsive, no release	Square wave anodic stripping voltammetry	[52]
	Lead/ cadmium phosphate	Acidic, complete, fast (5 min)	Voltammetry	[49]
	1 mM CuSO ₄ *5 H ₂ O (~1200 CuNPs/ apoferritin)	Acidic, complete, medium (20 min)	DPV ^[h]	[51]
Metal oxide	-	no	Conductometric	[27]
	-	no	Conductometric	[61]
	-	no	Conductometric	[62]
	-	no	Conductometric	[63]
Ln-MOF	-	no	Luminescence	[81]

[a] Photoelectrochemistry: electrochemical current is produced by electron transfer from photoactive materials to semiconductor electrodes via light irradiation. [b] ECL: electrochemiluminescence. [c] CL: chemiluminescence. [d] SWV: square wave voltammetry. [e] LSPR: localized surface plasmon resonance. [f] FRET: fluorescence resonance energy transfer. [g] QCM: quartz crystal microbalance. [h] DPV: differential pulse voltammetry. [g] PDA: polydiacetylene. [h] FCM: fluorescence correlation microscopy.

Successful entrapment of the signaling molecules is only possible if properties like size or hydrophilicity match with the nanocontainers' pores or cavities. The aqueous core of apoferritin can for example only be used for the entrapment of water-soluble compounds. For this the pH dependency of the

protein is exploited. At pH 2 it dissociates into its subunits and can be mixed with the entrapment molecules. Upon a rise in pH to 8.5 the protein reassembles into its native structure and encapsulation of the signaling molecules takes place.^[1,7,51]

Liposomes provide naturally the possibility to be loaded with both hydrophobic and hydrophilic components due to their bifunctional structure.^[38,67,68] Specifically, aqueous marker molecules can be entrapped in high concentrations within the inner cavity, while the membrane layer itself can be intercalated with hydrophobic components. Furthermore, the surface of the lipid bilayer can be functionalized with markers via covalent or adsorptive strategies.^[1] The hydrophilicity of the cavity of polymersomes depends on the polymeric membrane. In case of di-block polymeric membranes hydrophobic molecules can be entrapped and hydrophilic molecules in the case of tri-block polymeric membranes.^[13] In these cases the entrapment molecules are already added during vesicle formation. In the case of liposomes and polymersomes, their larger cavities in comparison to other nanocontainers (with pore sizes mostly below 10 nm) enable the entrapment of large numbers of signaling molecules, and even larger molecules (proteins, DNA) or nanoparticles can be loaded. In all instances, entrapment conditions play a crucial role for efficiency, yield and maintaining nanocontainer and entrapped molecule integrities. This is most critical for the entrapment of proteins where denaturation, unfolding and aggregation must be avoided.^[102] Therefore, mostly emulsion or rehydration methods under minimized harsh conditions have been applied for efficient protein encapsulation.^[102,103] In the case of nanoparticle entrapment into aqueous compartments, surface modification of the particles is necessary to render their usually hydrophobic surface hydrophilic.^[85] Moreover, the hydrodynamic diameter of nanoparticles restrict their overall number to be included in the inner cavity of a nanocontainer so that most nanoparticles used are smaller than 10 nm.^[47,85]

In the case of mesoporous silica nanocontainers the pore size and geometry can be tuned and can also be designed to bear either hydrophilic or hydrophobic characteristics.^[12] For example, the addition of MTMS to the formulation during synthesis provides an ideal environment for loading hydrophobic dyes such rhodamine 6g and fluorescein.^[40] Entrapment is usually conducted after synthesis either non covalently inside the pores or via covalent conjugation on the surface using *e.g.* dye-APS ((3-aminopropyl)triethoxysilane). The often occurring leakage of non-covalently loaded molecules^[91] can be avoided by using gatekeepers.^[24,41,42] These physically prevent the encapsulated material from leaking, and interestingly can also serve as target-responsive release systems. Here, the nanocontainer pores need to be big enough for the entrapment of the signaling molecules but at the same time small enough for a successful blocking of the pores.^[41] Such analytically highly interesting gatekeepers have also been successfully adapted to gold nanocontainers.^[55]

1.3.2. Signal Generation Through Controlled Release of Entrapped Molecules

Signal amplification of controlled release systems are based on the large amount of signal generating molecules entrapped inside the cavities or pores of a nanocontainer. Upon release, a signal is either obtained immediately or after reaction with molecules in the vicinity of the nanocontainer. For example, fluorescent dyes entrapped in self-quenching concentrations will emit fluorescence upon dilution in the outer media; electrochemical markers can react on electrode surfaces, enzymes can catalyze reactions etc.

Different mechanisms have been described for controlled release strategies. For example, the nanocontainers can react to external stimuli like temperature, pH or light irradiation.^[6] Bushan *et al.* demonstrated that by changing the pH from neutral and slightly basic conditions to acidic conditions the disassociation of apoferritin into its subunits takes place, which leads to the release of entrapped molecules.^[7] In addition to the same external stimuli,^[6] in case of polymeric nanocontainers also enzymes such as hyaluronidase have been used, which degrades specifically hyaluronic acid containing block copolymers.^[45] While liposomes also react to external stimuli as described above, detergents are mostly applied in bioassays to lyse the lipid bilayer.^[37,84] Somewhat slower release is obtained through enzymatic degradation using sphingomyelinase^[25] or phospholipase.^[104] For mesoporous silica and gold nanocontainers gatekeepers block the hollow pores. Here, the external stimulus is usually the target analyte, to which the gatekeeper binds more specifically than to the nanocontainer pores resulting in a concentration dependent release of signaling molecules.^[42,55] A detailed review on this topic was published by the group of Sancenón *et al.* in 2016.^[105]

1.3.3. Release-Independent Signal Generation Strategies

If no controlled release mechanism is applied, signal amplification is achieved by various strategies. In the case of liposomes, non-quenching concentrations of fluorescent dyes, absorption and refractive index can be detected optically, and size or weight acoustically or via impedance. Also here, the large surfaces and the larger inner cavities provide ultimate advantages. Gao *et al.* demonstrated that receptors are bound on outer and inner pore surfaces of gold nanocages and hence significantly enhance obtainable signals.^[54] Yildiz *et al.* showed that enzymes bound inside permeable pores of the nanocontainers can react with substrates diffusing into the pores.^[44] Similarly, in gas and metal ion sensing analyte molecules penetrate all pores of the metal oxide nanocontainers causing a change in resistance,^[27] a change in the luminescence properties of Ln-MOF structures,^[81] shifts in the LSPR spectrum of Ag/Au nanocages,^[82] or quench the fluorescence of carbon-based nanocontainers.^[11]

1.4. Analytical Applications of Nanocontainers

1.4.1. Bioassays

Table 1.3 provides an overview of analytes detected in recent years with the help of nanocontainers. Assay types, detection methods and corresponding detection limits are provided as well in order to allow a comparison between the analytical performance of nanocontainers described. The sheer number and breadth of analytes studied signify that general bioassay-related challenges have been overcome in the last decade and that nanocontainers can further develop into new standard strategies also applied in commercial products.

1.4.1.1. Heterogenous, Controlled Release Bioassays

In heterogeneous assays nanocontainers are used similar to enzyme labels,^[38,51] providing shorter assay times due to instant signal generation and in many instances enable very low limits of detection, as convincingly shown for liposomes, mesoporous silica particles and protein nanocages. For example, 1-methyl-1H-benzimidazole functionalized mesoporous silica nanocontainers were used for the development of a sandwich immunoassay for the detection of squamous cell carcinoma antigen. Under neutral conditions, β -cyclodextrin functionalized AuNPs serve as gatekeeper for the entrapment of a large amount of methylene blue molecules in the nanocontainer pores. After sandwich formation with the specific antigen on a gold electrode the pH is lowered to acidic conditions, which results in gate opening and release of the signaling molecules. Square wave voltammetry (SWV) was applied for analysis and a detection limit of 0.25 pg mL^{-1} was achieved. This signal amplification strategy can compete *e.g.* with immunoassays based on chemiluminescent (CL) labeled antibodies and achieves even lower detection limits than enzymatic amplification.^[41] Similarly, magnetic, mannose-functionalized mesoporous silica particles were used for the detection of aflatoxin B₁ (AFB₁). rhodamine B was entrapped inside the pores and capped with concanavalin A (ConA) via weak interactions with mannose. The mesoporous silica particles were also used for the attachment of capture antibodies. AuNPs were functionalized with the enzyme invertase and the analyte AFB₁. A competitive reaction between free analyte and the functionalized AuNPs took place. For signal generation, sucrose was enzymatically converted to glucose, which can also bind to ConA. This resulted in the displacement of mannose gatekeepers and release of the fluorescent dye. A limit of detection (LOD) of 8 pg mL^{-1} was achieved, which is up to 30 times lower than with commercially available ELISA kits.^[90]

Although low detection limits can be achieved using such setups, heterogenous assays using gatekeepers for signal generation can be very time-consuming as the reported release times range from 90 to 120 minutes to ensure complete release of the guest molecules. Thus, careful evaluation of the perceived improvements over standard materials needs to be considered.

External stimuli often provide faster signal release. For example, Wang *et al.* developed a sandwich immunoassay for the detection of an avian leukosis virus subgroup. A dual signal amplification strategy was applied here for further signal enhancement through a large number of electroactive copper nanoparticles inside apoferritin and by using quantum dot (QD) coated magnetic particles. These were also used for the attachment of multiple reporter antibodies and apoferritin. For the assay, a glassy carbon electrode (GCE) coated also with graphene quantum dots was used for the covalent attachment of the capture antibodies. After the immunocomplex formation acidic release of the entrapped copper nanoparticles was initiated and the virus subgroup was quantified using the oxidation peak in differential pulse voltammetry analysis. This resulted in a limit of detection of 115 TCID₅₀ mL⁻¹ (tissue culture infection dose), which outperforms single signal amplification strategies.^[51] Ge *et al.* used the apoferritin cavity for the formation of lead and cadmium phosphate for the simultaneous detection of different phosphorylation sites in phosphorylated p53 via a voltammetric sandwich immunoassay (Figure 1.1). For further signal amplification SiO₂/Au nanocomposites were applied for

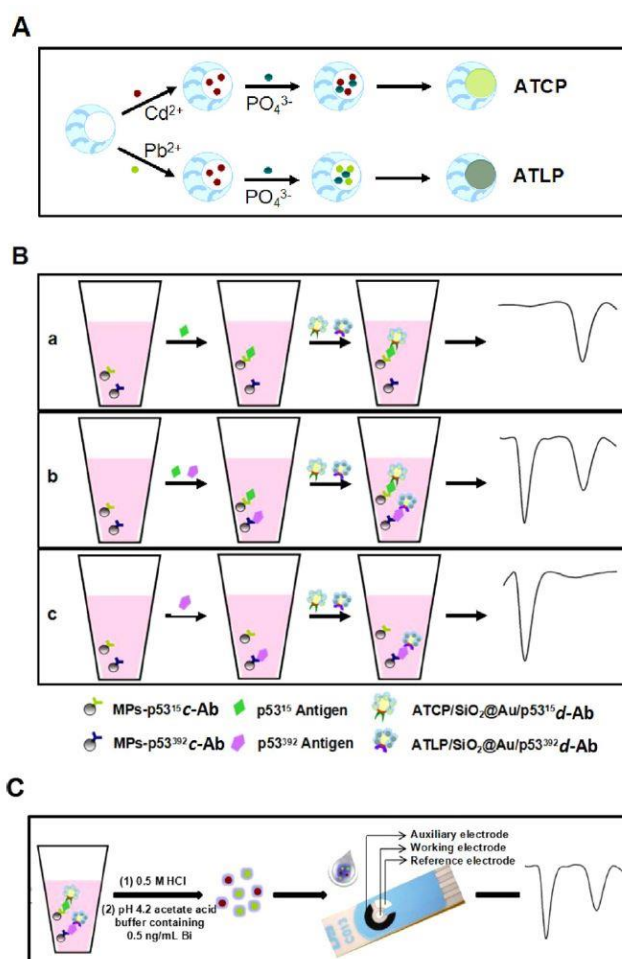


Figure 1.1. (A) Synthesis illustration of apoferritin templated metal phosphates; (B) Schematic illustration of simultaneous immune-detection of multiple phosphorylated proteins: sandwich-like immunoreaction with phospho-p53¹⁵ (a), phospho-p53¹⁵ and phospho-p53³⁹² (b), phospho-p53³⁹² (c). (C) The electrochemical measurement of multiple analytes. Reprinted from Ref. [49], with permission. Copyright 2016 Elsevier.

co-immobilization of the apoferritin signal reporters and the detection antibodies. After immunocomplex formation on magnetic beads the metal phosphates were released and quantified using square wave voltammetry. The different peaks could clearly be distinguished enabling the simultaneous detection of phospho-p53¹⁵ with a LOD of 0.05 ng mL⁻¹ and phospho-p53³⁹² with a LOD of 0.02 ng mL⁻¹.^[49] In the case of liposomes, instantaneous lysis can be achieved via detergent addition. Mayer *et al.* employed carboxy-luminol entrapping liposomes for the detection of *C. parvum* via a DNA sandwich hybridization assay. The release of the 100.000s of marker molecules and quantification via electrochemiluminescence (ECL) resulted in a detection limit of 3.2 pM, which is 150 times lower than the corresponding fluorescence approach.^[37] Similarly, Edwards *et al.* developed various liposome-based bioassays, *e.g.* for the detection of myoglobin in a simple immunoassay format using sulforhodamine B encapsulating liposomes. With fluorescence detection, a limit of detection of 11.3 pg mL⁻¹ was achieved, which was reported to be 1.5 times better than with enzymatic amplification.^[84] Similarly, such fluorescent liposomes were applied for thiamine detection. Here, the liposomal surface was functionalized with a periplasmic binding protein specific to thiamine. A polyethylene glycol modified (PEGylated) thiamine analogue was immobilized on a 96 well plate to compete with free thiamine for binding to the functionalized liposomes. Fluorescence analysis of the lysed liposomes resulted in a limit of detection of 0.5 nM, which is about 10 times lower than with a commercially available ELISA kit for thiamine detection.^[83] For further improvement of the assay sensitivity with respect to resolution and LOD, Edwards *et al.* developed fluorescent, magnetic DNA-tagged liposomes. This was demonstrated in a sandwich hybridization assay. Here, binding of the liposomes to the target DNA should be faster and more directed as in case of non-magnetic liposomes enabling a more sensitive detection. Signal amplification using magnetic, fluorescent liposomes resulted in a limit of quantification of 35 pM that was 15 times better than without directed magnetic attraction.^[38]

Mei *et al.* demonstrated recently that liposomes can successfully substitute enzymes and improve photoelectrochemical detection strategies which is an emerging and rapidly advancing field in bioanalyses.^[39,66,106] Here, large amounts of electron donors such as ascorbic acid are entrapped inside liposomes (Figure 1.2). An immune sandwich assay was conducted on electrodes coated with TiO₂ nanoparticles. Upon release of enediol ligands from the liposomes a chelate complex was formed with the uncoordinated Ti atoms on the surface of the TiO₂ nanoparticles. Irradiation with visible light leads to an electron transfer from the enediol ligands to the vacant conduction band of the TiO₂ nanoparticles, which enables the successful photoelectrochemical detection of the model analyte IgG with a LOD of 0.1 pg mL⁻¹.^[66] Similarly, dopamine encapsulating liposomes were applied for the detection of aflatoxin B₁ (AFB₁). The liposome surface was functionalized with AFB₁ resulting in a competitive reaction with free analyte for binding to antibody functionalized magnetic beads. The

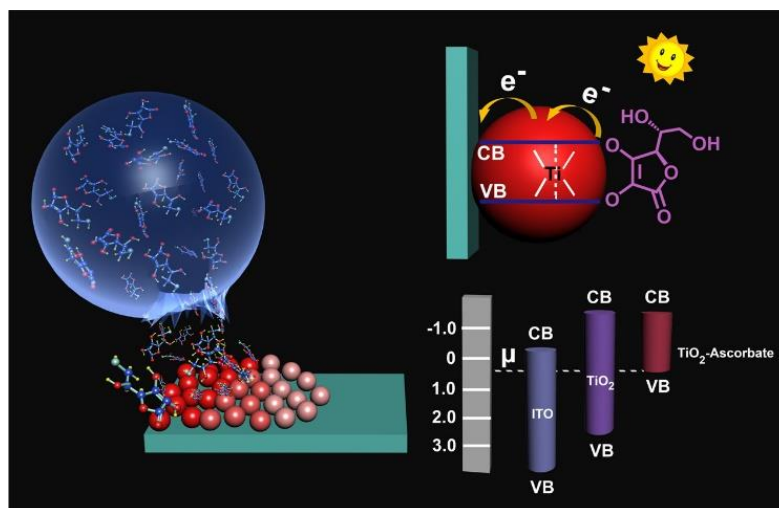


Figure 1.2. Schematic illustration of the enediol-ligands chelation against surface Ti atom with the charge transfer processes upon visible light irradiation and the corresponding energy-level diagram. Reprinted from Ref. [66], with permission. Copyright 2017 American Chemical Society.

loaded dopamine was released and served as electron donor to increase the photocurrent of Mn²⁺-doped nanobelt electrodes. AFB₁ could be detected down to 0.3 pg mL⁻¹, which is up to 1000 times lower than with commercially available ELISA kits.^[87] Another example for a photoelectrochemical based immunoassay relies on photocurrent inhibition (Figure 1.3). Here, indium tin oxide (ITO) electrodes coated with CdS quantum dots are applied, which gives a photoelectrochemical signal. Cu nanoclusters are entrapped inside liposomes and after immune sandwich formation the entrapped material is released and converted to Cu²⁺ using HNO₃. The free Cu²⁺-ions interact with the electrode and form Cu_xS, which inhibits the photocurrent. A LOD of 0.03 pg mL⁻¹ was achieved for the detection of the model antigen human cardiac troponin T, which is 4.5 times lower than reported for piezoelectric detection and even 3000 times lower than with surface plasmon resonance (SPR) spectroscopy.^[39]

1.4.1.2. Homogenous Controlled Release Bioassays

Homogenous assays usually enable simpler and faster assays since no washing steps are needed. However, higher background caused by the interference of unbound material often results in a less sensitive detection. Smart signal amplification strategies are therefore required which can be offered by nanocontainers, especially as the concentration dependent release of marker molecules can be realized through gatekeepers sensitive to analyte binding. Various nanocontainer strategies have hence been demonstrated.

For example, photoelectrochemical based bioassays have been reported such as with Cu²⁺-loaded mesoporous silica nanocontainers. Here, pore blocking was achieved using capture RNA functionalized AuNPs, which are complementary to the target analyte, microRNA-21. Thus, a concentration-dependent release of Cu²⁺-ions takes place upon binding of microRNA-21. An array of TiO₂ nanorods

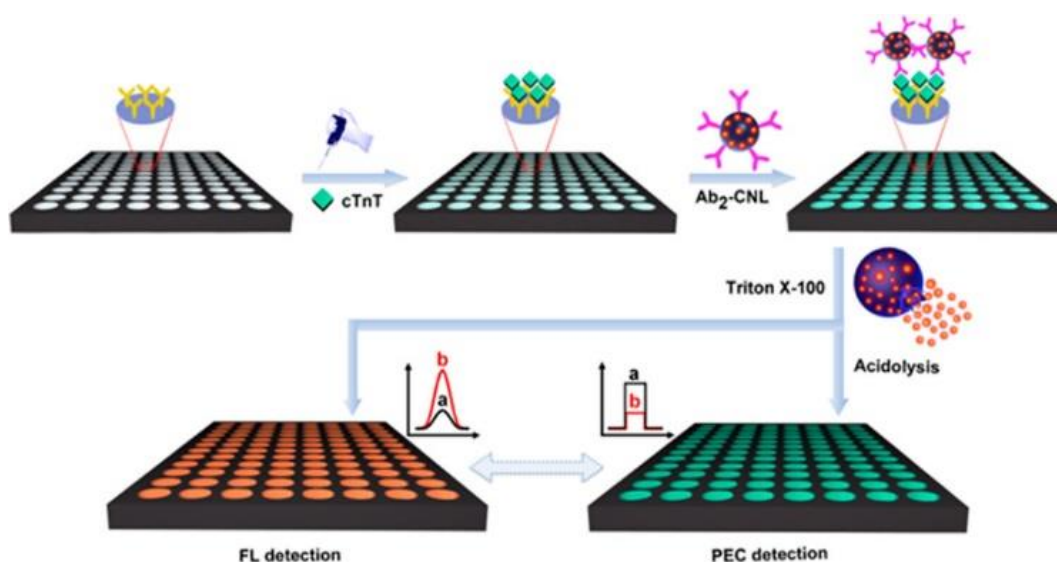


Figure 1.3. Illustration of the Cu nanocluster-loaded liposomal photoelectrochemical immunoassay accompanied by a complementary fluorescent detection. Reprinted from Ref. [39], with permission. Copyright 2018 American Chemical Society.

and of $\alpha\text{-Fe}_2\text{O}_3$ shells was applied as photoelectrode. The generated photoelectrons can be accepted by the released Cu^{2+} ions, which are reduced to Cu^0 at the counter electrode. The obtained photocurrent allowed the detection of microRNA-21 down to 0.74 fM .^[92] This result is comparable to other photoelectrochemical assays and even superior to some electrochemical approaches. The signal amplification here was attributed to the efficient charge separation of the hierarchical nanorod array in addition to the high loading capacity of the nanocontainers.^[92] Zhang *et al.* report on methylene blue encapsulating mesoporous silica nanocontainers that are functionalized with antibodies and applied to the detection of biotoxins. Aminated polystyrene microspheres were applied as gatekeeper by binding nonspecifically to the antibodies and blocking the pores. Upon binding of the analyte, the microspheres are replaced, the pores opened, methylene blue is released and can be used for analysis by square wave voltammetry. Biotoxins could be detected down to 6 pg mL^{-1} , which is a ~ 8 times lower LOD than with a commercially available ELISA kit.^[73] Such polystyrene-gated nanocontainers have also been applied for the detection of brevetoxin B. Here, entrapped glucose molecules were released upon replacement of the polystyrene particles by the analyte. The concentration-dependent release of glucose molecules was monitored using a glucometer. A LOD of 0.01 ng mL^{-1} was achieved, which was 5 times lower than with a commercially available ELISA kit.^[74] The simplicity and low-cost features of a glucometer readout was also exploited for aflatoxin detection. Here, antibody-functionalized gold nanoparticles are electrostatically attached to the nanocontainers to block the pores. Upon addition of the analyte, the gold nanoparticles are removed and monitoring of the concentration-dependent release of glucose molecules by a glucometer resulted in a LOD of $0.005 \text{ } \mu\text{g kg}^{-1}$, which is well below the allowed limit of $2 \text{ } \mu\text{g AFB}_1$ in foodstuff (EU) and shows a comparable LOD as commercially available ELISA kits.^[42] Aptamer-gated glucose loaded mesoporous silica nanocontainers have also been

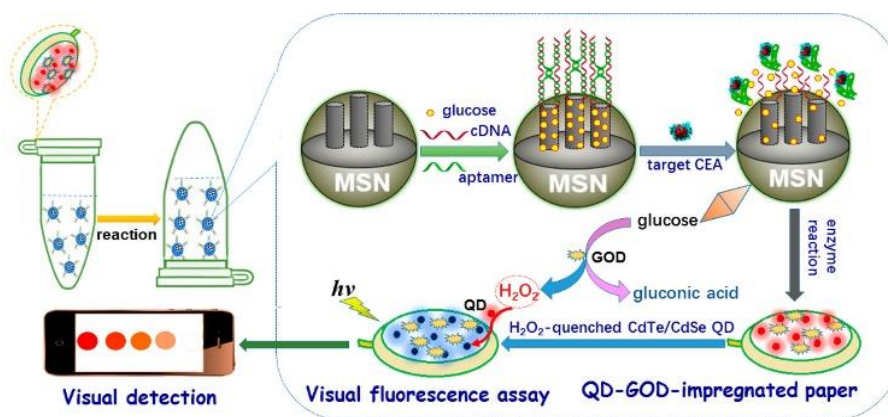


Figure 1.4. Schematic illustration of paper-based analytical device for the visual fluorescence detection of target carcinoembryonic antigen (CEA) biomarker in a 0.5 mL centrifugal tube based on CEA aptamer/complementary DNA-gated mesoporous silica nanocontainers loaded with glucose molecules by coupling with target-induced cargo release and cargo-promoted enzymatic amplification. Reprinted from Ref. [24], with permission. Copyright 2017 American Chemical Society.

described for the detection of carcinoembryonic antigen (Figure 1.4). Here, a paper-based homogenous assay using a centrifuge tube was applied. For detection the lid of this tube contains glucose oxidase modified CdTe/CdSe quantum dots immobilized on paper. The enzyme catalyzes the reaction of the released glucose to gluconic acid and H₂O₂ quenches the emission of the quantum dots. This yields a quantitative response with a detection limit of 6.7 pg mL⁻¹, which is 30-150 times lower than for most commercially available ELISA kits.^[24]

Also, the group of Félix Sancenón and Ramón Martínez-Máñez has published a number of bioassays and sensors using gated mesoporous silica nanocontainers.^[69] While other groups mainly report on electrostatic attachment of gatekeepers, they also investigated the effect of covalent attachment as for example for the detection of Ochratoxin A. Here, the nanocontainers were loaded with rhodamine B and the pores capped with aptamers using two different approaches, either by covalent blocking by hybridization with a short DNA sequence attached to the nanocontainer surface or by electrostatic blocking exploiting the aminopropyl functionalization of the nanocontainer surface. Although a faster dye release was observed in case of the covalent approach, a detection limit of only 0.5 nM was achieved here, whereas a 10 times lower LOD was observed for the electrostatic approach. This can be assigned to the weaker interaction between the gatekeeper and the nanocontainer surface. Both detection limits are comparable to reported LC-MS or HPLC-fluorescence approaches or even lower than those of many other reported aptasensors for ochratoxin A detection. Moreover, the assay provided good results with high accuracy with real samples.^[69] The same principle was applied to several other analytes by simply using a different aptamer. This enabled for example also the detection of genomic DNA down to 50 DNA copies μL⁻¹, which is similar to PCR-based approaches but enables a faster detection with less sources of error due to the omission of analyte amplification.^[94] Apart from the detection of biological molecules these nanocontainers also enable the quantification of chemical

substances. For example, bisphenol A (BPA) was successfully detected down to 3.5 μM . This is comparable to other setups based on aptamer recognition and sufficient to detect hazardous amounts of BPA in water, but electrochemical sensors based on rGO electrodes have been reported to work down to nM levels.^[93]

Similar approaches have also been reported with capped gold nanocages. The group of Wang *et al.* designed positively charged gold nanocages entrapping rhodamine B for adenosine triphosphate (ATP) detection. ATP-binding aptamers are electrostatically bound to the nanocages capping their pores. Upon ATP binding, the conformational changes of the aptamers lead to an opening of the pores and release of entrapped fluorescent cargo. The obtained LOD of 1 nM^[55] is ~ 50 times more lower than *e.g.* reported for a competitive aptamer bioassay using fluorescent gold nanoclusters, which in turn was reported to be comparable to electrochemical detection and even better than most fluorescence-based approaches.^[107]

If the analyte causes the degradation of a nanocontainer shell, homogeneous assays are equally straightforward to design. For example, Holme *et al.* designed a liposome-based assay for the detection of sphingomyelinase (Figure 1.5), which serves as biomarker for several diseases.^[25] The liposomes contained sphingomyelin lipids in their bilayer and cysteine molecules in their inner cavity. Upon addition of sphingomyelinase the phosphate-oxygen bonds of the sphingomyelin molecules are enzymatically hydrolysed to form phosphocholine and ceramide. The resulting change in the lipid bilayer composition causes a change in the membrane phase leading to leakage of the encapsulated

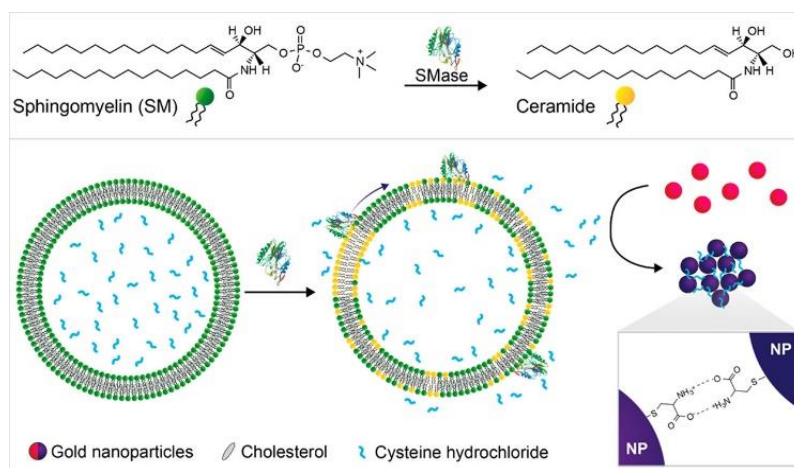


Figure 1.5. Assay schematic. (Top) Hydrolysis of the phosphate-oxygen bond of sphingomyelin (SM) by sphingomyelinase (SMase) to produce ceramide and phosphocholine (not shown). (Bottom) Action of SMase on BSM:Chol liposomes encapsulating cysteine leads to a composition-driven membrane phase change with the formation of ceramide-rich gel domains and partitioning of cholesterol into remaining SM domains. This causes cysteine leakage and aggregation of subsequently added gold nanoparticles by formation of hydrogen bonds between cysteine molecules on adjacent nanoparticles. Adapted from Ref. [25] with permission, <https://pubs.acs.org/doi/10.1021/acsnano.8b03308>, contact American Chemical Society for further permissions.

cysteine molecules. These can induce aggregation of AuNPs, which enabled bare eye detection of the enzyme activity down to 0.08 mU mL^{-1} (5.5 pM) and down to 0.02 mU mL^{-1} (1.4 pM) using absorbance spectra for quantification. The obtained LODs are lower than with commercially available colorimetric assays.^[25] Also, other encapsulants can be envisioned for fluorescence and electrochemical approaches.

In a slightly different approach, the enzyme hyaluronidase, which is a biomarker for *S. aureus* in wounds, was quantified via polymersomes formed by block-copolymers containing hyaluronic acid. The fluorogenic substrate 7-amino-4-methylcoumarin was entrapped inside the container. In the presence of hyaluronidase, the polymersomes were enzymatically degraded, the cargo was released and detected after cleavage of its peptide bond by α -chymotrypsin. Again, other entrapment molecules can easily lead to other read-out systems and strengthen the ability to create fast *in situ* sensors for bacterial infections.^[45]

1.4.1.3. Release-Independent Bioassays

In comparison to bioassays relying on the release of marker molecules for signal enhancement only few examples can be found for non-release bioassays. Here, signal enhancement is for example achieved by entrapping a large amount of dye molecules as described by the group of Tao *et al.* They used mesoporous silica particles loaded with rhodamine 6G and fluorescein for the detection of staphylococcal enterotoxin C1 in a classical sandwich immunoassay. However, due to the semi-hollow structure of the silica particles, the bis(2,4,6-trichlorophenyl)oxalate (TCPO)- H_2O_2 -imidazole reagent can enter the pores, react with the entrapped dyes and initiate a chemiluminescent reaction. With this, a limit of detection of 0.019 ng mL^{-1} was achieved, which is up-to 100 times lower than other reported methods using *e.g.* CL, fluorescence or electrochemical detection methods and also ~ 25 times lower than with an ELISA.^[40]

Another popular strategy for non-release bioassays is the use of polydiacetylene (PDA) vesicles. These polymeric structures exhibit a change in color from blue to red as well as an emergence of fluorescence upon changes in their environment. This has for example been exploited for the detection of surfactin producing bacteria. The negatively charged surfactin is able to interact with amine functionalized PDA vesicles. This induces conformational changes of the bilayer and a specific shift in absorbance, which also creates a strong fluorescence signal that enables detection down to $1.8 \cdot 10^3 \text{ cfu mL}^{-1}$. This enables an effective detection of bacteria classes, that *e.g.* all secrete the same molecule, without the need for a specific receptor.^[98] A dual signal amplification strategy can be achieved using an array of PDA vesicles in combination with an enzymatic reaction as shown for the detection of hIgE (human IgE). Here, a sandwich immunoassay was conducted on PDA vesicles. Each binding event causes a slight shift in color. Upon addition of the substrate and after binding of the horseradish peroxidase (HRP)-labeled

detection antibody, precipitation of the insoluble product of the enzymatic reaction takes place, which causes an enormous shift in absorbance. This results in a LOD of 0.01 ng mL^{-1} , which is a 1000 times lower than without the use of an enzyme-labeled detection antibody.^[99]

Moreover, vesicle fusion can be exploited for the design of release-independent assays. Here, mostly FRET-based approaches have been reported, *e.g.* by incorporation of membrane dyes like DiI or DiD into two different liposomes functionalized with dsDNA. For one type of liposome the sticky end of the liposome is blocked using a hairpin DNA to prevent fusion with the other vesicles by hybridization with the complementary DNA strands. In the presence of the target RNA hybridization with the hairpin DNA takes place, which causes its detachment from the sticky end and thus fusion of the two differently labeled liposomes. The resulting close proximity of the DiD and DiI dyes results in the emergence of FRET. This was applied for microRNA-29a quantification down to 18 nM using a simple microplate reader and could be further improved to 1.2 nM using two color fluorescence correlation microscopy in combination with intensity fluctuation analysis.^[86]

Table 1.3. Overview of analytes that have been detected using different nanocontainers and assay types.

Analyte	Nanocontainer	Detection/assay type	Assay type	LOD	Ref.	
Pathogens	Carcinoembryonic antigen	Mesoporous silica	Fluorescence	Homogenous	6.7 pg mL^{-1}	[24]
	Cell carcinoma antigen		SWV ^[a]	Sandwich immunoassay	0.25 pg mL^{-1}	[41]
	<i>C.parvum</i>	Liposomes	ECL ^[c]	Sandwich hybridization	3.2 pM	[37]
	Human cardiac troponin T		Photoelectrochemistry ^[b]	Sandwich immunoassay	0.03 pg mL^{-1}	[39]
	IgG		Photoelectrochemistry ^[b]	Sandwich immunoassay	0.1 pg mL^{-1}	[66]
	ssDNA		Fluorescence	Sandwich hybridization	35 pM	[38]
	hIgG	PDA ^[f]	Absorbance	Sandwich immunoassay	0.01 ng mL^{-1}	[99]
	Surfactin producing bacteria		Fluorescence	Homogenous	$1.8 \cdot 10^3 \text{ cfu mL}^{-1}$	[98]
Proteins	Myoglobin	Liposomes	Fluorescence	Sandwich immunoassay	11.3 pg mL^{-1}	[84]
Nucleic acids	MicroRNA-21	Mesoporous silica	Photoelectrochemistry ^[b]	Homogenous	0.74 fM	[92]
	Genomic DNA		Fluorescence	Homogenous	$50 \text{ copies } \mu\text{L}^{-1}$	[94]
	MicroRNA-29a	Liposomes	FRET, FCM ^[g]	Homogenous	18 nM; 1.2 nM	[86]

Nanocontainers for Analytical Applications

Toxins	AFB ₁	Mesoporous silica	Fluorescence	Competitive immunoassay	8 pg mL ⁻¹	[90]
	aflatoxins		Glucometer	Homogenous	0.005 µg kg ⁻¹	[42]
	BrevetoxinB		Glucometer	Homogenous	0.01 ng mL ⁻¹	[74]
	Biotoxin		SWV ^[a]	Homogenous	6 pg mL ⁻¹	[73]
	Staphylococcal enterotoxin C1		Fluorescence	Homogenous	0.019 ng mL ⁻¹	[40]
	Ochratoxin A		Fluorescence	Homogenous	0.05 nM	[69]
	AFB ₁	Liposomes	Photoelectrochemistry ^[b]	Competitive immunoassay	0.3 pg mL ⁻¹	[87]
Viruses	Avian leukosis virus subgroup	Apo ferritin	DPV ^[d]	Sandwich immunoassay	115 TCID ₅₀ mL ⁻¹	[51]
Enzymes	Sphingomyelinase	Liposomes	Absorbance	Homogenous	1.4 pM	[25]
	Hyaluronidase (<i>S.aureus</i>)	Polymersomes	Fluorescence	Homogenous	-	[45]
ATP	ATP	AuNC ^[e]	Fluorescence	Homogenous	1 nM	[55]
Bisphenol A	Bisphenol A	Mesoporous silica	Fluorescence	Homogenous	3.5 µM	[93]
Vitamins	Thiamine	Liposomes	Fluorescence	Competitive immunoassay	0.5 nM	[83]
Protein biomarker	Phosphorylation sites in p53	Apo ferritin	SWV ^[a]	Sandwich immunoassay, multiplexing	0.02 ng mL ⁻¹ and 0.05 ng mL ⁻¹	[49]

[a] SWV: square wave voltammetry. [b] Photoelectrochemistry: electrochemical current is produced by electron transfer from photoactive materials to semiconductor electrodes via light irradiation. [c] ECL: electrochemiluminescence. [d] DPV: differential pulse voltammetry. [e] AuNC: gold nanocage. [f] PDA: polydiacetylene. [g] FCM: fluorescence correlation microscopy

1.4.2. Chemosensors

Nanocontainers can also improve the sensitivity of chemosensors due to the large active surface area of their porous nanostructures,^[108] although these improved chemosensors don't approach sensitivities yet as achieved with ICP-MS, AAS and GC (gas chromatography) analyses. The overview in Table 1.4 shows that mainly gas and metal ion sensing have been reported recently. Most reported concepts are based on nanocages made from metal oxides, gold or carbon, but a few examples can also be found for mesoporous silica, polymer and lipid based nanocontainers. Oxidizing and reducing gases such as acetone and benzene can easily be detected using metal oxide nanocontainers,^[10] which often offer semiconductor properties. The gas sensing principle is based on the adsorption and oxidation of oxygen on the nanocontainer surface (Figure 1.6). Ionized oxygen species like O^- , O^{2-} or O_2^- are formed by capturing free electrons from the valence band of the nanostructure, which in turn results in the formation of a depletion layer on its surface. Thus, the electron concentration is decreased leading to an increase in resistance. Upon addition of an oxidizing or reducing gas, interaction with the adsorbed oxygen takes place, electrons are either released to the valence band resulting in a decreased resistance or more electrons are removed from the valence band. This results in a change in the depletion layer thickness and thus a concentration dependent change in resistance.^[61] This mechanism was for example exploited to detect the oxidizing gas acetone down to 1 ppm using $ZnO/ZnFe_2O_4$ nanocontainers prepared via a metal organic framework (MOF) strategy. Simple metal oxide films or nanostructures like rod-shaped nanoparticles or hollow microspheres could not provide such low LODs.^[61] In the case of the reducing gas xylene, $ZnO/ZnCo_2O_4$ hollow core-shell nanocontainers were used by Qu *et al.* They could demonstrate that not only the enlarged surface area of the pores but also electronic effects of the core-shell structures influenced the sensitivity of the gas sensor when compared to simple $ZnCo_2O_4$ shells or ZnO nanocages.^[62] Similarly, for toluene

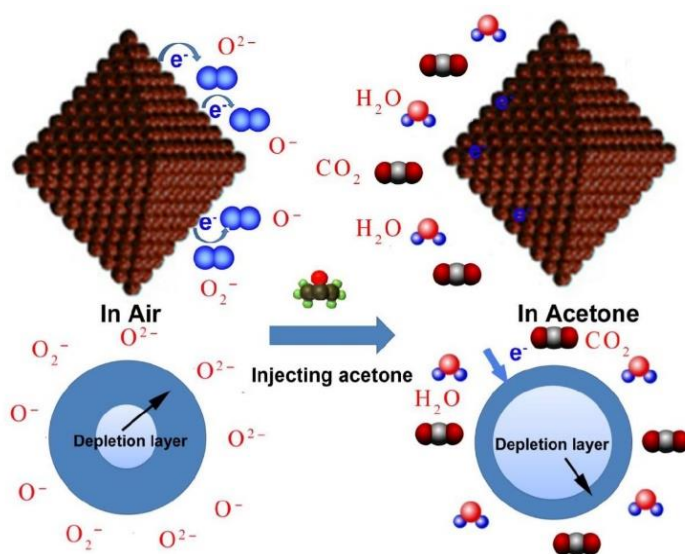


Figure 1.6. Schematic diagram of acetone sensing mechanism in $ZnO/ZnFe_2O_4$ hollow nanocages. Reproduced from Ref. [61], with permission Copyright 2017 Elsevier.

sensing cubic SnO₂ nanocontainers loaded with the catalyst Pd are described providing a LOD of only 0.1 ppm toluene.^[63] Due to synergistic effects, further signal enhancement can be achieved by the additional entrapment of metal catalysts. For example, Co₃O₄ nanocages functionalized with a PdO catalyst have been described for the sensing of acetone (Figure 1.7). The structure of the Co₃O₄ containers is again derived from a metal organic framework, which consists of small cavities for the entrapment of small metal nanoparticles. Preparation of these hollow structures is very simple as formation can be conducted simultaneously with nanoparticle functionalization using MOFs as template.^[27] For sensing, the hollow nanostructures were drop-coated in Al₂O₃ substrates consisting of two parallel gold electrodes for electrochemical analysis and Pt for heating the samples to 250-400 °C. High selectivity towards acetone was found and the ratios of the resistances $R_{\text{gas}}/R_{\text{air}}$ were used for the quantitative analysis of acetone down to 100 ppb.^[27]

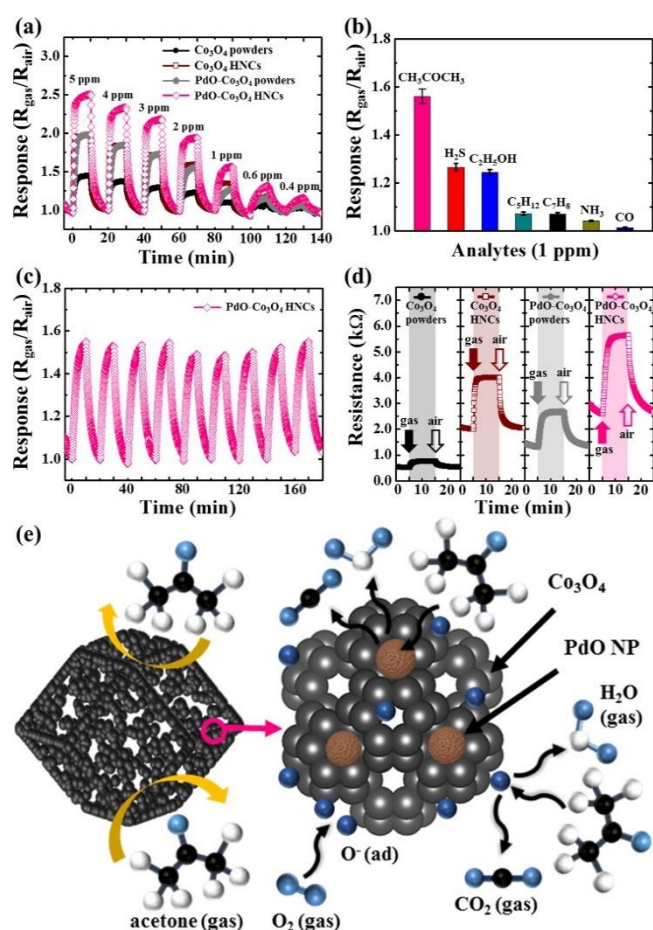


Figure 1.7. Sensing characteristics under highly humid condition (90% RH) at 350 °C. (a) Dynamic acetone sensing transient properties of Co₃O₄ powders, Co₃O₄ hollow nanocages (HNCs), PdO-Co₃O₄ powders and PdO-Co₃O₄ HNCs in the concentration range of 0.4-5.0 ppm. (b) Response values to 1 ppm of interfering analytes. (c) Cyclic sensing transient of PdO-Co₃O₄ HNCs toward 1 ppm acetone. (d) Dynamic resistance transition toward 5 ppm of acetone molecules. (e) Schematic illustration of acetone sensing mechanism for PdO-Co₃O₄ HNCs. Reprinted from Ref. [27], with permission. Copyright 2017 American Chemical Society.

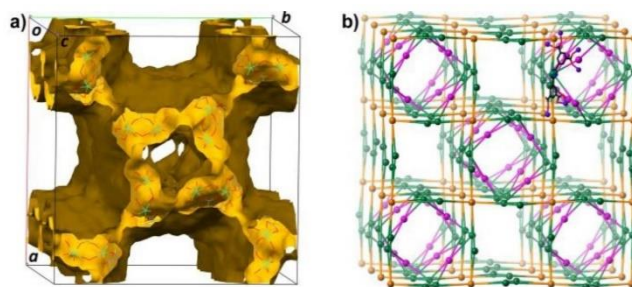


Figure 1.8. (a) 3D pores of Ln-metal organic framework structure (1-Tb), and (b) the (4,4,8)-connected topology (L^4 : green balls; Tb_2 clusters (SBU1 and SBU2), SBU1: orange balls; SBU2: purple balls). Reproduced from Ref. [81], with permission. Copyright 2016, Wiley-VCH Verlag GmbH & Co. KGaA.

The group of Liu *et al.* investigated Ln-MOF-based nanocage chemosensors (Figure 1.8 and 1.9) for the detection of the metal ions Fe^{3+} and $Cr_2O_7^{2-}$. Eu^{3+} and Tb^{3+} were introduced as lanthanoid ions. The ligand of the framework contains a triazolyl group, which presents potential nitrogen binding sites. These enhance the polarity of the framework and the sensing properties due to possible host-guest interactions. The framework is formed by M12L8-nanocages with a diameter of 1.7 nm. Each of these nanocages is connected to four other cages building a highly porous 3D structure consisting of nanocages and channels. The introduced lanthanoid ions Eu^{3+} and Tb^{3+} exhibit specific emission peaks that change upon addition of different metal ions. For example, $Cr_2O_7^{2-}$ is able to strongly quench the Eu luminescence and Fe^{3+} , in addition, significantly reduces the fluorescence lifetime. For Fe^{3+} , a detection limit of 18 μM was achieved. The detection limit is similar or even better compared to other Ln-MOF based sensing approaches but cannot compete with carbon or gold NP approaches, yet.^[81]

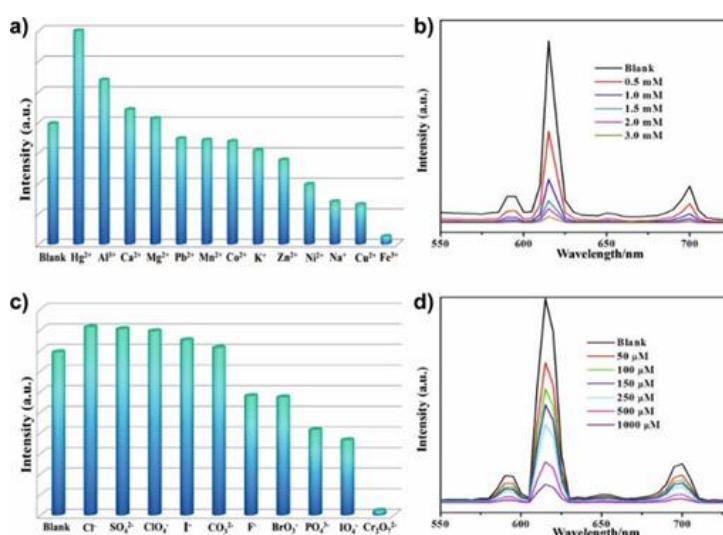


Figure 1.9. Luminescence intensity at 615 nm of Ln-MOF structure (1-Eu) treated with different metal cations (a) and anions (c) (10^{-2} M) in DMF solutions, and luminescence spectra of 1-Eu in DMF solutions with $Fe(NO_3)_3$ (b) and $Cr_2O_7^{2-}$ (d) at different concentrations. Reproduced from Ref. [81], with permission. Copyright 2016, Wiley-VCH Verlag GmbH & Co. KGaA.

Metal ion sensing using carbon nanocages usually exploits the intrinsic fluorescence of the material. The nanocages offer good binding ability to metal ions, which are able to quench the nanocontainer fluorescence. The group of Bi *et al.* for example developed a sensor using fluorescent carbon nanocages for the detection of ascorbic acid. Here, Fe^{3+} -ions are applied, which could be detected down to 3.96 μM . Moreover, in the presence of ascorbic acid Fe^{3+} is reduced to Fe^{2+} , which interacts not as strongly as with the carbon nanocages. Thus, fluorescence is turned on and can be used for the quantification of ascorbic acid. This resulted in a detection limit of 97.2 nM, which is comparable with fluorescence detection using graphene quantum dots and even lower than HPLC-based detection or electrochemical detection using $\text{Ni}(\text{OH})_2$ nanoboxes.^[11]

Kosaki *et al.* describe the synthesis of carbon nanocages using mesoporous silica as template. To further increase available sensing surface area, the nanocages were mixed with polymethylmethacrylate (PMMA) and electrospun to create a thin fibrous film on the surface of quartz crystal microbalance (QCM) electrodes.^[58] Aniline could be selectively detected in ppm levels, which is comparable *e.g.* to amperometric sensing using nanoporous gold electrodes.^[58,109] The selective response to aniline vs. other aromatic molecules such as benzene can be ascribed to the presence of alcohol, carbonyl or carboxyl groups in the nanocages, which interact stronger with aromatic amines.^[58]

Finally, also Ag/Au nanocages have been proposed for the detection of metal ions replacing fluorescent probes such as rhodamine and fluorescein. The chelation with metal ions changes the LSPR spectrum and enables highly sensitive measurements that don't suffer from photobleaching as observed with most fluorescent approaches.^[82,110] A LSPR-based sensing approach for the detection of mercury ions has for example been reported by the group of Huang *et al.* Ag/Au nanocages were synthesized by depositing AgNPs onto an ITO electrode followed by the growth of thin porous gold shells. This resulted in a framework containing a partial hollow center and multiple pinholes. The authors detect mercury ions, which are reduced while at the same time Ag atoms in the Ag/Au nanocages are oxidized and a shell of mercury is formed on the surface of the cages. This results in a blue shift in the LSPR spectrum, which can be used for mercury quantification providing a detection limit of 5 ppb Hg^{2+} , which is comparable to other reported optical sensors.^[82] Bi *et al.* use the large surface area and electrochemical properties of gold for the enzyme-free detection of hydrogen peroxide. They designed 25 nm small gold nanocages, which were deposited on GCE electrodes for voltammetric quantification of H_2O_2 . This resulted in a limit of detection of 11 μM , which is not significantly low but comparable to other H_2O_2 sensors based on gold nanocaged structures.^[26] With a similar approach, the group of Zhang *et al.* was able to reach a LOD of only 0.1 μM , which is comparable to H_2O_2 sensing with simple Prussian blue-coated electrodes.^[97,111]

Moreover, the use of mesoporous silica nanocontainers has been reported for chemosensing. For example, boron-dipyrromethene (BODIPY) can be covalently attached to the inner walls of mesoporous silica particles to prevent aggregation of the dye. In the presence of phosph(on)ate substrates a reaction to phosph(on)ate esters takes place via acylation of the hydroxyl group of BODIPY, which results in intramolecular N-alkylation and thus the formation of a bicyclic ring. This bicyclic product is non-fluorescent. This mechanism enables the quantification of chemical warfare agents containing phosph(on)ate groups such as Sarin, Soman or Tabun using the fluorescence quenching of BODIPY. The 3 analytes were quantified in the pM range, which is in all cases below the maximum permitted concentrations in drinking water.^[95] Another example can be found, where rhodamine 6G has been attached to a mesoporous silica particle surface. Rhodamine 6G consists of a spiro lactam ring, which opens in the presence of Fe^{3+} forming a complex with the metal ion. Due to the chelation of rhodamine 6G and Fe^{3+} a strong fluorescence enhancement can be observed, which allows for the quantitative analysis of Fe^{3+} down to low ppb levels, which is slightly below the recommended level in drinking water. Reversibility of the sensor was demonstrated by the addition of EDTA, which resulted in a quenching of the emission due to detachment of the Fe^{3+} ions from rhodamine 6G.^[96]

Recently, several concepts have been proposed that also improve the sensitivity of PDA vesicle-based sensors. Frequently, the additional incorporation of a fluorophore creates a sensor that is independent of incomplete photopolymerization of the vesicles. For example, a 1,8-naphthalimide derivative has been reported, whose emission is quenched in the blue phase of the vesicles via a Förster energy transfer. Conversion to the red phase in the presence of cationic surfactants results in a decrease in quenching and concentration-dependent re-occurrence of the fluorophore emission. This enabled a detection of CTAB down to $0.18 \mu\text{M}$ which is up to 10 times lower than with conventional PDA vesicles and comparable to other reported methods based on fluorometric analysis.^[100] A different concept is based on the attachment of the deprotonated form of cresol red molecules to the surface of polymer vesicles functionalized with tertiary amine alcohol groups. These vesicles exhibit a purple color. Competitive binding between cresol red and the analytes SO_2 or HSO_3^- results in the attachment of the analyte to the vesicle surface while at the same time the protonated form of cresol red is detached. This causes a color shift from purple to yellow, which enables colorimetric detection of SO_2 and HSO_3^- down to 25 nM. This LOD is comparable or even lower than other reported SO_2 probes, which are typically in the range of $5 \mu\text{M}$ to 3 nM.^[101]

A smart surface design is also crucial for liposome-based chemosensors. Here, the group of B. König has synthesized different receptors that enable the recognition of various analytes. For example, a

thiolated bis-Zn²⁺-cyclen receptor attached to the liposomes has been reported to be suitable for the detection of phosphate moieties.^[88]

Table 1.4. Overview of analytes that have been detected using chemosensors based on different nanocages.

Analyte	Nanocage	Detection	LOD	Ref.
Acetone	Co ₃ O ₄	Conductometry	100 ppb	[27]
	ZnO/ZnFe ₂ O ₄	Conductometry	1 ppm	[61]
Xylene	ZnO/ZnCo ₂ O ₄	Conductometry	-	[62]
Toluene	SnO ₂	Conductometry	0.1 ppm	[63]
Aniline	Carbon NCs ^[c]	QCM ^[a]	ppm level	[58]
Cations/Anions	Ln-MOF ^[d]	Luminescence	0.018 mM (Fe ³⁺)	[81]
Mercury	Ag/AuNCs ^[e]	LSPR ^[b]	5 ppb	[82]
Chemical warfares	Mesoporous silica	Fluorescence	0.12-90.8 pM	[95]
PO ₄ ³⁻	Liposomes	Fluorescence	52 μM	[89]
	Liposomes	Fluorescence	-	[88]
SO ₂ /HSO ₃ ⁻	Polymersomes	Absorbance	25 nM	[101]
Fe(III)	Mesoporous silica	Fluorescence	ppb level	[96]
H ₂ O ₂	AuNCs ^[e]	Voltammetry	11 μM	[26]
	AuNCs ^[e]	Voltammetry	0.1 μM	[97]
Cationic surfactants	PDA	Fluorescence	0.18 μM	[100]
Ascorbic acid	Carbon NCs ^[c]	Fluorescence	97.2 nM	[11]

[a] QCM: quartz crystal microbalance. [b] LSPR: localized surface plasmon resonance. [c] carbon NC: carbon nanocage. [d] Ln-MOF: lanthanoid- metal organic framework. [e] AuNC: gold nanocage.

Moreover, they developed a template-assisted post-functionalization strategy to introduce two-dimensional receptors via molecular imprinting, enabling the design of various receptors and thus the recognition of a large variety of analytes. The sensor principle relies on the co-embedding of the amphiphilic reporter dyes and receptor moieties close to each other in the lipid bilayer, which quenches the emission of the fluorescent probe. Target binding induces a restructuring of the membrane, which increases the distance of receptor and dye and thus enhances the emission.^[88] Phosphate quantification has also been reported with liposomes embedding a cationic conjugated polyfluorene in the vesicle membrane. The blue emission of the polymer can be quenched by p-nitrophenol (PNP), which is the product of the enzymatic degradation of p-nitrophenylphosphate

(PNPP) by alkaline phosphatase. PO_4^{3-} can inhibit this conversion resulting in the emergence of a strong vesicle emission. This enables the detection of PO_4^{3-} down to $52 \mu\text{M}$, which is comparable to conductometric sensors based on alkaline phosphatase inhibition but cannot compete with standard methods for ion analysis.^[89]

1.4.3. Bioimaging and *in vivo* Applications

Nanocontainers can bring their full range of capabilities to bear in *in vivo* applications, where fully reversible and long-term stable signaling means are necessary that function in homogeneous assays under physiological conditions. Also, here gated mesoporous silica nanocontainers have been successfully applied. They can for example be doped with black hole quenchers and simultaneously loaded with the fluorescent dye rhodamine B. Due to the high quenching efficiency of the nanocontainers, the rhodamine B fluorescence is turned on only upon dye-release triggered by specific binding of the analyte to the gatekeeper anti-GSH (glutathione). *In vitro* tests proved the ability to sense free glutathione as well as protein S-glutathionylation (PSSG) down to 52 pM and 0.03 pM , respectively. After coating the surface of the nanocontainers also with cell penetrating poly(disulfide)s, they could successfully be delivered into live mammalian cells, which enables live intracellular imaging of the target analytes.^[72] However, the use of fluorescent dyes like rhodamine B. for bioimaging is not ideal. Typically, near infrared (NIR) fluorophores are preferred as interferences by absorption of water or lipids, scattering of tissue and autofluorescence is low and hence high tissue penetration depth can be achieved. A common strategy has hence been to entrap large amounts of NIR probes inside nanocontainers to enhance the contrast between area of interest and background compared to single fluorophores.^[78] Mesoporous silica nanocontainers for example have been applied for the imaging of sentinel lymph nodes. The containers were loaded with the NIR dye Cy754 enabling fluorescent and

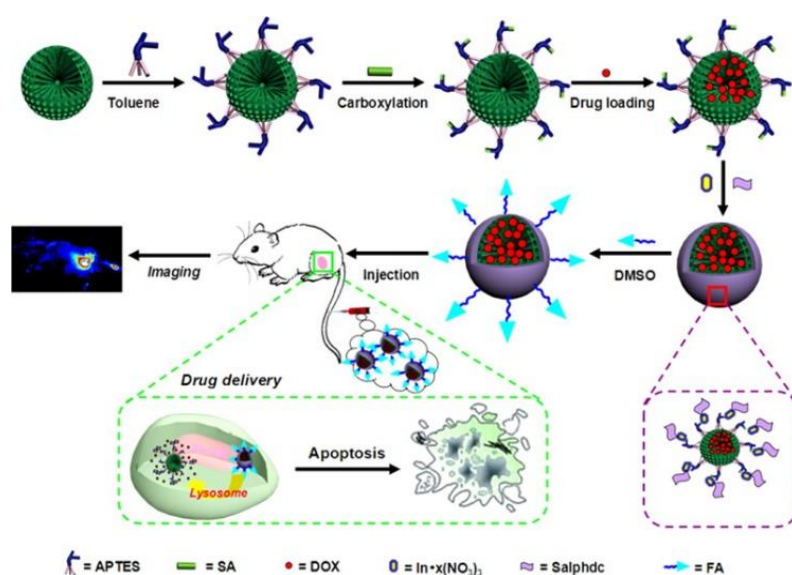


Figure 1.10. Construction of pH-responsive HPSN-Salphdc-FA system: drug-loaded HPSN-Salphdc-FA system for tumor therapy and bioimaging *in vivo*. Adapted from Ref. [79], with permission. Copyright 2015 American Chemical Society.

photoacoustic *in vivo* imaging of regional lymph nodes in a dual modality imaging mode.^[91] Silica nanoparticles with hierarchical pores (HPSNs) are also very well suited for such applications. They serve as nanocontainers with unique mesoporous characteristics as their pore sizes decrease from surface to center. Dai *et al.* use a N,N-phenylenebis(salicylideneimine)dicarboxylic acid (Salphdc) complex as gatekeeper to entrap the model drug doxorubicin (DOX) but can also be applied as autofluorescent probe for bioimaging (Figure 1.10). Folic acid was attached to the particle surface as targeting unit for tumor cells. Under acidic pH values, the Salphdc complex is dissolved, which results in the release of the entrapped drug molecules. At physiological pH, the Salphdc complex stays intact.^[79]

Also liposomes have been applied for the imaging of cancer cells. For example, folic acid-modified liposomes entrapping an amphiphilic fluorescent squaraine dye have been designed by Dong *et al.* Squaraine is embedded in the hydrophobic membrane to prevent fluorescence quenching otherwise caused by aggregation in an aqueous environment. Those liposomes are able to bind to cancer cells, which overexpress folate receptors. The squaraine dye emits light in the red region (640-665 nm), which minimizes the interference with biological cells or tissues and enhances the tissue penetration depth and results in a good contrast suitable for imaging applications.^[22]

A different bioimaging approach is described using self-assembled amphiphilic polyesters (formed by π - π stacking of oligo-phenylenevinylene (OPV) and L-aspartic acid) that form OPV-coated polyester nanocontainers smaller than 200 nm in size. By entrapping Nile Red in their interior, a fluorescence resonance energy transfer (FRET) couple is obtained, *i.e.* the blue luminescence of the nanocage serves as FRET donor, Nile Red as FRET acceptor. Thus, while the nanocontainers are intact FRET occurs. The nanocontainers are taken up by cancer cells through endocytosis, accumulate in the cytoplasm and are degraded in the presence of lysosomal enzymes. This concept not only allows imaging of the cellular uptake but also of its successful degradation and hence removal from the body, which is crucial for biomedical applications.^[23] Another possibility for *in vivo* imaging is the use of fluorescence quenching. Here, *e.g.* polymeric nanocontainers have been applied for the imaging of ATP degradation. The di-block-copolymer used to form the polymersomes gives the vesicles a membrane, which is permeable for small molecules such as ATP. A conjugated polymer served as fluorescent reporter probe and the ATP degrading enzyme alkaline phosphatase was entrapped inside the polymersomes. ATP can passively diffuse through the permeable pores of the membrane and induce conformational changes of the fluorescent probe causing quenching of its emission. The enzymatic ATP degradation can then be quantified by fluorescence recovery of the quenched probe.^[44]

Also the entrapment of upconverting nanoparticles for bioimaging is gaining in interest as they can overcome some of the disadvantages of simple fluorophores. They provide low autofluorescence background, no photobleaching, no phototoxicity, long luminescence lifetime and deep tissue

penetration due to excitation in the NIR region.^[65,78] However, as water quenches the emission of the upconversion nanoparticles, surface design is mandatory which is also needed to obtain colloidal stability under physiological conditions and to provide functional groups for tagging. Here, embedding the particles within shells, nanocontainers, fibers etc. has been suggested.^[47] For example, multifunctional liposomes have been designed by co-loading them with Er^{3+} and Yb^{3+} doped NaGdF_4 upconverting nanoparticles in their aqueous core and the drug doxorubicin (DOX) in their hydrophobic membrane (Figure 1.11). DOX quenches the nanoparticle emission when excited at 980 nm, which allows the monitoring of drug loading and release. This makes them promising candidates for theranostic applications.^[85]

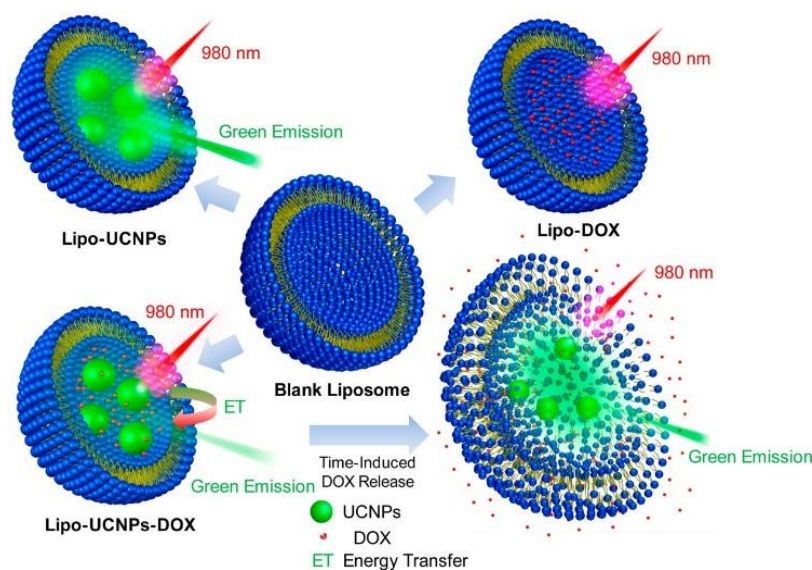


Figure 1.11. Schematic representation showing the structures of the blank liposome, Lipo-UCNPs, Lipo-DOX, and Lipo-UCNPs-DOX. Reprinted from Ref. [85], with permission. Copyright 2016 American Chemical Society.

Similarly, multimodal liposomes for theranostic applications have been designed by the group of Ma *et al.* They synthesized folic acid functionalized liposomes entrapping DOX and conjugated polymer dots simultaneously in the lipid bilayer. The liposomes were specifically taken up by the tumor cells and drug accumulation could be observed enabling cancer diagnosis and drug release at the same time.^[67]

1.5. Conclusion, Future Perspectives and Challenges

Over the course of the last five years a variety of nanocontainers were created, characterized and applied in bioanalysis, in chemosensors, and for *in vitro* and *in vivo* imaging. In all cases, their two distinguishing characteristics of a high functional surface area and often a large inner cavity are exploited for surface functionalization and signal amplification. Thus, limits of detection were demonstrated in many cases competing and outperforming commercially available gold standard detection strategies. Here, mainly liposomes and ferritin nanocages gave excellent results in

heterogeneous assays with detection limits up-to 1000 times lower than those achieved with commercially available ELISAs. In homogeneous assays especially gatekeeper-based approaches with mesoporous silica particles and gold nanocages have been superior, which also outperformed the detection limits of commercially available assays by up to 100 times. However, for many other instances, the use of nanocontainers is not convincing. For example, H₂O₂ sensing using gold nanocage-modified electrodes show no improvement over already implemented sensors based on quite traditional mechanisms, *e.g.* Prussian blue-coated electrodes. In the case of sensing of ions, gases and volatile substances, nanocontainer-based approaches rarely can compete with gold standard analytical techniques such as ICP-OES/MS, GC or GC-MS, which may not be too surprising considering the difference in device complexity employed. A typical example is mercury detection, with a maximum concentration allowed by WHO of 6 ppb,^[112] which can barely be achieved by the nanocontainer-based mercury sensor in this review. Hence, much emphasis should focus in the future on combining these types of sensors as small arrays with appropriate read-out algorithms and artificial intelligence in order to overcome their often inherent non-specific responses and perceived limited sensitivity. Then, detection ranges comparable to spectrophotometry may soon be reached and the device and assay simplicity of the sensing approach can be taken advantage of.

In contrast, nanocontainers developed for imaging are not only very successful but also hold much promise especially in clinical diagnostics and therapy. Multimodal and theranostic strategies can easily be implemented such as for drug delivery and photodynamic therapy, as the nanocontainers can provide imaging through inherent material characteristics and also enable localized treatment through release of drugs or catalysis of reactions on their surface.^[80] The biggest hurdle for nanocontainers here may only be biocompatibility and possible toxicity, which is part of overall toxicological studies on nanomaterials that include not only other types of materials than those used for nanocontainers, but also investigates hazards caused by their production and disposal.

For applications such as point-of-care diagnosis parameters like long-term stability, simple assay setups, short assay times, possible miniaturization and integration into chips play an important role. Many nanocontainer-based bioassays pay attention to these requirements, such as liposome stability of over 1 year by Edwards *et al.*,^[84] yet the practicality of some examples is questionable. Long operation times don't seem feasible for example with marker release via gatekeepers. In other instances, low limits of detection were only achieved through a series of cumbersome assay setups, and compatibility with sample matrices is doubtful and not demonstrated.

Thus, nanocontainers serve an important role in (bio)analytical chemistry and can ameliorate challenging tasks such as those described in biosensors and imaging, however, their usefulness should always be critically assessed to warrant that they only solve a problem and don't create a new one.

Acknowledgements

We would like to thank Vanessa Tomanek for the drawing of the frontispiece and TOC graphic.

References

- [1] Q. Liu, B. J. Boyd, *Analyst* **2013**, *138*, 391.
- [2] A. Gómez-Hens, J. Manuel Fernández-Romero, *TrAC, Trends Anal. Chem.* **2005**, *24*, 9.
- [3] A. Jesorka, O. Orwar, *Annu. Rev. Anal. Chem.* **2008**, *1*, 801.
- [4] K. A. Edwards, A. J. Baeumner, *Talanta* **2006**, *68*, 1421.
- [5] A. Graff, S. M. Benito, C. Verbert, W. Meier, Polymer Nanocontainers in *Nanobiotechnology: Concepts, Applications and Perspectives* (Eds.: C. M. Niemeyer, C. A. Mirkin), Wiley-VCH, Weinheim, **2007**, pp. 168–184.
- [6] A. Feng, J. Yuan, *Macromol. Rapid Commun.* **2014**, *35*, 767.
- [7] B. Bhushan, S. U. Kumar, I. Matai, A. Sachdev, P. Dubey, P. Gopinath, *J. Biomed. Nanotechnol.* **2014**, *10*, 2950.
- [8] A. R. Chandrasekaran, O. Levchenko, *Chem. Mater.* **2016**, *28*, 5569.
- [9] Y. Xia, W. Li, C. M. Cobley, J. Chen, X. Xia, Q. Zhang, M. Yang, E. C. Cho, P. K. Brown, *Acc. Chem. Res.* **2011**, *44*, 914.
- [10] W. Li, X. Wu, N. Han, J. Chen, X. Qian, Y. Deng, W. Tang, Y. Chen, *Sens. Actuators, B* **2016**, *225*, 158.
- [11] J. Bi, H. Wang, T. Kamal, B.-W. Zhu, M. Tan, *RSC Adv.* **2017**, *7*, 30481.
- [12] M. Misson, H. Zhang, B. Jin, *J. R. Soc. Interface* **2015**, *12*, 20140891.
- [13] P. Broz, S. Driamov, J. Ziegler, N. Ben-Haim, S. Marsch, W. Meier, P. Hunziker, *Nano Lett.* **2006**, *6*, 2349.
- [14] K. T. Kim, S. A. Meeuwissen, R. J. M. Nolte, van Hest, Jan C M, *Nanoscale* **2010**, *2*, 844.
- [15] J. Gaitzsch, X. Huang, B. Voit, *Chem. Rev.* **2016**, *116*, 1053.
- [16] J. Li, S. Lu, H. Huang, D. Liu, Z. Zhuang, C. Zhong, *ACS Sustainable Chem. Eng.* **2018**, *6*, 10021.
- [17] a) E. Petala, Y. Georgiou, V. Kostas, K. Dimos, M. A. Karakassides, Y. Deligiannakis, C. Aparicio, J. Tuček, R. Zbořil, *ACS Sustainable Chem. Eng.* **2017**, *5*, 5782; b) S. Dib, M. Boufatit, S. Chelouaou, F. Sadi-Hassaine, J. Croissant, J. Long, L. Raehm, C. Charnay, J.-O. Durand, *RSC Adv.* **2014**, *4*, 24838.

- [18] a) Y. Wang, G. Wang, H. Wang, C. Liang, W. Cai, L. Zhang, *Chem. - Eur. J.* **2010**, *16*, 3497; b) Y. Zhang, S. Xu, Y. Luo, S. Pan, H. Ding, G. Li, *J. Mater. Chem.* **2011**, *21*, 3664.
- [19] a) L. Messenger, J. R. Burns, J. Kim, D. Cecchin, J. Hindley, A. L. B. Pyne, J. Gaitzsch, G. Battaglia, S. Howorka, *Angew. Chem. Int. Ed.* **2016**, *55*, 11106; b) T. Trantidou, M. Friddin, Y. Elani, N. J. Brooks, R. V. Law, J. M. Seddon, O. Ces, *ACS Nano* **2017**, *11*, 6549; c) L. Otrin, N. Marušič, C. Bednarz, T. Vidaković-Koch, I. Lieberwirth, K. Landfester, K. Sundmacher, *Nano Lett.* **2017**, *17*, 6816.
- [20] P. Sahandi Zangabad, M. Karimi, F. Mehdizadeh, H. Malekzad, A. Ghasemi, S. Bahrami, H. Zare, M. Moghoofei, A. Hekmatmanesh, M. R. Hamblin, *Nanoscale* **2017**, *9*, 1356.
- [21] B. Iyisan, J. Kluge, P. Formanek, B. Voit, D. Appelhans, *Chem. Mater.* **2016**, *28*, 1513.
- [22] S. Dong, J. D. W. Teo, L. Y. Chan, C.-L. K. Lee, K. Sou, *ACS Appl. Nano Mater.* **2018**, *1*, 1009.
- [23] S. Saxena, M. Jayakannan, *Biomacromolecules* **2017**, *18*, 2594.
- [24] Z. Qiu, J. Shu, D. Tang, *Anal. Chem.* **2017**, *89*, 5152.
- [25] M. N. Holme, S. Rana, H. M. G. Barriga, U. Kauscher, N. J. Brooks, M. M. Stevens, *ACS Nano* **2018**, *12*, 8197.
- [26] H. Li, Y. Li, S. Wang, *CrystEngComm* **2015**, *17*, 2368.
- [27] W.-T. Koo, S. Yu, S.-J. Choi, J.-S. Jang, J. Y. Cheong, I.-D. Kim, *ACS Appl. Mater. Interfaces* **2017**, *9*, 8201.
- [28] a) F. Sancenón, L. Pascual, M. Oroval, E. Aznar, R. Martínez-Máñez, *ChemistryOpen* **2015**, *4*, 418; b) A. Mirzaei, S. G. Leonardi, G. Neri, *Ceram. Int.* **2016**, *42*, 15119; c) T. Wagner, S. Haffer, C. Weinberger, D. Klaus, M. Tiemann, *Chem. Soc. Rev.* **2013**, *42*, 4036.
- [29] X. Wang, J. Feng, Y. Bai, Q. Zhang, Y. Yin, *Chem. Rev.* **2016**, *116*, 10983.
- [30] Z. Dai, H. Ju, *TrAC, Trends Anal. Chem.* **2012**, *39*, 149.
- [31] Y. Li, J. Shi, *Adv. Mater. (Weinheim, Ger.)* **2014**, *26*, 3176.
- [32] S.-H. Wu, C.-Y. Mou, H.-P. Lin, *Chem. Soc. Rev.* **2013**, *42*, 3862.
- [33] F. Tang, L. Li, D. Chen, *Adv. Mater. (Weinheim, Ger.)* **2012**, *24*, 1504.
- [34] L. Schoonen, van Hest, Jan C M, *Nanoscale* **2014**, *6*, 7124.
- [35] M. Marguet, C. Bonduelle, S. Lecommandoux, *Chem. Soc. Rev.* **2013**, *42*, 512.
- [36] A. B. T. Ghisaidoobe, S. J. Chung, *Nanomedicine (London, U. K.)* **2015**, *10*, 3579.

- [37] M. Mayer, S. Takegami, M. Neumeier, S. Rink, A. Jacobi von Wangelin, S. Schulte, M. Vollmer, A. G. Griesbeck, A. Duerkop, A. J. Baeumner, *Angew. Chem. Int. Ed.* **2018**, *57*, 408.
- [38] K. A. Edwards, A. J. Baeumner, *Anal. Chem.* **2014**, *86*, 6610.
- [39] L.-P. Mei, X.-Y. Jiang, X.-D. Yu, W.-W. Zhao, J.-J. Xu, H.-Y. Chen, *Anal. Chem.* **2018**, *90*, 2749.
- [40] L. Tao, C. Zhang, J. Zhang, Y. Sun, X. Li, K. Yan, B. Jin, Z. Zhang, K. Yang, *Microchim. Acta* **2016**, *183*, 2163.
- [41] H. Ma, Y. Wang, D. Wu, Y. Zhang, J. Gao, X. Ren, B. Du, Q. Wei, *Sci. Rep.* **2016**, *6*, 19797.
- [42] D. Tang, Y. Lin, Q. Zhou, Y. Lin, P. Li, R. Niessner, D. Knopp, *Anal. Chem.* **2014**, *86*, 11451.
- [43] X. Yang, A. Wang, J. Liu, *Talanta* **2013**, *114*, 5.
- [44] U. H. Yildiz, H.-P. M. de Hoog, Z. Fu, N. Tomczak, A. N. Parikh, M. Nallani, B. Liedberg, *Small* **2014**, *10*, 442-7, 441.
- [45] S. Haas, N. Hain, M. Raoufi, S. Handschuh-Wang, T. Wang, X. Jiang, H. Schönherr, *Biomacromolecules* **2015**, *16*, 832.
- [46] B. Kulkarni, M. Jayakannan, *ACS Biomater. Sci. Eng.* **2017**, *3*, 2185.
- [47] U. Bazylińska, D. Wawrzyńczyk, J. Kulbacka, R. Frąckowiak, B. Cichy, A. Bednarkiewicz, M. Samoć, K. A. Wilk, *Sci. Rep.* **2016**, *6*, 29746.
- [48] W. C. de Vries, D. Grill, M. Tesch, A. Ricker, H. Nüsse, J. Klingauf, A. Studer, V. Gerke, B. J. Ravoo, *Angew. Chem. Int. Ed.* **2017**, *56*, 1.
- [49] X. Ge, A. Zhang, Y. Lin, D. Du, *Biosens. Bioelectron.* **2016**, *80*, 201.
- [50] a) A. Chen, Y. Bao, X. Ge, Y. Shin, D. Du, Y. Lin, *RSC Adv.* **2012**, *2*, 11029; b) N. Liao, Y. Zhuo, Y. Chai, Y. Xiang, Y. Cao, R. Yuan, J. Han, *Chem. Commun. (Cambridge, U. K.)* **2012**, *48*, 7610; c) S. Kashanian, F. Abasi Tarighat, R. Rafipour, M. Abbasi-Tarighat, *Mol. Biol. Rep.* **2012**, *39*, 8793.
- [51] X. Wang, L. Chen, X. Su, S. Ai, *Biosens. Bioelectron.* **2013**, *47*, 171.
- [52] A. Abbaspour, A. Noori, *Biosens. Bioelectron.* **2012**, *37*, 11.
- [53] J. P. Laulhere, A. M. Lescure, Briat J F, *J. Biol. Chem.* **1988**, *263*, 10289.
- [54] C. Gao, M. Su, Y. Wang, S. Ge, J. Yu, *RSC Adv.* **2015**, *5*, 28324.
- [55] W. Wang, C. Chen, X. Li, S. Wang, X. Luo, *Chem. Commun. (Cambridge, U. K.)* **2015**, *51*, 9109.

- [56] A. Vinu, M. Miyahara, V. Sivamurugan, T. Mori, K. Ariga, *J. Mater. Chem.* **2005**, *15*, 5122.
- [57] H. Zhang, O. Noonan, X. Huang, Y. Yang, C. Xu, L. Zhou, C. Yu, *ACS Nano* **2016**, *10*, 4579.
- [58] Y. Kosaki, H. Izawa, S. Ishihara, K. Kawakami, M. Sumita, Y. Tateyama, Q. Ji, V. Krishnan, S. Hishita, Y. Yamauchi *et al.*, *ACS Appl. Mater. Interfaces* **2013**, *5*, 2930.
- [59] H. Zhang, M. Yu, H. Song, O. Noonan, J. Zhang, Y. Yang, L. Zhou, C. Yu, *Chem. Mater.* **2015**, *27*, 6297.
- [60] F. Qu, B. Zhang, X. Zhou, H. Jiang, C. Wang, X. Feng, C. Jiang, M. Yang, *Sens. Actuators, B* **2017**, *252*, 649.
- [61] X. Wang, S. Zhang, M. Shao, J. Huang, X. Deng, P. Hou, X. Xu, *Sens. Actuators, B* **2017**, *251*, 27.
- [62] F. Qu, H. Jiang, M. Yang, *Nanoscale* **2016**, *8*, 16349.
- [63] L. Qiao, Y. Bing, Y. Wang, S. Yu, Z. Liang, Y. Zeng, *Sens. Actuators, B* **2017**, *241*, 1121.
- [64] a) W. Zhao, T. M. H. Lee, S. S. Y. Leung, I.-M. Hsing, *Langmuir* **2007**, *23*, 7143; b) A. P. Stevenson, D. Blanco Bea, S. Civit, S. Antoranz Contera, A. Iglesias Cerveto, S. Trigueros, *Nanoscale Res. Lett.* **2012**, *7*, 151; c) D. J. A. Crommelin, van Bommel, E. M. G., *Pharm. Res.* **1984**, *1*, 159; d) B. S. Pattni, V. V. Chupin, V. P. Torchilin, *Chem. Rev.* **2015**, *115*, 10938.
- [65] V. Muhr, S. Wilhelm, T. Hirsch, O. S. Wolfbeis, *Acc. Chem. Res.* **2014**, *47*, 3481.
- [66] L.-P. Mei, F. Liu, J.-B. Pan, W.-W. Zhao, J.-J. Xu, H.-Y. Chen, *Anal. Chem.* **2017**, *89*, 6300.
- [67] M. Ma, M. Lei, X. Tan, F. Tan, N. Li, *RSC Adv.* **2016**, *6*, 1945.
- [68] G. Chen, I. Roy, C. Yang, P. N. Prasad, *Chem. Rev.* **2016**, *116*, 2826.
- [69] À. Ribes, S. Santiago-Felipe, A. Bernardos, M. D. Marcos, T. Pardo, F. Sancenón, R. Martínez-Mañez, E. Aznar, *ChemistryOpen* **2017**, *6*, 653.
- [70] X. Yang, F. Pu, C. Chen, J. Ren, X. Qu, *Chem. Commun. (Cambridge, U. K.)* **2012**, *48*, 11133.
- [71] M. Chen, C. Huang, C. He, W. Zhu, Y. Xu, Y. Lu, *Chem. Commun. (Cambridge, U. K.)* **2012**, *48*, 9522.
- [72] X. Mao, P. Yuan, C. Yu, L. Li, S. Q. Yao, *Angew. Chem. Int. Ed.* **2018**, *130*, 10414.
- [73] B. Zhang, B. Liu, J. Liao, G. Chen, D. Tang, *Anal. Chem.* **2013**, *85*, 9245.
- [74] Z. Gao, D. Tang, M. Xu, G. Chen, H. Yang, *Chem. Commun. (Cambridge, U. K.)* **2014**, *50*, 6256.

- [75] M. Holzinger, A. Le Goff, S. Cosnier, *Front. Chem.* **2014**, *2*, 63.
- [76] F. Mazur, M. Bally, B. Städler, R. Chandrawati, *Adv. Colloid Interface Sci.* **2017**, *249*, 88.
- [77] a) R. Weissleder, U. Mahmood, *Radiology* **2001**, *219*, 316; b) T. Yamaoka, Bioimaging Materials in *Encyclopedia of Polymeric Nanomaterials* (Eds.: S. Kobayashi, K. Müllen), Springer Berlin Heidelberg, Berlin, Heidelberg, **2016**, pp. 1–6.
- [78] Q. Le Trequesser, H. Seznec, M.-H. Delville, *Nanotechnol. Rev.* **2013**, *2*, 125.
- [79] L. Dai, Q. Zhang, J. Li, X. Shen, C. Mu, K. Cai, *ACS Appl. Mater. Interfaces* **2015**, *7*, 7357.
- [80] J. Jia, Y. Zhang, M. Zheng, C. Shan, H. Yan, W. Wu, X. Gao, B. Cheng, W. Liu, Y. Tang, *Inorg. Chem.* **2018**, *57*, 300.
- [81] J.-Q. Liu, G.-P. Li, W.-C. Liu, Q.-L. Li, B.-H. Li, R. W. Gable, L. Hou, S. R. Batten, *ChemPlusChem* **2016**, *81*, 1299.
- [82] D. Huang, T. Hu, N. Chen, W. Zhang, J. Di, *Anal. Chim. Acta* **2014**, *825*, 51.
- [83] K. A. Edwards, W. J. Seog, L. Han, S. Feder, C. E. Kraft, A. J. Baeumner, *Anal. Chem.* **2016**, *88*, 8248.
- [84] K. A. Edwards, K. J. Meyers, B. Leonard, A. J. Baeumner, *Anal. Bioanal. Chem.* **2013**, *405*, 4017.
- [85] Y. Huang, E. Hemmer, F. Rosei, F. Vetrone, *J. Phys. Chem. B* **2016**, *120*, 4992.
- [86] C. Jumeaux, O. Wahlsten, S. Block, E. Kim, R. Chandrawati, P. D. Howes, F. Höök, M. M. Stevens, *ChemBiochem* **2018**, *19*, 434.
- [87] Y. Lin, Q. Zhou, D. Tang, *Anal. Chem.* **2017**, *89*, 11803.
- [88] A. Müller, B. König, *Org. Biomol. Chem.* **2015**, *13*, 1690.
- [89] Z. Kahveci, M. J. Martínez-Tomé, R. Mallavia, C. R. Mateo, *ACS Appl. Mater. Interfaces* **2017**, *9*, 136.
- [90] D. Tang, B. Liu, R. Niessner, P. Li, D. Knopp, *Anal. Chem.* **2013**, *85*, 10589.
- [91] Z. Liu, P. Rong, L. Yu, X. Zhang, C. Yang, F. Guo, Y. Zhao, K. Zhou, W. Wang, W. Zeng, *Mol. Pharm.* **2015**, *12*, 3119.
- [92] Y. Wang, H. Shi, K. Cui, L. Zhang, S. Ge, M. Yan, J. Yu, *Biosens. Bioelectron.* **2018**, *117*, 515.
- [93] À. Ribes, E. Aznar, A. Bernardos, M. D. Marcos, P. Amorós, R. Martínez-Mañez, F. Sancenón, *Chem. - Eur. J.* **2017**, *23*, 8581.

- [94] E. Climent, L. Mondragón, R. Martínez-Máñez, F. Sancenón, M. D. Marcos, J. R. Murguía, P. Amorós, K. Rurack, E. Pérez-Payá, *Angew. Chem. Int. Ed.* **2013**, *52*, 8938.
- [95] E. Climent, M. Biyikal, K. Gawlitza, T. Dropa, M. Urban, A. M. Costero, R. Martínez-Máñez, K. Rurack, *Sens. Actuators, B* **2017**, *246*, 1056.
- [96] H. Kim, B. A. Rao, J. Jeong, S. Angupillai, J. S. Choi, J.-O. Nam, C.-S. Lee, Y.-A. Son, *Sens. Actuators, B* **2016**, *224*, 404.
- [97] Y. Zhang, Y. Sun, Z. Liu, F. Xu, K. Cui, Y. Shi, Z. Wen, Z. Li, *J. Electroanal. Chem.* **2011**, *656*, 23.
- [98] J. Park, S. K. Ku, D. Seo, K. Hur, H. Jeon, D. Shvartsman, H.-K. Seok, D. J. Mooney, K. Lee, *Chem. Commun. (Cambridge, U. K.)* **2016**, *52*, 10346.
- [99] J. U. Lee, J. H. Jeong, D. S. Lee, S. J. Sim, *Biosens. Bioelectron.* **2014**, *61*, 314.
- [100] D.-E. Wang, L. Zhao, M.-S. Yuan, S.-W. Chen, T. Li, J. Wang, *ACS Appl. Mater. Interfaces* **2016**, *8*, 28231.
- [101] T. Huang, Z. Hou, Q. Xu, L. Huang, C. Li, Y. Zhou, *Langmuir* **2017**, *33*, 340.
- [102] M. X. L. Tan, M. K. Danquah, *Chem. Eng. Technol.* **2012**, *35*, 618.
- [103] a) I. Petrikovics, K. Hong, G. Omburo, Q. Z. Hu, L. Pei, W. D. McGuinn, D. Sylvester, C. Tamulinas, D. Papahadjopoulos, J. C. Jaszberenyi *et al.*, *Toxicol. Appl. Pharmacol.* **1999**, *156*, 56; b) D. Brady, J. Jordaan, *Biotechnol. Lett.* **2009**, *31*, 1639.
- [104] H. Xing, C. L. Zhang, G. Ruan, J. Zhang, K. Hwang, Y. Lu, *Anal. Chem.* **2016**, *88*, 1506.
- [105] E. Aznar, M. Oroval, L. Pascual, J. R. Murguía, R. Martínez-Máñez, F. Sancenón, *Chem. Rev.* **2016**, *116*, 561.
- [106] W.-W. Zhao, J.-J. Xu, H.-Y. Chen, *Chem. Soc. Rev.* **2015**, *44*, 729.
- [107] J.-M. Liu, X.-P. Yan, *Biosens. Bioelectron.* **2012**, *36*, 135.
- [108] S. Sharma, M. Madou, *Philos. Trans. R. Soc. A* **2012**, *370*, 2448.
- [109] B. T. P. Quynh, J. Y. Byun, S. H. Kim, *Sens. Actuators, B* **2014**, *193*, 1.
- [110] J. Zhang, F. Cheng, J. Li, J.-J. Zhu, Y. Lu, *Nano Today* **2016**, *11*, 309.
- [111] M. P. O'Halloran, M. Pravda, G. G. Guilbault, *Talanta* **2001**, *55*, 605.
- [112] Z. Abrego, N. Unceta, A. Sánchez, A. Gómez-Caballero, L. M. Berrio-Ochoa, M. Aranzazu Goicolea, R. J. Barrio, *Analyst* **2017**, *142*, 1157.

2 Introduction and Structure of the Thesis

This thesis focuses on the preparation, the controlled surface design and characterization of colloiddally stable liposomes to serve as analytical tools such as for signal enhancement for the detection of bacteria or for the preconcentration of DNA.

The contamination of food or drinking water by pathogens or hazardous substances like heavy metal ions can cause serious diseases or even death.^[4,5] Therefore, the fast and early detection of such hazards is very important. Various (bio)analytical assays and sensors have for example been developed to solve this problem.^[5] To achieve the required sensitivity of such tests mostly signal enhancement is necessary. Common strategies include amplification via enzymes or PCR, which already find their application in clinical diagnosis or point-of-care devices.^[3,6] In the last years also the use of nanomaterials has become more interesting as they often provide an excellent sensitivity.^[1] The use of gold or polymer (nano)particles is for example well established for the development of lateral flow-based devices,^[2] but also other nanomaterials like quantum dots or up-converting phosphor have been successfully applied as optical labels.^[3] Among the various types of nanomaterials, nanocontainers have been shown to be ideal signal amplification tools. Here, signal enhancement is usually achieved by the entrapment of a large number of signaling molecules in their hollow interior or pores. **Chapter 1** gives an overview of the most important nanocontainers and their applications in (bio)assays, chemosensors and *in vitro* and *in vivo* imaging and provides a critical discussion of the different applications, challenges and restrictions regarding the nanocontainer-based analytical assays. Liposomes combine all the features of nanocontainers that are relevant for (bio)analytical applications, such as their relatively simple preparation and surface functionalization, their large inner cavity and variety of possible entrapped molecules, short assay response times due to an efficient lysis of the membrane as well as their natural biocompatibility.

Liposomes were discovered by Bangham *et al.* in 1964 and originally used as models for biological membranes.^[16] These artificial spherical vesicles consist of a lipid bilayer that is formed by the hydrophobic tails of the lipids while the polar headgroups are pointing towards the big hydrophilic inner cavity and the extraventricular solution.^[7,8] Liposomes can be composed of a variety of lipids. However, often phospholipids build the main component.^[8] Phospholipids are available with different chain lengths and polar headgroups.^[9,10] While chain length and the degree of saturation influence the phase transition temperature of the lipids and thus also the characteristics of the vesicle membrane, the polar headgroups are responsible for the stability of the vesicle dispersions in aqueous solutions or provide functionalities for the attachment of surface modifications.^[9] Charged headgroups improve

e.g. the colloidal stability due to electrostatic repulsion between the liposomes.^[11] Cholesterol is also a common component of the lipid bilayer and reduces the permeability of the membrane and thus leakage of molecules that can be entrapped inside the big, hydrophilic inner cavity of the liposomes.^[12] At the same time it increases the headgroup spacing between charged lipids and therefore the membrane stability due to a reduced repulsion between the lipids.^[13] Molecules that can be entrapped inside the inner cavity of the liposomes are salts or dyes, biomolecules like enzymes or DNA but also nanoparticles or drugs.^[8] The ability of liposomes to encapsulate molecules in their interior has made them a versatile tool for a variety of applications, *e.g.* in the cosmetic industry,^[14] for therapeutic or diagnostic applications,^[15] as delivery vehicles for vaccines and drugs, in gene therapy^[17] or in the field of (bio)analytical assays.^[8,18]

For most applications like targeted delivery to specific cells or tissues not only the entrapment of molecules is important but also the functionalization of the vesicles surface with specific recognition elements. Receptors on the vesicle surface not only allow for targeted drug delivery but also for specific binding to surfaces or analytes, which is crucial for most (bio)analytical tests. Surface functionalization can be achieved by several methods. The challenges and limitations of the different standard techniques, which are based on the incorporation of functionalized lipids during synthesis or on post-modifications via covalent coupling, are discussed in **Chapter 3**. In this chapter also an alternative method is developed for the modification of liposomes based on the insertion of a biotinylated lipopeptide into preformed vesicles. The method was optimized with respect to incubation parameters like time and temperature and in view of the vesicle stability regarding dye leakage and the loss of membrane material. Size, ζ -potential and binding functionality of the obtained vesicles were directly compared to standard modified liposomes and proved the superior performance of liposomes prepared via insertion of the lipopeptide. Functionalization of the vesicle surface is not limited to biotin as applied in **Chapter 3**. A variety of molecules can serve as receptors, *e.g.* enzymes, antibodies or ssDNA (**Chapter 4**).^[8]

A common application of DNA-functionalized vesicles is their use in sandwich hybridization assays,^[19] where *e.g.* the analyte *C.parvum* could be detected down to 3.2 pM.^[20] The sensitive detection can be ascribed to the large amount of marker molecules that can be entrapped in the vesicle interior.^[8] However, before applying such vesicles to analytical problems, a detailed characterization of the vesicles and their surface functionalization is crucial. For the characterization of the standard parameters such as vesicle size, ζ -potential or the phospholipid concentration well-established methods exist, *e.g.* dynamic light scattering, the Bartlett assay or ICP-based methods.^[21,22] In **Chapter 4** the vesicles are not only characterized by these standard methods. This chapter also provides an insight into several possibilities for the optical characterization of DNA-tagged liposomes ranging from

simple fluorescence measurements to fluorescence correlation spectroscopy and imaging techniques. Thereby, also information on the particle number, DNA surface coverage and functionality of the vesicles can be obtained.

The surface of liposomes cannot only be tuned via ligands and receptors but also by the surface charge.^[10] In bioanalysis mostly anionic liposomes are applied as they prevent non-specific binding to most surfaces and analytes.^[22] However, by introduction of positively charged lipids or amphiphiles into the lipid bilayer also the preparation of cationic liposomes is possible.^[23] These have been widely applied to form lipoplexes with DNA which renders them suitable *e.g.* for gene delivery.^[24] Their application in bioanalysis has seldomly been reported as the positive surface charge causes interference with most biological molecules. However, this can also be exploited to create very simple assays based on electrostatic interactions as for example for the detection of bacteria as in case of chitosan-coated Fe₃O₄ particles in combination with a magnetoelastic sensor^[25] or in case of PDA vesicles.^[26] **Chapter 5** discusses the preparation of cationic liposomes and how their electrostatic properties can be exploited for the detection of bacteria cells with *E.coli* as model analyte. The liposomes were loaded either with sulforhodamine B or *m*-carboxy-luminol to enable the analysis via fluorescence or chemiluminescence, respectively. Different lipid compositions, assay setups and readout mechanisms were investigated and optimized and the capability of these cationic liposomes to serve as analytical tool for the detection of bacteria was critically discussed with respect to remaining challenges and limitations.

Besides their use in bioanalysis the electrostatic interactions of nanovesicles or -particles have also been reported for other applications. For example, the bactericidal action of some nanomaterials can be ascribed to electrostatic interactions such as in case of some cationic liposomes or chitosan nanoparticles.^[27] Moreover, the electrostatic interactions can be used for the assembly of building blocks based for the formation of peptide- or protein-based nanomaterials^[28] or for the attachment of surface coatings or gatekeepers to nanoparticles.^[29] A very popular application is the use of DNA for the attachment to liposomes. Due to the negative charge of the phosphate backbone of DNA, cationic liposomes can electrostatically bind to the DNA molecules which has been widely applied in gene therapy.^[17] However, also other applications can be envisioned such as the extraction, purification and preconcentration of DNA which is necessary in several cases to enable a reliable analysis, *e.g.* via PCR which has a low tolerance towards impurities.^[30] This is often achieved via alcohol precipitation or magnetic beads which suffer from drawbacks like the need for organic solvents or chaotropic salts.^[30,31] In **Chapter 6** a fast and simple method for the preconcentration of DNA has been developed which is based on the use of cationic liposomes. The method was optimized and critically discussed regarding

the influences caused by the incubation time, temperature, centrifugation speed and liposome concentration and remaining challenges were addressed.

Finally, the main results and insights of this thesis are discussed in **Chapter 7** with respect to the advantages and disadvantages of liposomes and the influence of the vesicle surface design on applications in the field of bioanalysis. Moreover, this chapter addresses the challenges and future perspectives of applications of liposomes within this field.

References

- [1] J. Wang, *Biosens. Bioelectron.* **2006**, *21*, 1887.
- [2] V. Gubala, L. F. Harris, A. J. Ricco, M. X. Tan, D. E. Williams, *Anal. Chem.* **2012**, *84*, 487.
- [3] F. B. Myers, L. P. Lee, *Lab Chip* **2008**, *8*, 2015.
- [4] a) G. Tóth, T. Hermann, M. R. Da Silva, L. Montanarella, *Environ. Int.* **2016**, *88*, 299; b) P. K. Pandey, P. H. Kass, M. L. Soupir, S. Biswas, V. P. Singh, *AMB Express* **2014**, *4*, 51.
- [5] J. T. Connelly, A. J. Baeumner, *Anal. Bioanal. Chem.* **2012**, *402*, 117.
- [6] a) R. M. Lequin, *Clin. Chem.* **2005**, *51*, 2415; b) P. Miao, Y. Tang, B. Wang, J. Yin, L. Ning, *Trends Anal. Chem.* **2015**, *67*, 1.
- [7] A. Jesorka, O. Orwar, *Annu. Rev. Anal. Chem.* **2008**, *1*, 801.
- [8] Q. Liu, B. J. Boyd, *Analyst* **2013**, *138*, 391.
- [9] J. M. Zook, W. N. Vreeland, *Soft Matter* **2010**, *6*, 1352.
- [10] P. P. Karmali, A. Chaudhuri, *Med. Res. Rev.* **2007**, *27*, 696.
- [11] M. Grit, D. J.A. Crommelin, *Chem. Phys. Lipids* **1993**, *64*, 3.
- [12] a) A. Laouini, C. Jaafar-Maalej, I. Limayem-Blouza, S. Sfar, C. Charcosset, H. Fessi, *J. Coll. Sci. Biotechnol.* **2012**, *1*, 147; b) H. Ohvo-Rekilä, *Prog. Lipid Res.* **2002**, *41*, 66.
- [13] S. Bhattacharya, S. Haldar, *Biochim. Biophys. Acta* **2000**, *1467*, 39.
- [14] H.A.H. Rongen, A. Bult, W.P. van Bennekom, *J. Immunol. Methods* **1997**, *204*, 105.
- [15] N. Kamaly, A. D. Miller, *Int. J. Mol. Sci.* **2010**, *11*, 1759.
- [16] a) A. D. Bangham, M. W. Hill, N. G. A. Miller, "Preparation and Use of Liposomes as Models of Biological Membranes" in *Methods in Membrane Biology* (Ed.: E. D. Korn), Springer, Boston, MA, **1974**, pp. 1–68; b) A. D. Bangham, R. W. Horne, *J. Mol. Biol.* **1964**, *8*, 660–668.

- [17] A. Akbarzadeh, R. Rezaei-Sadabady, S. Davaran, S. W. Joo, N. Zarghami, Y. Hanifehpour, M. Samiei, M. Kouhi, K. Nejati-Koshki, *Nanoscale Res. Lett.* **2013**, *8*, 102.
- [18] K. A. Edwards, A. J. Baeumner, *Talanta* **2006**, *68*, 1421.
- [19] K. A. Edwards, A. J. Baeumner, *Anal. Chem.* **2014**, *86*, 6610.
- [20] M. Mayer, S. Takegami, M. Neumeier, S. Rink, A. Jacobi von Wangelin, S. Schulte, M. Vollmer, A. G. Griesbeck, A. Duerkop, A. J. Baeumner, *Angew. Chem. Int. Ed. Engl.* **2018**, *57*, 408.
- [21] K. A. Edwards, A. J. Baeumner, *Talanta* **2006**, *68*, 1432.
- [22] C. Fenzl, C. Genslein, C. Domonkos, K. A. Edwards, T. Hirsch, A. J. Baeumner, *Analyst* **2016**, *141*, 5265.
- [23] a) R. C. MacDonald, G. W. Ashley, M. M. Shida, V. A. Rakhmanova, Y. S. Tarahovsky, D. P. Pantazatos, M. T. Kennedy, E. V. Pozharski, K. A. Baker, R. D. Jones *et al.*, *Biophys. J.* **1999**, *77*, 2612; b) C. Montis, S. Sostegni, S. Milani, P. Baglioni, D. Berti, *Soft Matter* **2014**, *10*, 4287.
- [24] a) G. Caracciolo, H. Amenitsch, *Eur. Biophys. J.* **2012**, *41*, 815; b) C. R. Safinya, K. K. Ewert, R. N. Majzoub, C. Leal, *New journal of chemistry = Nouveau journal de chimie* **2014**, *38*, 5164.
- [25] H. Lin, Q. Lu, S. Ge, Q. Cai, C. A. Grimes, *Sens. Actuators, B* **2010**, *147*, 343.
- [26] J. Park, S. K. Ku, D. Seo, K. Hur, H. Jeon, D. Shvartsman, H.-K. Seok, D. J. Mooney, K. Lee, *Chem. Commun.* **2016**, *52*, 10346.
- [27] a) A. Shrestha, A. Kishen, *J. Endod.* **2016**, *42*, 1417; b) M. T. Campanhã, E. M. Mamizuka, A. M. Carmona-Ribeiro, *J. Lipid Res.* **1999**, *40*, 1495.
- [28] a) L. Miao, Q. Fan, L. Zhao, Q. Qiao, X. Zhang, C. Hou, J. Xu, Q. Luo, J. Liu, *Chem. Commun.* **2016**, *52*, 4092; b) M. Abbas, Q. Zou, S. Li, X. Yan, *Adv. Mater.* **2017**, *29*.
- [29] a) A. Sedlmeier, H. H. Gorris, *Chem. Soc. Rev.* **2015**, *44*, 1526; b) D. Tang, Y. Lin, Q. Zhou, Y. Lin, P. Li, R. Niessner, D. Knopp, *Anal. Chem.* **2014**, *86*, 11451.
- [30] T. Demeke, G. R. Jenkins, *Anal. Bioanal. Chem.* **2010**, *396*, 1977.
- [31] a) J. Prodělalová, B. Rittich, A. Španová, K. Petrová, M. J. Beneš, *J. Chromatogr. A* **2004**, *1056*, 43; b) L. Griffiths, D. Chacon-Cortes, *J. Biorepos. Sci. Appl. Med.* **2014**, *1*.

3 Tethering Functionality to Lipid Interfaces by a Fast, Simple and Controllable Post Synthesis Method

Abstract

Hypothesis: Liposomes require careful control of the surface design to ensure colloidal stability in complex matrices and target-specific binding to desired receptor units. Ideally, surface functionalization should be smart and controllable in terms of composition which is seldomly achieved by conventional methods. Therefore, a new strategy (insertion method) was developed and compared to the standard method (modification post-synthesis) using the model receptor biotin.

Experiments: Dipalmitoylphosphatidylethanolamine-biotin (DPPE-biotin) was used in both procedures, lipopeptide-biotin and cholesterol-biotin were tested additionally for insertion into the intact lipid bilayer. The insertion method was optimized regarding incubation time, temperature and vesicle stability. The biotinylated vesicles of both functionalization methods were characterized with respect to their size, ζ -potential and binding functionality.

Findings: Standard incorporation resulted in large variations in insertion-efficiency, high batch-to-batch differences, and an incorporation limit of 4 mol%. Best results were obtained through effortless insertion of the lipopeptide-biotin at room temperature. The concentration-controlled functionalization of liposomes (up to 10 mol%) could easily be monitored by the ζ -potential, resulted in reliable, quantitative binding to streptavidin and did not affect the analytical properties of the nanomaterial. This offers the possibility for a general modification strategy for lipid-based nanomaterials ideal for assay optimizations or multi-analyte detection

This chapter has been published.

C. Hofmann, G. Roth, T. Hirsch, A. Duerkop, A. J. Baeumner, *Colloids Surf., B* **2019**, *181*, 325-332, 10.1016/j.colsurfb.2019.05.049.

Author contributions:

The experimental work was carried out by CH. GR provided the lipopeptide-biotin. TH, AD and AJB contributed with strategic discussions. The manuscript was written by CH and revised by GR, TH, AD and AJB. AJB is corresponding author.

This chapter contains paragraphs that were in part already described in Carola Figalist's master's thesis. This includes paragraphs within the introduction or the experimental part regarding the liposome preparation and characterization. The master's thesis is entitled "Positively Charged Liposomes for Signal Enhancement via Electrostatic Interactions" and was submitted to the Faculty of Chemistry and Pharmacy at the University of Regensburg in December 2014. Sections that are identical or similar to the master's thesis are listed here in detail and are indicated in this chapter by the citation "M":

- p.56, subchapter 3.1., sentence 2 (introduction)
- p.60, subchapter 3.2.2.1.1. (experimental)
- p.61, subchapter 3.2.2.2., 3.2.2.2.1., 3.2.2.2.2. (experimental)

3.1. Introduction

Liposomes are membrane-based nanovesicles that can be used as model membranes for studying membrane interactions, or are applied as nanoreactors or functional components in medicine for therapeutic and diagnostic reasons, such as in delivery systems for drugs or vaccines, gene therapy or diagnostic imaging.^[1,2] They are commonly used in the cosmetic industry^[3] and are also well-established in the field of bioanalytical assays.^[4,M] All of these different application areas take benefit of the ability to encapsulate molecules within the aqueous cavity formed by a lipid bilayer membrane which can be varied in composition and functionalities. Liposome synthesis protocols can be optimized to entrap a variety of marker or drug molecules with high yield^[5] and their membrane surface can be modified to bear *e.g.* specific lipids, receptors, markers or recognition molecules to ensure specific binding and targeting capabilities. This surface modification is then exploited for specific targeting as in drug delivery^[6] and *in vivo* medical diagnostics^[7] as well as for specific analyte binding in bioanalytical assays.^[8]

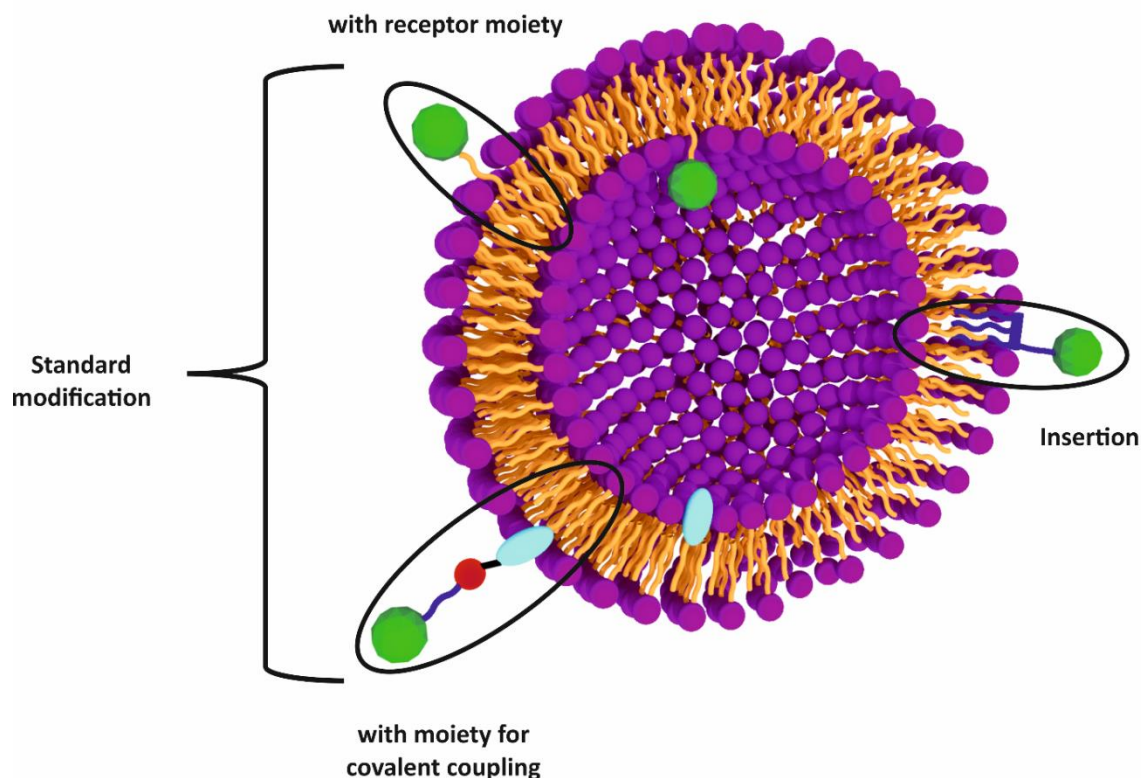
In these cases, the membrane surface becomes a critical feature of each liposome as it not only needs to afford specific binding or targeting but also needs to render liposomes colloidal stability over a long period of time in various buffer systems. In order to obtain stable liposome dispersions, the vesicle membranes are usually composed of a mixture of lipids. Charged phospholipids are for example applied to increase the colloidal stability by electrostatic repulsion of the vesicles.^[9] The addition of cholesterol favors the stability of the liposomal membrane by decreasing the membrane permeability which prevents leakage of entrapped molecules.^[10] PEGylation of liposomes, which finds its application mainly in drug delivery due to its ability to increase their blood circulation time, also leads to a higher steric stabilization.^[11] Nevertheless, it is challenging to find the ideal composition to control non-specific binding, spontaneous fusion or cellular uptake of liposomes. Thus, the interplay of the

membrane lipid composition and modification with specific recognition molecules require special attention in the design and synthesis of liposomes.

For the use of functionalized liposomes in classical bioassays, as *e.g.* described for microtiter plates,^[12] microfluidic lab on chip systems^[13] or lateral flow assays,^[14] two standard methods have mostly been reported; (i) direct modification during synthesis (Scheme 3.1, standard method with receptor moiety) using receptor modified lipids like biotinylated phospholipids,^[15] DNA-probes with cholesterol tags,^[12] gangliosides,^[16] or dye-coupled phospholipids^[17] or (ii) post modifications by covalent coupling. In the first case, the main advantage is the formation of a large amount of readily functionalized liposomes without the need for further coupling reactions and purification steps. This is very beneficial when liposomes and their surface tags have been optimized and are used in larger quantities for assay development or performance. This method is very cumbersome and wasteful when different tags and different tag concentrations are being studied. Furthermore, variations between liposome lots like the efficiency of the incorporation of receptor tags or signaling molecules may overlay effects caused by variations to the modification itself. In the case of post modifications by covalent coupling commonly lipids with functionalized headgroups like phosphatidylethanolamines, N-glutaryl-PE or cholesterol are added to the initial lipid composition during synthesis (Scheme 3.1, standard method with coupling moiety).^[18,19] Subsequently, these are used for conjugation to a desired biorecognition element, hapten or functional moiety. However, post-modifications via covalent coupling often suffer from low coupling yields, can cause leakage of entrapped marker molecules and require additional separation from by-products and blocking steps to cover remaining active groups on the vesicle surface. In general, both standard methods yield a large number of liposomes readily available for many applications but suffer from distinct disadvantages that cannot always be compensated for. Specifically, the preparations are time-consuming and require elevated temperatures during liposome formation. This renders these methods unsuitable for fragile functional moieties. Furthermore, preparations are accompanied by a loss of material during the many synthesis and purification steps as well as the loss of half of the functional moieties due to decoration of the outer and inner layer of the liposome membrane.

A third method for liposome surface modification takes advantage of the insertion ability of certain molecules into the membranes of liposomes (Scheme 3.1, insertion). This method is especially interesting as only the outer leaflet is functionalized without the need for chemical coupling reactions. Therefore, side reactions like crosslinking are avoided and no by-products are formed which enables easy purification. Also, insertion lends itself very well to optimization procedures as many different modifications of liposomes from the same synthesis batch can be studied. The main challenge here is to find amphiphilic molecules consisting of a hydrophobic part which efficiently inserts into the

Scheme 3.1. Overview of different methods for the surface modification of liposomes. Standard modification either by incorporation of receptor modified phospholipids (method 1; e.g. biotin, green) or by phospholipids with functional moieties for covalent coupling (method 2; e.g. carboxyl groups, light blue). The statistical coverage of the inner liposome surface is also indicated for method 1 and 2. Method 3: Modification via insertion of functionalized amphiphilic molecules (e.g. biotin-lipopeptide) which exclusively covers the outside surface of the liposome.



membrane and a hydrophilic part which renders them water soluble to preserve the preformed liposomes from being ruptured during insertion. Successful strategies for this insertion-method have used modified fatty acids,^[20] distearoylphosphoethanolamine (DSPE)-derivatives,^[21] and pH-low insertion peptides^[22] or self-designed peptides.^[23] However, a common problem reported with the use of peptides for insertion-based modification of liposomes is a resulting fusion of the vesicles.

Another interesting class of molecules are therefore lipopeptides that show the ability to successfully insert into phospholipid membranes.^[24] According to the group of Lin and Grossfield, who investigated the mechanism and thermodynamics of some lipopeptides, the fatty acid part is mainly responsible for the interaction with membranes.^[25] Steinhäuser *et al.* used this effect of Lipobiotin and a Pam3Cys-biotin for the successful labeling of gram-positive and gram-negative bacteria and subsequent isolation via magnetic beads.^[26] Such a labeling can also be achieved using cholesterol-derivatives.^[27] Kuhn *et al.* applied this ability of cholesterol-PEG-biotin for simple immobilization strategy of vesicles and cells onto surfaces in microfluidic channels.^[28]

However, the insertion-method has not been reported and studied with respect to their bioanalytical functionality so far. Therefore, we investigated another approach for the design of functionalized

vesicles suitable for bioassays. We developed an insertion strategy for the surface modification of marker encapsulating liposomes composed of DPPC, DPPG and cholesterol. For this, different anchor molecules were investigated with respect to their ability to effectively insert into the vesicle membrane. The best system for insertion was then compared to liposomes prepared via the standard method in terms of zeta potential, binding capability and encapsulation efficiency of entrapped marker molecules. It was found that insertion is possible up to 10 mol% without affecting the liposome stability. It can be conducted very fast under gentle conditions; all receptor moieties are distributed on the outer vesicle surface and also the loss of material is minimized as there is no need for complex purification steps.

3.2. Experimental

3.2.1. Materials

1,2-dipalmitoyl-sn-glycero-3-phosphatidylcholine (DPPC), 1,2-dipalmitoyl-sn-glycero-3-[phosphor-rac-(1-glycerol)] (DPPG), 1,2-dipalmitoyl-sn-glycero-3-phosphoethanolamine-N-(biotinyl) (biotin-DPPE), cholesterol and the extrusion kit and membranes were purchased from Avanti Polar Lipids (www.avantilipids.com). The dialysis membrane spectra/por 4 with a MWCO of 12-14 kDa was purchased from spectrum labs (www.spectrumlabs.com). Cholesterol-PEG-biotin was purchased from nanocs (www.nanocs.net). Lipopeptide-biotin is a Pam3Cys-SK4 (N-Palmitoyl-S-[2,3-bis(palmitoyloxy)-(2RS)-propyl]-[R]-cysteinyl]-seryl-lysyl-lysyl-lysyl-lysine(beta-alanyl-beta-alanyl-epsilon-aminocaproyl-epsilon-aminocaproyl-biotinyl)-NH₂) kindly supplied by Guenter Roth from the ZBSA, University of Freiburg and synthesized at EMC microcollections GmbH, Tübingen (<http://www.microcollections.de>). The Lipopeptide-biotin is structurally related to Lipobiotin and Pam3Cys-biotin^[26] but shows higher solubility at lesser tendency to vesicle building. Sulforhodamine B monosodium salt (SRB), 4-(2-Hydroxyethyl)piperazine-1-ethanesulfonic acid (HEPES) and sodium azide were bought from Sigma Aldrich (www.sigmaaldrich.com). n-Octyl-β-D-glucopyranoside (OG) was purchased from Roth (www.carlroth.com). For binding experiments either white streptavidin coated microtiterplates C96 from Kaivogen (kaivogen.com) were used or black MaxiSorp plates from Nunc (www.sigmaaldrich.com) were self-coated with streptavidin from Invitrogen (www.thermofisher.com). All other chemicals were of analytical grade and purchased from VWR (de.vwr.com). Millipore water ($\geq 18.2 \text{ M}\Omega \text{ cm}$) was used for the preparations of all buffers and aqueous solutions.

3.2.2. Methods

3.2.2.1. Liposome Preparations

3.2.2.1.1. Preparation of Liposomes by Reverse Phase Evaporation

DPPC (30 mg), DPPG (15 mg) and cholesterol (20 mg) were dissolved in chloroform (3 mL) and methanol (0.5 mL) and sonicated with a bath sonicator (Bandelin Sonorex Digitec, DT 255 H) at 45 °C for 1 minute. 2 mL of SRB-solution (150 mM, dissolved in 0.02 M HEPES) were added and the mixture sonicated at 45 °C for 4 minutes. The organic solvent was removed by using a rotary evaporator at 45 °C and a pressure of 380 mbar for 40 minutes. The solution was vortexed for 30 s and another 2 mL of the SRB-solution were added. After vortexing again, the solution was rotated at 45 °C and 380 mbar for 20 minutes and then again at 45 °C and 280 mbar for 20 minutes. The solution was being extruded through polycarbonate membranes (1 μm and 0.4 μm) at 50 °C by pushing the syringes back and forth 21 times for each membrane. Excess of SRB was removed by size exclusion chromatography with a Sephadex G-50 column (24x2 cm) and HSS buffer as eluent (10 mM HEPES, 200 mM NaCl, 200 mM sucrose, 0.01 % NaN₃, pH 7.5) followed by dialysis against HSS buffer (800 mL) for 24 h.^[M]

3.2.2.1.2. Insertion Method

A solution of anionic SRB encapsulating liposomes (25 μL) and a solution of biotinylated lipopeptide, DPPE-biotin or cholesterol-biotin (1-8 mol% phospholipid) were mixed in a 1.5 mL Eppendorf vial and shaken at elevated times (1, 2, 4 and 8 h) at 25 °C or at elevated temperatures (25, 30, 40, 50 °C) for 2 h. Then the mixture was diluted in HSS buffer to a total volume of 2 mL. To remove an excess of biotinylated molecules dialysis against HSS buffer (250 mL) was applied for 24 h.

3.2.2.1.3. Direct Modification

Liposomes were prepared by reverse phase evaporation at 60 °C and purified as described above. The desired amount of DPPE-biotin was added to the lipid composition prior to synthesis in order to obtain biotin modified liposomes.

3.2.2.2. Characterization

All measurements were performed at room temperature and ultrapure water (≥ 18.2 MΩ cm) was used for all experiments unless stated otherwise.^[M]

3.2.2.2.1. Dynamic Light Scattering and ζ-Potential

Dynamic light scattering (DLS) and ζ-potential measurements were carried out with a Malvern Zetasizer Nano-ZS (www.malvern.com). For all measurements the temperature was set to 25 °C. Semi-micro PMMA cuvettes were used for size determinations, disposable folded capillary cells for the ζ-potential measurements. The samples were diluted 1:100 prior to the measurements. The following settings were applied for the material liposomes: $n_D^{20} = 1.34$ and Abs = 0.000 and HSS buffer as

dispersant: $n_D^{20} = 1.342$, viscosity = $1.1185 \text{ kg} \cdot \text{m}^{-1} \cdot \text{s}^{-1}$, dielectric constant: 78.5. An equilibration time of 60 s was applied before each measurement.^[M] DLS spectra were plotted as intensity size distributions with the relative % of light scattered by the particles in a size class on the y-axis vs. the diameter of the particles on the x-axis.

3.2.2.2.2. Determination of Phospholipid Concentration

The phospholipid concentration was determined by using a Spectroflame-EOP inductively coupled plasma optical emission spectrometer (ICP-OES) from Spectro (www.spectro.com). Therefore, 20 μL of the liposome sample was diluted in 2980 μL 0.5 M HNO_3 and could then be used for the measurement. 0.5 M HNO_3 and a solution of 100 μM of PO_4^{3-} in 0.5 M HNO_3 were used for calibration before each measurement.^[M]

3.2.2.2.3. Microtiterplate Coating with Streptavidin

Streptavidin (100 $\mu\text{L}/\text{well}$, 10 $\mu\text{g}/\text{mL}$ in PBS) was added to the wells of a MaxiSorp microtiterplate (Nunc) and incubated overnight at 4 °C. After the coating step, the streptavidin solution was removed and the wells were washed with PBS buffer (2x200 μL). Blocking was conducted by incubating a solution of BSA/Tween 20 (0.1%/0.05% in PBS, 200 $\mu\text{L}/\text{well}$) for 1 h at room temperature. Before using the plates, the wells were washed twice with PBS buffer (200 μL) and once with HSS buffer (200 μL).

3.2.2.2.4. Fluorescence Measurements of Liposomes Immobilized in Streptavidin Coated Plates

The liposome dispersions (100 $\mu\text{L}/\text{well}$, $c(\text{phospholipid}) = 5 \mu\text{M}$, in HSS) were incubated on a streptavidin coated microtiter plate for 30 minutes at room temperature. After washing twice with HSS-buffer (200 μL) the fluorescence signal was read out with a FLUOStar OPTIMA microplate reader at wavelengths of $\lambda_{\text{ex}} = 544 \text{ nm}$ and $\lambda_{\text{em}} = 575 \text{ nm}$ and a gain of 1500 before (in 100 μL HSS) and after lysis with 30 mM n-octyl- β -D-glucopyranoside (OG, 100 μL). Triplicates were applied for each concentration.

3.2.2.2.5. Fluorescence Measurements to Determine the Retained Sulforhodamine B

For characterization liposome dispersions were diluted to 5 μM phospholipid once in HSS buffer and once in 30 mM OG solution. The fluorescence intensities were read out on a FLUOStar OPTIMA microplate reader at wavelengths of $\lambda_{\text{ex}} = 544 \text{ nm}$ and $\lambda_{\text{em}} = 575 \text{ nm}$ and a gain of 1500. Triplicates were applied for each concentration. For analysis the signal obtained in HSS buffer was subtracted from the corresponding signal in the OG solution to calculate the SRB concentration contained inside the liposomes. Therefore, also a SRB standard curve between 0 and 8 μM was recorded.

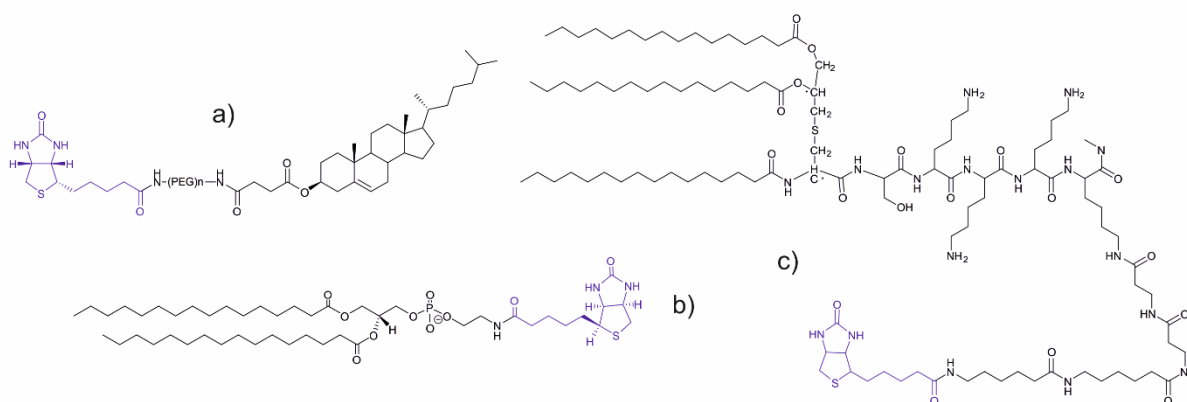
3.3. Results and Discussion

3.3.1. Insertion Method – Preparation and Characterization

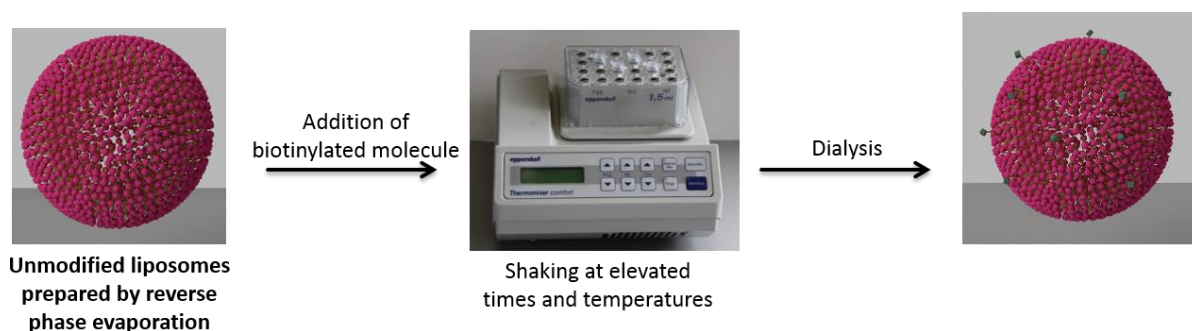
Liposomes are formed by self-assembly of either one phospholipid or a mixture of lipids which can be achieved by several techniques.^[1] This study focuses on large unilamellar vesicles, which are most commonly prepared using the reverse-phase evaporation strategy. This method leads to a large amount of liposomes sufficient *e.g.* for hundreds to thousands of bioassays.

For insertion, unmodified standard liposomes were synthesized consisting of DPPC, DPPG and cholesterol. As many assays are based on biotin as recognition element, this functionality was chosen as a model moiety. Here commercially available DPPE-biotin (Chart 3.1b) was tested for its ability to efficiently insert into phospholipid bilayers. Cholesterol-biotin (Chart 3.1a) was commercially obtained with a PEG linker ensuring good water solubility, which is desirable as the insertion process takes place in an aqueous environment. As a third modifying agent for insertion a lipopeptide-biotin (Chart 3.1c) was chosen. This molecule is known for its ability to insert into DPPC membranes and contains a hydrophilic linker to ensure good water solubility.

Chart 3.1. Chemical structures of investigated insertion molecules. a) cholesterol-(PEG)2000-biotin, b) DPPE-biotin, c) lipopeptide-biotin.



Insertion is simply performed by mixing and incubating vesicle dispersion and solutions of different modifying agents in an Eppendorf shaker (Scheme 3.2). After functionalization, all preparations resulted in liposomes with average diameters of 160 nm. Also, as the vesicle diameter didn't change after insertion, no aggregation was observed, and the ζ -potentials were all < -13 mV. Thus, the obtained modified liposomes remain colloidally stable (Figure 3.1a, Table 3.1). Interestingly, the ζ -potential decreases with increasing number of inserted molecules (Figure 3.1b). Such a change after insertion can be observed for all modifications (Table 3.1). Obviously, the extent of this decrease strongly depends on the size and nature of the headgroups of the inserted molecule as they shield the overall negative charge of the liposome surface.

Scheme 3.2. Schematic overview on the preparation of biotin-functionalized liposomes via the insertion-method.

Consequently, as cholesterol-biotin and lipopeptide-biotin both have a rather long spacer, higher decreases in the zeta-potential were observed, whereas the zeta potential of DPPE-modified liposomes does not change significantly. It can be concluded that this change in the zeta potential can serve as a quick and simple indication for the successful insertion of molecules.

Table 3.1. Characterization of liposome dispersions before and after modification with biotinylated molecules by DLS and ζ -potential measurements ($n=4$). The DLS data presented are for 10 mol% biotin inserted in all cases. The ζ -potential data show 10 mol% inserted DPPE-biotin and cholesterol-biotin and 7 mol% inserted lipopeptide-biotin. Errors are given as standard deviation.

	Unmodified	Lipopeptide-biotin	Cholesterol- biotin	DPPE-biotin
Diameter [nm]	156	178	169	161
Pdl	0.07	0.17	0.19	0.18
ζ -potential [mV]	-29 ± 1	-20 ± 3	-13 ± 1	-25 ± 3

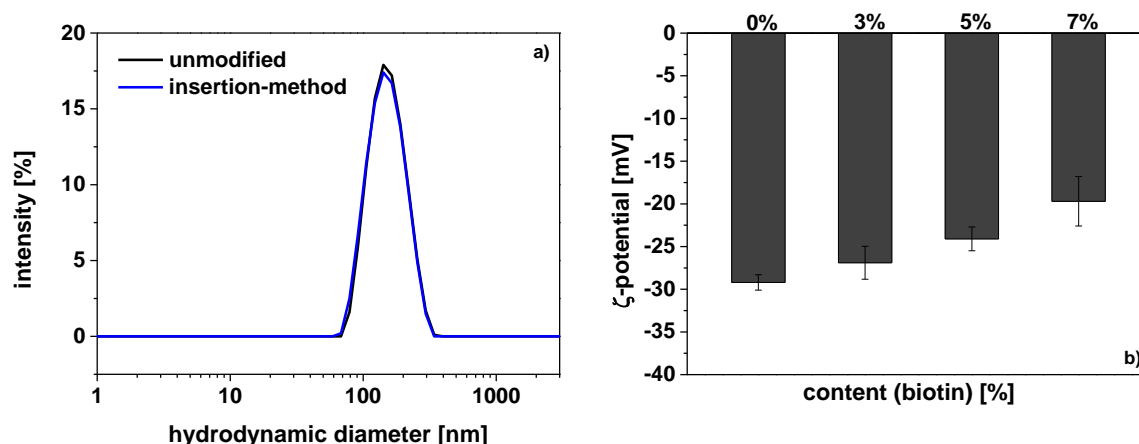
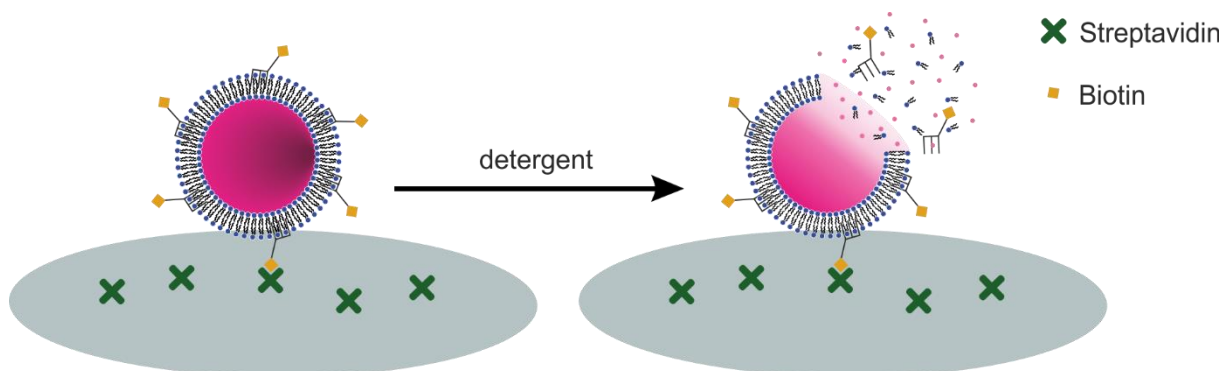


Figure 3.1. Characterization of liposome dispersions before and after modification with biotinylated lipopeptide by a) DLS and b) ζ -potential measurements. Error bars display the standard deviation, $n=4$.

3.3.2. Optimization of Insertion Conditions

Insertion of the three molecules was optimized with respect to incubation time and temperature. Here, the successful surface modifications were characterized with respect to their effective biological targeting functionality by binding to streptavidin-coated microtiter plates. The fluorescence intensity of sulforhodamine B (SRB) entrapped inside the liposomes was quantified after removal of unbound vesicles before and after lysis with octyl glucopyranoside (OG) (Scheme 3.3).

Scheme 3.3. Measurement setup for the biotin-streptavidin binding assay on streptavidin coated 96 well plates.



It was expected that the more efficient the insertion is, the more liposomes are able to bind to the plate and thus a higher signal is obtained. The plotted data were normalized to the lowest insertion time or temperature. As shown in Figure 3.2a an increase in the insertion time had no influence on the insertion efficiency in all cases suggesting a very fast process, an even shorter incubation time could be investigated in the future. The high standard deviations observed for insertion of DPPE-biotin are likely due to experiments being performed at 25 °C instead of at elevated temperatures. In general, due to higher membrane mobility at insertion temperatures above the phase transition temperature also a higher insertion efficiency should be achieved as was observed for cholesterol-biotin and DPPE-biotin modified liposomes (Figure 3.2b).

Here 40 °C and 50 °C showed an improved insertion. In case of DPPE-biotin the signal increased 25-fold when applying 50 °C during insertion. This is likely due to a decreased presence of DPPE-micelles in solution because of its enhanced solubility at higher temperatures. At the same time, the still significantly higher standard deviations indicate an unreliable insertion. Interestingly, for the insertion of lipopeptide-biotin neither the insertion time nor the temperature had any influence on the insertion efficiency. So, functionalization using this modifying agent is not only very fast but can also be conducted simply at room temperature without any loss in insertion efficiency. In subsequent experiments respective optimal conditions were used, *i.e.* an insertion time of 1 h in all cases and an insertion temperature of 25 °C for lipopeptide-biotin, 40 °C for cholesterol-biotin and 50 °C for DPPE-biotin.

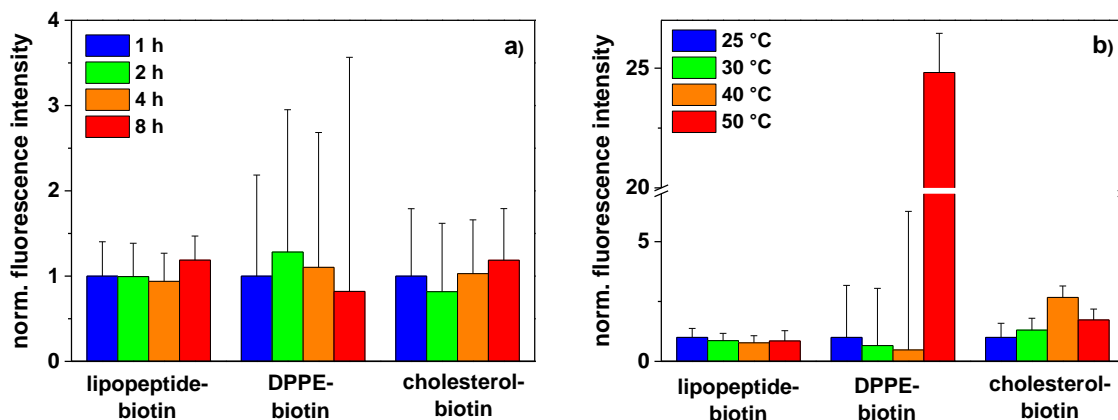


Figure 3.2. Insertion efficiency of biotin-lipopeptide, DPPE-biotin and cholesterol-biotin into SRB-encapsulating liposomes (150 mM SRB, HSS buffer) for a) different insertion times (1, 2, 4, 8 h, 25 °C insertion temperature) and b) different insertion temperatures (25, 30, 40, 50 °C, 2 h insertion time each), $n=3$. The plotted data were normalized to the lowest insertion time or temperature. Error bars display the relative standard deviations.

3.3.3. Binding Behaviour of Functionalized Liposomes

Finally, liposomes with varying contents of biotin (from 0-8 mol% with respect to the phospholipid concentration) were prepared for each of the modifying agents. An increase in the binding ability to streptavidin-modified surfaces was expected with increasing biotin surface loads as known from other studies investigating surface-tag concentrations.^[12] This direct correlation was found for DPPE-biotin and lipopeptide-biotin modified liposomes, but not for cholesterol-biotin (Figure 3.3). Overall, the lipopeptide-modified liposomes had a superior performance providing double the signal intensity in comparison to DPPE-biotin (Figure 3.3). We assume that this is in part due to a better insertion

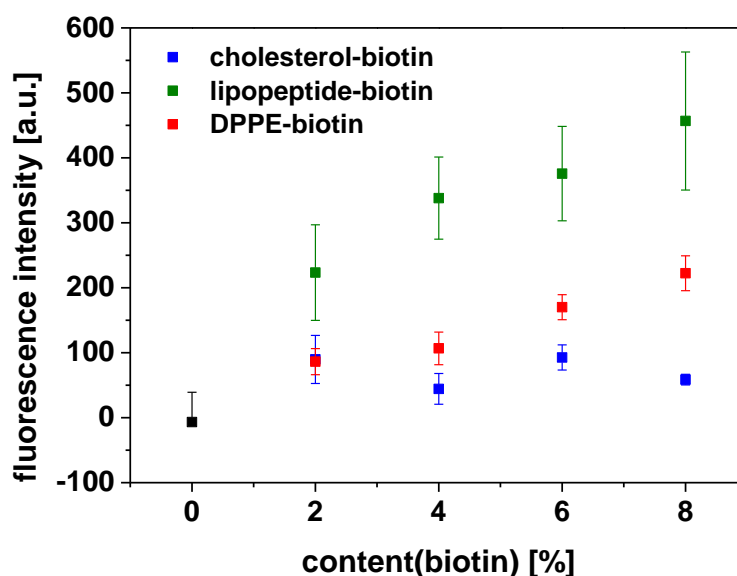


Figure 3.3. Binding capability of SRB-encapsulating, anionic liposomes (150 mM SRB, HSS buffer) modified by insertion of either lipopeptide-biotin, DPPE-biotin or cholesterol-biotin under optimized conditions. Error bars display the standard deviation, $n=3$. The content of biotin refers to the provided amount of biotin.

efficiency but also due to the less stringent preparation conditions at room temperature. In the case of DPPE-biotin incubation is done at 50 °C and 10% ethanol is required for a better dissolution of the molecule. While the addition of ethanol did not affect the liposome stability as determined by DLS, it caused an increase in dye leakage of 7%. Also, incubation at 50 °C resulted in a lower concentration of entrapped SRB after modification (Figure 3.4). Moreover, DPPE-biotin tends to form micellar structures in aqueous solutions with a similar diameter as the modified liposomes as confirmed by DLS measurements (data not shown). Thus, unloaded DPPE-micelles may still be present in addition to the modified liposomes in the final dispersion which will block some binding sites on the microtiter plate and hinder the loaded functionalized liposomes from binding. In the case of cholesterol-biotin, minimal binding was observed which was essentially independent of the amount of tag used. DLS spectra of cholesterol-biotin dispersions showed a peak around 20 nm which suggests that no micellar structures are present and rather corresponds to the lipid molecules themselves with their long PEG spacer. As after insertion only the liposome peak can be observed in the DLS spectra the molecules either inserted completely or were successfully removed during purification and thus do not interfere with the binding of the functionalized liposomes. Also, we had chosen a PEG linker to increase the tags solubility, however, in the end, this long linker may sterically hinder the cholesterol moiety's insertion resulting in only few molecules to anchor into the liposomal membrane.

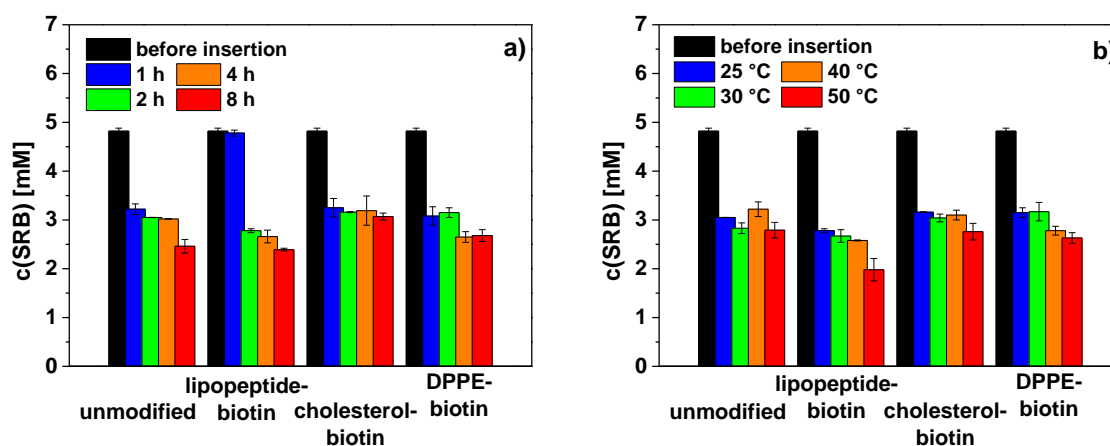


Figure 3.4. Effect of different shaking times (1, 2, 4, 8 h, 25 °C incubation temperature; a) and temperatures (25, 30, 40, 50 °C, 2 h incubation time each; b)) on the concentration of sulforhodamine B contained within the liposomes during insertion of biotin-lipopeptide, DPPE-biotin and cholesterol-biotin into SRB-encapsulating liposomes (150 mM SRB, HSS buffer), $n=3$. Unmodified liposomes were treated the same way as negative control.

The dye leakage during insertion was investigated for all three anchor molecules. Due to the insertion of the receptor tags into the tightly packed membrane of the liposomes their stability may be affected. This was determined by measuring the concentration of entrapped SRB before insertion and after different insertion times and temperatures (Figure 3.4). As negative control, unmodified liposomes without the addition of a modifying agent were treated alongside. The initial drop in signal intensity

after insertion is most probably due to the fact that the liposomes before insertion were not freshly dialyzed, so that also some free dye molecules were present. However, in almost all cases a further decrease in the SRB concentration was observed with increasing insertion time and temperature (Figure 3.4).

This was also the case for the negative control liposomes, which leads to the conclusion that this loss is not caused by the insertion process itself but mainly due to the subsequent purification by dialysis. Also, a decrease in the phospholipid concentration could be observed after incubation at different shaking times and temperatures (Figure 3.5). This would indicate a simple loss of liposomes through the process. In the end, since longer incubation times and higher temperatures did increase the loss of dye molecules to a certain extent, an incubation time of 1 h was used for the following preparations and the optimized incubation temperatures of 25, 40 and 50 °C for lipopeptide-biotin, cholesterol-biotin and DPPE-biotin, respectively.

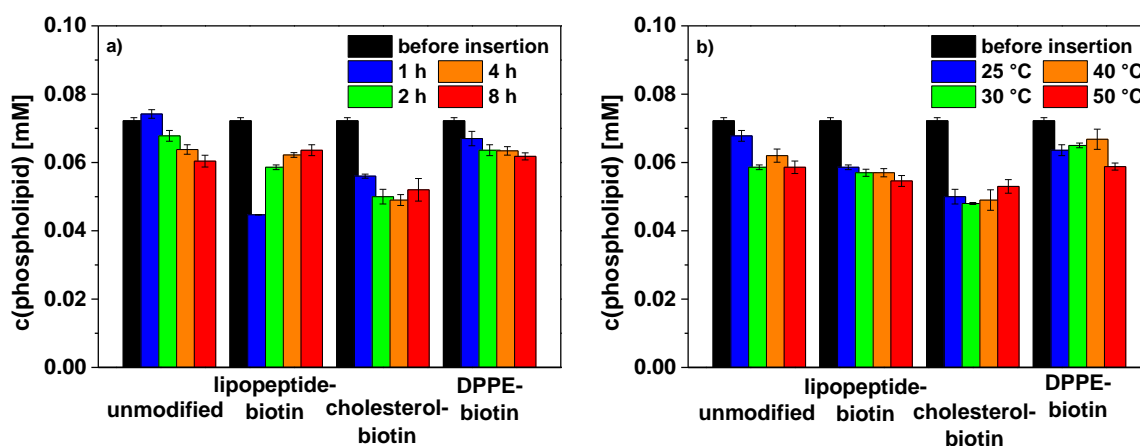


Figure 3.5. Phospholipid concentration before and after insertion of biotin-lipopeptide, DPPE-biotin and cholesterol-biotin into SRB-encapsulating, anionic liposomes (150 mM SRB, HSS buffer) for different shaking times (1, 2, 4, 8 h) and temperatures (25, 30, 40, 50 °C), determined by ICP-OES, $n=3$. Unmodified liposomes were treated the same way as negative control.

In conclusion, lipopeptide insertion was the most promising of these three systems due to its fast and controllable execution under gentle conditions. This enables the efficient functionalization of the vesicle surface even with temperature-sensitive or otherwise fragile biological molecules, which can either be attached to such a lipopeptide or a different suitable lipophilic anchor molecule.

The reliability of the lipopeptide insertion was proven by repeating the insertion of different amounts of lipobiotin into a second lot of liposomes consisting of the same formulation and dye concentration and by analyzing the binding behavior of the two different batches to streptavidin on different plates. As shown in Figure 3.6 the binding behavior is very similar, proving a very good reproducibility of the insertion of lipobiotin into the liposomes used in this work.

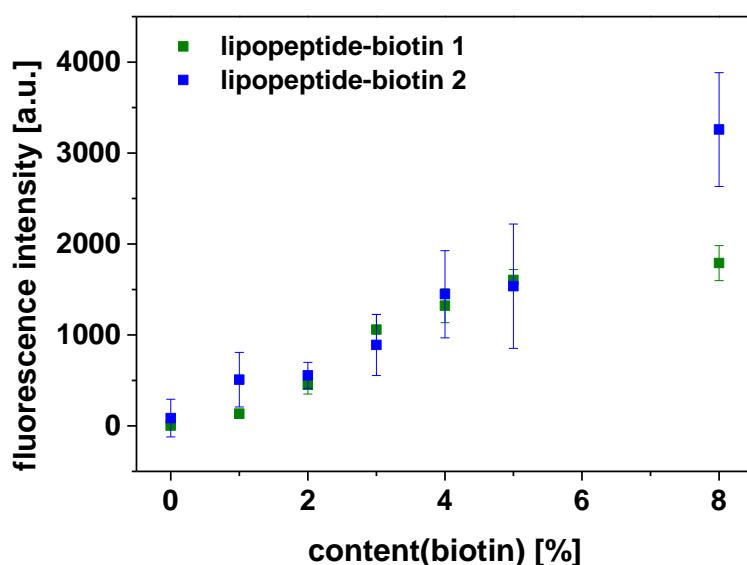


Figure 3.6. Reproducibility of the insertion of lipopeptide-biotin for 2 different batches of SRB-encapsulating, anionic liposomes (150 mM SRB, HSS buffer), $n=3$.

3.3.4. Comparison of Lipopeptide-Insertion and Standard Modification

The insertion-method using the lipopeptide-biotin, which performed best in this study, was then compared to the standard modification method with DPPE-biotin which is commonly used for the functionalization of liposomes.^[18] Here, different batches with varying DPPE-biotin contents (0 to 16 mol% regarding the total phospholipid concentration) were prepared by adding it directly to the lipid mixture prior to liposome synthesis. As it is assumed that biotin will be statistically distributed between inner and outer liposome surface, double the amount of biotin moieties were used for preparation. This enables the comparison of similar biotin amounts available for binding in both methods, as in case of insertion all moieties will be at the outer surface due to an unlikely flip-flop of the large peptide headgroups between outer and inner membrane.^[29]

All separately synthesized liposome batches resulted in colloidal stable vesicle dispersions with average diameters of 200 nm and ζ -potentials below -20 mV (Figure 3.7, Table 3.2).

Moreover, the long-term stability of the liposomes was tested and no change in vesicle diameter or colloidal stability was observed (Figure 3.8 and Figure 3.9). Non-modified liposomes showed highest stability (as expected),^[30] liposomes with DPPE-biotin made through the direct method showed 14-16% dye leakage after 5 months, and liposomes prepared via the insertion method showed similar leakage after 3 months of storage (17% lipopeptide, 30% cholesterol, 23% DPPE) (Table 3.3 and Table 3.4).

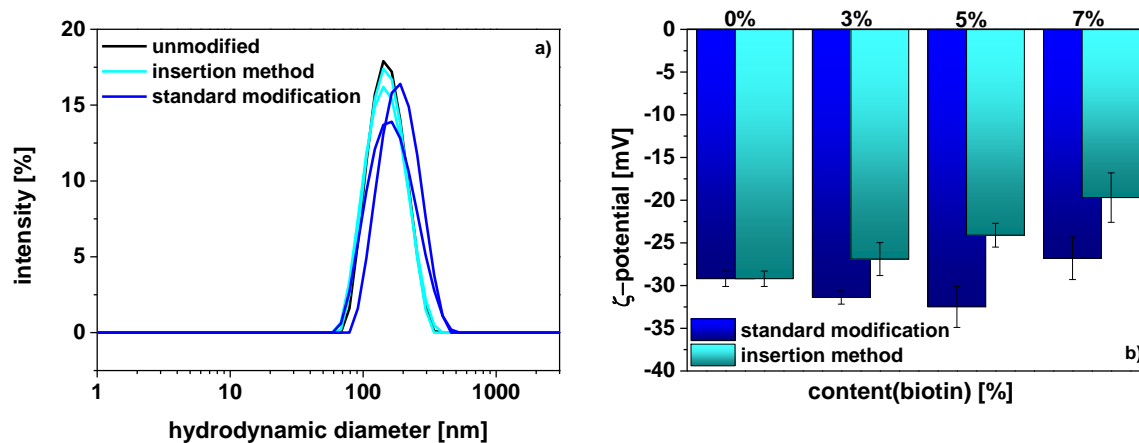


Figure 3.7. Characterization of liposome dispersions by DLS (a) and ζ -potential measurements (b), $n=4$. Lipopeptide-biotin was used for insertion and DPPE-biotin for standard modification.

Table 3.2. Characterization of liposomes prepared by standard modification using DPPE-biotin.

Content (biotin) [%]	Diameter [nm]	Pdl	ζ -potential [mV]
0	156 \pm 44	0.07	-29.2 \pm 0.9
3	162 \pm 48	0.13	-31.4 \pm 0.8
5	184 \pm 70	0.18	-32.5 \pm 2.4
7	196 \pm 64	0.20	-26.8 \pm 2.5
12	240 \pm 126	0.23	-18.5 \pm 2.4
16	216 \pm 89	0.24	-22.6 \pm 3.5

Table 3.3. Dye leakage of liposomes modified via the insertion method using lipopeptide-biotin, DPPE-biotin and cholesterol-biotin, $n=3$.

	Lipopeptide-Biotin	Cholesterol-Biotin	DPPE-Biotin
Day 1	2 \pm 0.10%	7 \pm 0.08%	2 \pm 0.12%
After 3 months	17 \pm 0.04%	30 \pm 0.05%	23 \pm 0.07%

Table 3.4. Dye leakage of unmodified liposomes and liposomes modified via the direct method using DPPE-biotin, $n=3$.

	Unmodified	DPPE-biotin/3%	DPPE-biotin/7%
Day 1	4 \pm 0.13%	12 \pm 0.05	6 \pm 0.08
After 5 months	4 \pm 0.12%	16 \pm 0.06%	14 \pm 0.05

Further studies are needed, however, to determine whether this trend continues with longer storage or can be avoided by shortening the insertion incubation periods. As the DPPE-biotin headgroup is so

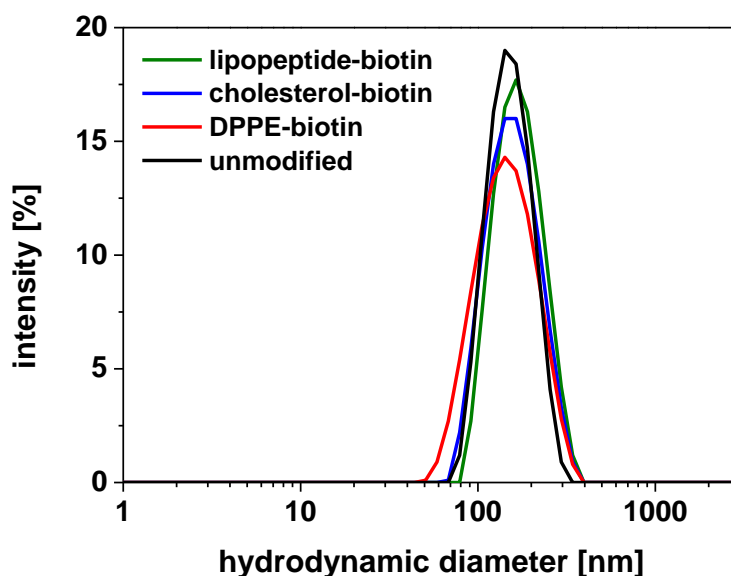


Figure 3.8. DLS spectra of unmodified liposomes and liposomes modified via insertion after 3 months.

small, the zeta-potential could not be used as indicator for a successful incorporation of the modifying agent. Biological targeting functionality was again proven using binding assays to streptavidin-coated microtiter plates and directly compared to the lipopeptide-modified liposomes (Figure 3.10). In the case of standard-modified liposomes only the contents of available biotin groups on the outer surface of the liposomes were plotted which were estimated to be half of the total biotin content. In case of the insertion method all biotin molecules are expected to be on the outer surface. While the lipopeptide-modified liposomes provided expected signals, *i.e.* increasing signal with increasing amount of available biotin groups on the surface, no such relationship was found for liposomes prepared by the standard method using DPPE-biotin. Here, amounts above 4 mol% of total DPPE-biotin are not effectively incorporated into the lipid bilayer during the synthesis anymore because even the

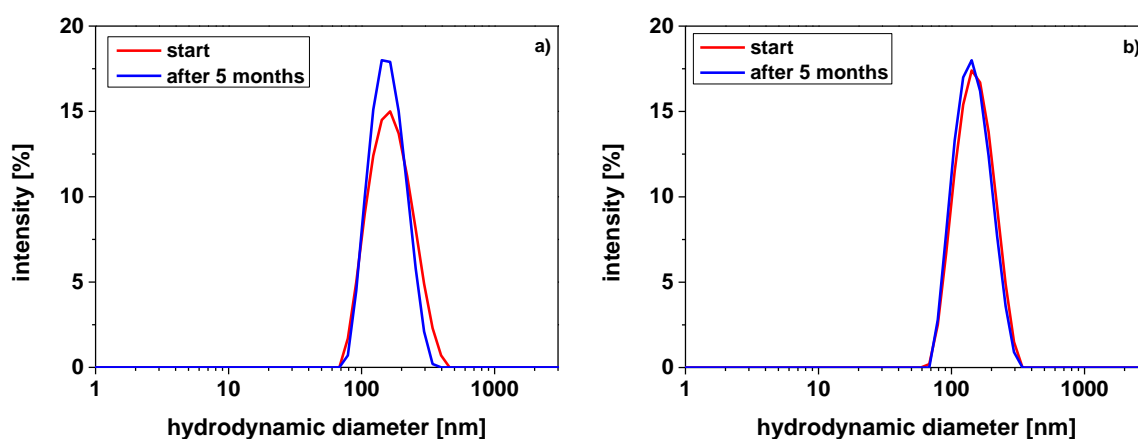


Figure 3.9. DLS spectra of liposomes right after the preparation and after 5 months. a) Direct modification using DPPE-biotin, b) Insertion-method using lipopeptide-biotin.

addition of 16 mol% of total DPPE-biotin showed no increase in the binding capability compared to 4 mol%. Thus, the incorporation of DPPE-biotin by direct modification at higher concentrations doesn't seem to be successful. We also observed that the presence of higher amounts of DPPE-biotin has a negative impact on the yield of liposome preparations as well as on the encapsulation efficiency as shown in Chapter 3.3.5. However, the insertion of lipopeptide-biotin shows that a decoration of the surface with more biotin groups is possible and also results in a higher binding capability. For the lipopeptide-insertion even 10 mol% can still be incorporated and a direct correlation between the biotin content and the signal intensity can be observed which makes this method much more reliable than standard modification with DPPE-biotin. The observed higher error bars at 10 mol% and the saturation of the signal indicate that higher concentrations are less likely to be useful. We assume that this is due to steric hindrance in the insertion process.

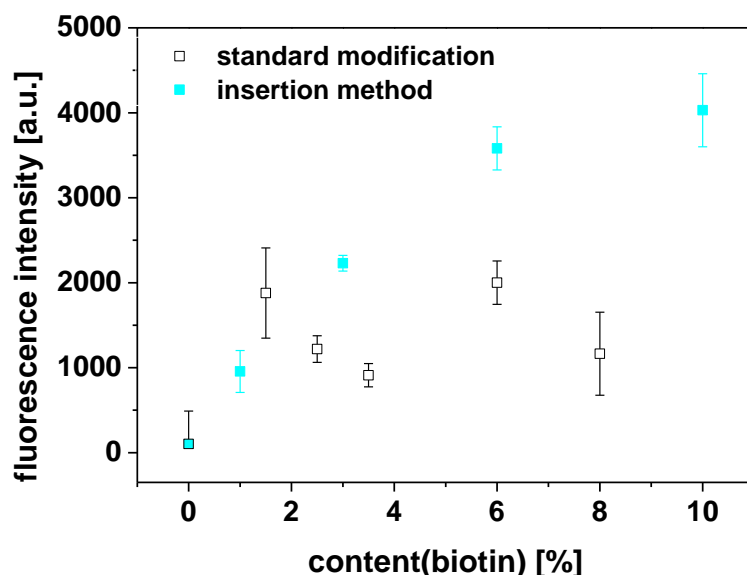


Figure 3.10. Insertion efficiency as obtained from fluorescence measurements of biotinylated liposomes functionalized either by direct modification or by the insertion-method with different biotin concentrations. Error bars display the standard deviation, $n=3$. The content of biotin refers to the provided amount of biotin. In the case of standard-modified liposomes only the contents of available biotin groups on the outer surface of the liposomes were plotted, which were estimated to be half of the total biotin content. In case of insertion all biotin molecules are expected to be on the outer surface.

In addition to this determination of biological functionality of the biotin-modified liposomes, it was tried to determine the actual biotin concentration in the liposomes via orthogonal approaches. However, no approach provided reliable data, specifically, the HABA/Avidin assay, which is commonly used for characterization of biotinylated proteins, led to a crosslinking of the liposomes and prevented correct data acquisition. ICP-OES was studied for the quantification of the total sulfur contained in biotin. However, the emission spectral lines of sulfur overlap with those of phosphorus. In the future,

the use of labeled monomeric streptavidin or radiolabels might be a possible alternative to provide an answer to this question.

3.3.5. Influence of the Preparation Methods on Liposome Signaling Capability - Effect of Dye Loading

The insertion method has shown to be a significantly more reliable and reproducible method for the surface modification of liposomes than the standard method. It will have highest impact during the development of liposome reagents with new surface modification groups, as during these optimization efforts ideally large numbers of variants are being investigated. The second most important impact it will have on the development of multi-analyte and multi-modal liposomes to generate the same type of liposome for any surface tag. In both scenarios not only the effective surface tag concentration is of utmost importance but also the signaling power through the entrapped marker molecules. We therefore compared entrapment efficiencies between the standard and insertion methods. They were determined and calculated using equation 3.1.

$$EE(\%) = \frac{c_{after\ lysis}(SRB) - c_{before\ lysis}(SRB)}{c_0(SRB)} \cdot 100\% \quad (3.1)$$

In case of the insertion method, all liposome variations are derived from the same original liposome preparation. No changes in encapsulation efficiency are therefore expected, which was also confirmed by our measurements (Table 3.5). However, in case of liposomes prepared by the standard modification method, a functionalized lipid is already present during liposome formation. This impacts the vesicle formation during the preparation process. As it is based on self-assembly of the lipids the efficiency of the vesicle formation and the entrapment of molecules are directly influenced. As shown in Table 5 varying encapsulation efficiencies were observed for the direct modification with DPPE-biotin. It is known that the encapsulation efficiency can vary significantly with changing lipid compositions^[31] and is evidenced here as increasing amounts of DPPE-biotin in the lipid mixture had a negative effect on the encapsulation efficiency (Table 3.5).

Table 3.5. Encapsulation efficiencies determined by fluorescence measurements of different preparations of biotinylated liposomes prepared either by direct modification or insertion-method. Errors are given as standard deviation, n=3. This table shows the total content of biotin in both cases.

Total content(biotin) [%]	EE(direct modification) [%]	EE(insertion-method) [%]
0	3.8 ± 0.2	
3	1.6 ± 0.1	3.5 ± 0.2
5	0.80 ± 0.04	3.6 ± 0.4
7	0.85 ± 0.04	3.3 ± 0.4

This in turn has a direct effect on the overall suitability of liposomes as signaling reagents in binding assays. As lower dye entrapment leads to less signaling power, comparison between varying surface tag concentrations becomes even more complex, if not the exact same liposome population can be used. It is therefore mandatory to be able to optimize surface modification of liposomes with a reliable method, as is enabled by the insertion method.

3.4. Conclusions

Modification of the liposome surface using the insertion method was demonstrated to be a highly efficient method depending on the type of the insertion molecule used. The high solubility, independency of insertion temperature and fast and effective insertion ability of the biotinylated lipopeptide makes it superior to simple cholesterol-PEG and DPPE-moieties. Up to 10 mol% of lipopeptide-biotin can easily be inserted without any negative impact on vesicle size or membrane stability. In case of the standard modification an increase in the surface tag concentration resulted in lower incorporation yields and lower signaling power due to decreased encapsulation efficiencies of the marker molecules. This suggests that concentrations above 4 mol% of total DPPE-biotin are not useful for binding assays. Most interesting for future applications is the fact that lipopeptide-inserted liposomes keep their analytical characteristics and only differ by the tag concentration used. This feature is of utmost importance to analytical applications of liposomes, *e.g.* as signal enhancers in bioassays, for assay development or multi-analyte detection. Furthermore, this surface modification strategy can be used for the functionalization of any lipid-bilayer surface or micellar structure and this expands its importance beyond liposome-based bioanalysis to general analytical and drug delivery applications.

Acknowledgements

We would like to thank Sandy Franziska Himmelstoß for her help with the 3D drawings.

References

- [1] A. Akbarzadeh, R. Rezaei-Sadabady, S. Davaran, S. W. Joo, N. Zarghami, Y. Hanifehpour, M. Samiei, M. Kouhi, K. Nejati-Koshki, *Nanoscale Res. Lett.* **2013**, *8*, 102.
- [2] a) N. Kamaly, A. D. Miller, *Int. J. Mol. Sci.* **2010**, *11*, 1759; b) G. Clergeaud, R. Genç, M. Ortiz, C. K. O'Sullivan, *Langmuir* **2013**, *29*, 15405; c) M. J. Richards, C.-Y. Hsia, R. R. Singh, H. Haider, J. Kumpf, T. Kawate, S. Daniel, *Langmuir* **2016**, *32*, 2963; d) Q. Han, X. Jia, Y. Qian, Z. Wang, S. Yang, Y. Jia, W. Wang, Z. Hu, *J. Mater. Chem. B* **2016**, *4*, 7087.
- [3] a) A. Jesorka, O. Orwar, *Annu. Rev. Anal. Chem.* **2008**, *1*, 801; b) H.A.H. Rongen, A. Bult, W.P. van Bennekom, *J. Immunol. Methods* **1997**, *204*, 105.

- [4] a) Q. Liu, B. J. Boyd, *Analyst* **2013**, *138*, 391; b) W.-C. Liao, J.-A. A. Ho, *Anal. Chem.* **2009**, *81*, 2470; c) B. Lin, D. Liu, J. Yan, Z. Qiao, Y. Zhong, J. Yan, Z. Zhu, T. Ji, C. J. Yang, *ACS Appl. Mater. Interfaces* **2016**, *8*, 6890.
- [5] T. Nii, F. Ishii, *Int. J. Pharm.* **2005**, *298*, 198.
- [6] a) A. R. Hilgenbrink, P. S. Low, *J. Pharm. Sci.* **2005**, *94*, 2135; b) S. Dong, J. D. W. Teo, L. Y. Chan, C.-L. K. Lee, K. Sou, *ACS Appl. Nano Mater.* **2018**, *1*, 1009; c) M. Miyazaki, E. Yuba, H. Hayashi, A. Harada, K. Kono, *Bioconjug. Chem.* **2018**, *29*, 44.
- [7] G. Tripathi, K. Chaurasiya, P. Katare, *Int. J. Curr. Pharm. Res.* **2013**, *5*, 4.
- [8] a) J. Wang, *Small* **2005**, *1*, 1036; b) Y.-F. Chang, C. Fu, Y.-T. Chen, A. Fang-Ju Jou, C.-C. Chen, C. Chou, J.-A. Annie Ho, *Biosens. Bioelectron.* **2016**, *77*, 1201; c) M. Mayer, S. Takegami, M. Neumeier, S. Rink, A. Jacobi von Wangelin, S. Schulte, M. Vollmer, A. G. Griesbeck, A. Duerkop, A. J. Baeumner, *Angew. Chem. Int. Ed.* **2018**, *57*, 408.
- [9] M. Grit, D. J.A. Crommelin, *Chem. Phys. Lipids* **1993**, *64*, 3.
- [10] H. Ohvo-Rekilä, B. Ramstedt, P. Leppimäki, J. P. Slotte, *Prog. Lipid Res.* **2002**, *41*, 66.
- [11] a) L. Kong, S. H. C. Askes, S. Bonnet, A. Kros, F. Campbell, *Angew. Chem. Int. Ed.* **2016**, *55*, 1396; b) M. Kanamala, B. D. Palmer, H. Ghandehari, W. R. Wilson, Z. Wu, *Pharm. Res.* **2018**, *35*, 154; c) D. Paolino, M. L. Accolla, F. Cilurzo, M. C. Cristiano, D. Cosco, F. Castelli, M. G. Sarpietro, M. Fresta, C. Celia, *Colloids Surf. B Biointerfaces* **2017**, *155*, 266; d) Y. Zhang, E. Mintzer, K. E. Uhrich, *J. Colloid Interface Sci.* **2016**, *482*, 19.
- [12] K. A. Edwards, A. J. Baeumner, *Anal. Bioanal. Chem.* **2006**, *386*, 1613.
- [13] N. Bunyakul, C. Promptmas, A. J. Baeumner, *Anal. Bioanal. Chem.* **2015**, *407*, 727.
- [14] Y. Xu, Y. Liu, Y. Wu, X. Xia, Y. Liao, Q. Li, *Anal. Chem.* **2014**, *86*, 5611.
- [15] X. Zhang, J. Qi, Y. Lu, W. He, X. Li, W. Wu, *Nanomedicine* **2014**, *10*, 167.
- [16] S. Ahn-Yoon, T. R. DeCory, A. J. Baeumner, R. A. Durst, *Anal. Chem.* **2003**, *75*, 2256.
- [17] Guohua Lei, Robert C. MacDonald, *Biophys. J.* **2003**, *85*, 1585.
- [18] K. A. Edwards, A. J. Baeumner, *Talanta* **2006**, *68*, 1421.
- [19] J. O. Eloy, R. Petrilli, L. N. F. Trevizan, M. Chorilli, *Colloids Surf. B Biointerfaces* **2017**, *159*, 454.

- [20] a) I. Haralampiev, M. Mertens, R. Schwarzer, A. Herrmann, R. Volkmer, P. Wessig, P. Müller, *Angew. Chem. Int. Ed.* **2015**, *54*, 323; b) H. M. Ekrami, A. R. Kennedy, W.-C. Shen, *FEBS Lett.* **1995**, *371*, 283.
- [21] a) T. M. Allen, P. Sapra, E. Moase, *Cell. Mol. Biol. Lett.* **2002**, *7*, 217; b) T. Perrier, P. Saulnier, F. Fouchet, N. Lautram, J.-P. Benoît, *Int. J. Pharm.* **2010**, *396*, 204; c) A. Cieślak, N. Wauthoz, A. Nieto Orellana, N. Lautram, J. Béjaud, J. Hureaux, M. Lafleur, J.-P. Benoit, C. J. Salomon, G. Bastiat, *Eur. J. Pharm. Biopharm.* **2017**, *115*, 31.
- [22] V. Vasquez-Montes, J. Gerhart, K. E. King, D. Thévenin, A. S. Ladokhin, *Biochim. Biophys. Acta* **2018**, *1860*, 534.
- [23] a) S. Aoki, R. M. Epand, *Biochim. Biophys. Acta* **2012**, *1818*, 12; b) C. Chen, Z. Duan, Y. Yuan, R. Li, L. Pang, J. Liang, X. Xu, J. Wang, *ACS Appl. Mater. Interfaces* **2017**, *9*, 5864.
- [24] M. Hagimori, Y. Chinda, T. Suga, K. Yamanami, N. Kato, T. Inamine, Y. Fuchigami, S. Kawakami, *Eur. J. Pharm. Sci.* **2018**, *123*, 153.
- [25] D. Lin, A. Grossfield, *Biophys. J.* **2014**, *107*, 1862.
- [26] C. Steinhäuser, T. Dallenga, V. Tchikov, U. E. Schaible, S. Schütze, N. Reiling, *Curr. Protoc. Immunol.* **2014**, *105*, 14.
- [27] a) S. B. Sato, K. Ishii, A. Makino, K. Iwabuchi, A. Yamaji-Hasegawa, Y. Senoh, I. Nagaoka, H. Sakuraba, T. Kobayashi, *J. Biol. Chem.* **2004**, *279*, 23790; b) S.-M. Lee, *Langmuir* **2017**, *33*, 6751.
- [28] P. Kuhn, K. Eyer, T. Robinson, F. I. Schmidt, J. Mercer, P. S. Dittrich, *Integr. Biol.* **2012**, *4*, 1550.
- [29] a) R. Homan, H. J. Pownall, *Biochim. Biophys. Acta* **1988**, *938*, 155; b) R. Volinsky, L. Cwiklik, P. Jurkiewicz, M. Hof, P. Jungwirth, P. K. J. Kinnunen, *Biophys. J.* **2011**, *101*, 1376.
- [30] K. A. Edwards, K. J. Meyers, B. Leonard, A. J. Baeumner, *Anal. Bioanal. Chem.* **2013**, *405*, 4017.
- [31] a) L. M. Were, B. D. Bruce, P. M. Davidson, J. Weiss, *J. Agric. Food Chem.* **2003**, *51*, 8073; b) J. M. López-Pinto, M. L. González-Rodríguez, A. M. Rabasco, *Int. J. Pharm.* **2005**, *298*, 1; c) K. P. McNamara, Z. Rosenzweig, *Anal. Chem.* **1998**, *70*, 4853.

4 Optical Characterization of DNA-tagged Fluorescent Liposomes

Abstract

DNA-tagged nanoparticles or vesicles are important analytical and biomedical tools and find their application *e.g.* in hybridization assays, targeted imaging, targeted drug delivery or in the isolation and purification of proteins. For all applications a detailed characterization of the functionalized particles or vesicles is important to ensure the suitability for each application. In this chapter, phospholipids were functionalized with different concentrations of ssDNA and the vesicle properties characterized via DLS, zeta-potential, ICP-OES, fluorescence spectroscopy, imaging and fluorescence correlation spectroscopy (FCS). A hybridization assay with complementary dye-tagged oligonucleotides followed by centrifugation confirmed the successful functionalization and allows an estimation of the DNA concentration on the vesicle surface. Control experiments using oligo-tagged magnetic particles and fluorescence microscopy proved a sufficient purification via centrifugation. Moreover, no quenching of oligo-A647 could be observed after hybridization with the complementary strand. After hybridization, also fluorescence correlation spectroscopy (FCS) was applied to determine the particle numbers and concentrations. Concentrations of around 4 nM and a loss during purification of 80-90% are in agreement with the theoretical calculations. Moreover, fluorescence imaging of dye-loaded liposomes showed that the DNA-tagged liposomes bind specifically to magnetic particles bearing the complementary strand. For some applications also lysis of the liposomes is crucial, and it was found that a concentration of 22 mM OG is sufficient for complete lysis of the liposomes.

This chapter has not been published.

Author contributions:

Most of the experimental work was solely done by the author. The author also wrote this chapter. The experimental work was partly done at Abbott Diagnostics in Lake Forest, IL in cooperation with Qiaoqiao Ruan. Sergey Tetin, Thomas Hirsch, Axel Duerkop and Antje J. Baeumner contributed with strategic discussions. Antje J. Baeumner was the leader of this project.

This chapter contains paragraphs that were in part already described in Carola Figalist's master's thesis. This includes paragraphs within the experimental part regarding the liposome preparation and characterization. The master's thesis is entitled "Positively Charged Liposomes for Signal Enhancement via Electrostatic Interactions" and was submitted to the Faculty of Chemistry and Pharmacy at the University of Regensburg in December 2014. Sections that are identical or similar to the master's thesis are listed here in detail and are indicated in this chapter by the citation "M":

- p.80, subchapter 4.2.1., paragraph 2 (experimental)
- p.81, subchapter 4.2.2.1., 4.2.2.2. (experimental)
- p.82, subchapter 4.2.2.3.

4.1. Introduction

Surface functionalization of nanoparticles or vesicles is a widespread analytical and biomedical tool as it allows the specific binding to analytes, cells or tissues. Thus, such materials can *e.g.* be applied for targeted drug delivery, imaging, the development of bioassays or for the separation or preconcentration of analytes. Several examples can be found for AuNPs. Here often thiolated ssDNA is applied for modification, which can be covalently attached to the particles.^[1] Bioanalytical applications of DNA-functionalized gold nanoparticles include *e.g.* colorimetric assays that exploit the change in the optical properties of the particles upon aggregation.^[2] Also DNA functionalized magnetic particles or microbeads can be found. In bioanalysis, they often serve as solid support for modification with the capture DNA and have been applied for several DNA hybridization assays.^[3,4] Their magnetic properties make them ideal materials for simple separation or purification means.^[4] Also the preconcentration of analytes using such magnetic particles has been reported.^[5] Another material that is often found in combination with DNA functionalization are silica nanoparticles as they also provide a simple surface chemistry for modifications. They find their application in controlled release mechanisms for drug delivery,^[6] for nucleic acid extraction and purification or in bioanalysis.^[7] Here, they can *e.g.* serve as label bearing the probe DNA on the particle surface as in case of sandwich hybridization assays,^[8] or the DNA is attached to block the pores of mesoporous silica particles and serves as gate-keeper.^[9] Such applications can also be found for liposomes, which provide more natural properties as they usually consist of phospholipids. For functionalization with oligonucleotides often cholesterol-tagged ssDNA is applied and added to the lipid composition of the lipid bilayer.^[10] This has for example been exploited for the FRET-based detection of micro-RNA^[11] or in classical sandwich hybridization assays.^[12] Also the formation of so-called lipoplexes has been intensively studied. Here the liposomes serve as DNA carrier by forming a complex with the DNA molecules.^[13] This can *e.g.* be applied for DNA vaccination or gene therapy.^[14]

However, before application to bioassays or drug delivery systems such functionalized materials need to be characterized carefully to ensure the suitability for each application. Here, factors like the size, morphology, colloidal stability or biocompatibility of particles or vesicles are important but also the number of surface tags and their functionality. Especially the determination of the amount of surface tags often remains a challenge. In case of biotin modifications *e.g.* a HABA/avidin assay can be applied.^[15] However, its application is restricted to problems with crosslinking and a low sensitivity as observed *e.g.* for liposomes.^[16] For the quantification of carboxyl groups on particle surfaces often conductometric titration is applied.^[17] The group of Resch-Genger also developed a simple method for the quantification of PEG maleimide ligands on polymeric microparticles based on the use of the Ellman's reagent.^[18] Also the use of FT-IR, XPS, solid state NMR, fluorescence labeling or dye adsorption assays can help to assess the number of functional groups on the surface of particles.^[19]

In this chapter a hybridization assay using fluorophore-tagged oligonucleotides was applied for the quantification of available ssDNA on the surface of liposomes. Several control experiments were conducted to proof the reliability of this method and the specific binding of the functionalized liposomes to their complementary DNA strand. Moreover, the DNA-tagged liposomes were characterized in detail with respect to their hydrodynamic diameter, zeta-potential, ICP-OES, fluorescence spectroscopy, imaging and fluorescence correlation spectroscopy (FCS).

4.2. Experimental

4.2.1. Materials

1,2-dipalmitoyl-sn-glycero-3-phosphatidylcholine (DPPC), 1,2-dipalmitoyl-sn-glycero-3-[phosphor-rac-(1-glycerol)] (DPPG), cholesterol and the extrusion kit and membranes were purchased from Avanti Polar Lipids (www.avantilipids.com). The cholesterol and dye-tagged oligonucleotides were either purchased from metabion (www.metabion.com) or from Integrated DNA Technologies (www.idtdna.com). The dialysis membrane spectra/por 4 with a MWCO of 12-14 kDa was purchased from spectrum labs (www.spectrumlabs.com). Sulforhodamine B monosodium salt (SRB), 4-(2-Hydroxyethyl)piperazine-1-ethanesulfonic acid (HEPES), sodium azide and black 96 well plates from Nunc were bought from Sigma Aldrich (www.sigmaaldrich.com). n-Octyl- β -D-glucopyranoside (OG) was purchased from Roth (www.carlroth.com). Magnetic microparticles and microtiter plate with glass bottom were provided by Abbott Diagnostics.

All other chemicals were of analytical grade and purchased from VWR (de.vwr.com). Millipore water ($\geq 18.2 \text{ M}\Omega \text{ cm}$) was used for the preparations of all buffers and aqueous solutions.^[M]

4.2.2. Methods

4.2.2.1. Preparation of Liposomes by Reverse Phase Evaporation

Liposomes were prepared via a modified protocol by Edwards *et al.*^[10] DPPC (40.3 μmol), DPPG (21 μmol) and cholesterol (51.7 μmol) were dissolved in chloroform (3 mL) and methanol (0.5 mL).^[M] Then the cholesterol-tagged oligo (sequence: 5' AAT CCA CCT TAG AGT ACA AAC GGA ACA CGA GAA AAG 3'- cholesterol) was dissolved in a MeOH:water mixture (1:4) added to the lipids and the mixture sonicated for 1 min. Table 4.1 shows the different liposome batches with varying amounts of the added cholesterol-tagged oligo.

Table 4.1. Overview of the different batches of DNA-tagged liposomes.

	ACF#1	ACF#2	ACF#7	ACF#9
c(chol-oligo)	350 pmol μl^{-1}	350 pmol μl^{-1}	350 pmol μl^{-1}	1 nmol μl^{-1}
V [μl]	50	50	250	204
xDNA	1x	1x	5x	25x
Encapsulant	150 mM NaCl	150 mM NaCl + 1 mM SRB	150 mM NaCl	150 mM NaCl + 1 mM SRB

Next, 2 mL encapsulant (either 150 mM NaCl or 150 mM NaCl+1 mM SRB, dissolved in 7.5 mM HEPES, pH 7.5) were added and the mixture sonicated for 4 min. The organic solvent was removed by using a rotary evaporator at 45 °C and a pressure of 380 mbar for 40 minutes. The solution was vortexed and another 2 mL of encapsulant were added. After vortexing again the solution was rotated at 45 °C and 380 mbar for 20 minutes and then again at 45 °C and 280 mbar for 20 minutes. The solution was being extruded through polycarbonate membranes (1 μm , 0.4 μm) at 50 °C by pushing the syringes back and forth 21 times for each membrane. Excess of encapsulant was removed by size exclusion chromatography with a Sephadex G-50 column followed by dialysis against HEPES buffer (10 mM HEPES, 200 mM NaCl, pH 7.5).^[M]

4.2.2.2. Dynamic Light Scattering and ζ -Potential

Dynamic light scattering (DLS) and ζ -potential measurements were carried out with a Malvern Zetasizer Nano-ZS (www.malvern.com). For all measurements the temperature was set to 25 °C. Semi-micro PMMA cuvettes were used for size determinations, disposable folded capillary cells for the ζ -potential measurements. The samples were diluted 1:100 prior to the measurements. The following settings were applied for the material liposomes: $n_D^{20} = 1.34$ and Abs = 0.000 and HSS buffer as dispersant: $n_D^{20} = 1.342$, viscosity = 1.1185 $\text{kg}\cdot\text{m}^{-1}\cdot\text{s}^{-1}$, dielectric constant: 78.5. An equilibration time of 60 s was applied before each measurement.^[16,M]

4.2.2.3. Phospholipid Determination by ICP-OES

The phospholipid concentration was determined by using a Spectroflame-EOP inductively coupled plasma optical emission spectrometer (ICP-OES) from Spectro (www.spectro.com). Therefore, 20 μL of the liposome sample was diluted in 2980 μL 0.5 M HNO_3 and could then be used for the measurement. 0.5 M HNO_3 and a solution of 100 μM of PO_4^{3-} in 0.5 M HNO_3 were used for calibration before each measurement.^[16,M]

4.2.2.4. Determination of ssDNA Content on the Liposomal Surface Using Cy5-Labeled Oligonucleotides

The liposome dispersions (200 μL in HEPES buffer) were mixed with an aqueous solution of Cy5-labeled oligonucleotide strands complementary to the strands incorporated in the liposomal membrane (12 μL , 300 pmol/ μL , sequence: Cy5- 3' TTA GGT GGA ATC TCA TGT TTG 5'). The mixture was shaken for 1 h at 23 °C and 300 rpm using an Eppendorf shaker. Excess of non-hybridized oligonucleotides was removed by centrifugation at 10000 g for 1 h at 25 °C. The pellet was resuspended in 200 μL HEPES buffer and centrifuged again for 1 h at 10000 g and 25 °C. After washing twice with HEPES buffer the pellet was again resuspended in HEPES buffer (200 μL) and diluted 1:3 for fluorescence measurements. 100 μL of the diluted dispersions was added to the wells of a black microtiter plate. The fluorescence signal of Cy5 was read out with a FLUOStar OPTIMA microplate reader at wavelengths of $\lambda_{\text{ex}}=640$ nm and $\lambda_{\text{em}}=675$ nm and a gain of 2900. To determine the corresponding Cy5 concentration a calibration curve of the Cy5-labeled DNA strand was recorded under the same conditions with concentrations ranging from 0-2 μM . All measurements were conducted in quadruplicates.

4.2.2.5. Estimation of ssDNA Content on the Liposomal Surface Using Alexa647-Labeled Oligonucleotides

The liposome dispersions (50 μL) were mixed with an aqueous solution of A647-labeled oligonucleotide strands complementary to the strands incorporated in the liposomal membrane (30 μM , 15 μL for ACF#1 and 2, 50 μL for ACF#7). The mixture was incubated for 30 min at room temperature under shaking at 300 rpm and purified via centrifugation as described in Chapter 4.2.2.4. Finally, the pellet was resuspended in 100 μL HEPES buffer and diluted 1:50 for fluorescence analysis.

Spectra of liposomes hybridized with oligoA647 were recorded on a Fluorolog (Horiba Scientific) between 660 and 800 nm at $\lambda_{\text{ex}}=650$ nm. The peak maxima at 666 nm were taken for analysis and background correction was conducted.

4.2.2.6. Absorbance Spectra

Absorbance spectra were recorded between 250 and 800 nm on a Cary4000 (Agilent Technologies). To determine the concentration of oligo-A647 in the stock solution the absorbance maximum at 650 nm with and $\epsilon=267\text{mmol}^{-1}\text{cm}^{-1}$ was used.

4.2.2.7. Determination of Free Oligo-A649 After Purification by Centrifugation

Streptavidin coated, magnetic polystyrene particles (5 μm , 0.1%, 50 μL) were mixed with an aqueous solution of biotinylated oligo (same as on liposomes, 1 μM , 50 μL) and incubated for 1 h at room temperature. Magnetic separation was applied, the supernatant containing unbound oligos was removed and the pellet resuspended in HEPES buffer (100 μL). This washing was repeated several times. A 96 well plate with glass bottom was prepared for the microscopic studies. A 100 μL of HEPES buffer was applied to each of the wells. Then 100 μL of 50fold diluted liposomes that had been hybridized with oligo-A647 before and purified by centrifugation was added to row A of the plate. A 3.8 nM solution of oligo-A647 was added to create a standard curve. Serial dilutions of 2 fold each were conducted by removing 100 μL and adding it to the row below. Then 1 μL of the oligo tagged microparticles was added to each of the wells and the mixtures incubated for 30 min at 30 °C and shaking at 750 rpm on a BioShake iQ. Then washing was conducted using a magnetic plate washer (BioTek ELx50). An Olympus Ix81 fluorescence microscope at 20x magnification was used to read out the signal intensity/particle. Four images of each well were taken and pixel analysis was automatically conducted by the software.

4.2.2.8. Fluorescence Correlation Spectroscopy

After hybridization with A647, 40 μL of ACF#1 and 2 were added to the wells of a 384 well plate. ACF#7 was diluted 1:5 before adding it to the wells. A solution of oligo-A647 was measured as control. Measurements were conducted on an ISS Alba fluorescence correlation spectrometer with an A402 scanning mirrors module, a fianium laser module and a Nikon confocal microscope with a 20x water objective. To detect liposomes labeled with oligoA647 an excitation wavelength of 640 nm, 20 kHz and 25% power were applied.

4.2.2.9. Hybridization of Liposomes to Microparticles

A solution of SRB liposomes (1:1000 dilution, 200 μL) was added to the wells of a black 96well plate with glass bottom. A dilution series with 2-fold dilution each was conducted (From row A-H). Magnetic polystyrene microparticles coated with a strand complementary to the liposome strand (0.1% solid particles, 2 μL) was added and the mixture incubated for 30 min at 30 °C and shaking at 750 rpm on a BioShake iQ. Then washing was conducted using a magnetic plate washer (BioTek ELx50). An Olympus Ix81 fluorescence microscope at 20x magnification was used to read out the signal intensity/particle. Four images of each well were taken and pixel analysis was automatically conducted by the software.

4.2.2.10. Hybridization of Liposomes to Antibody-Microparticle Conjugate

A solution of mouse antibody (200 μL , pM range) was added to the wells of a black 96 well plate with glass bottom. A dilution series with 2fold dilution each was conducted (From row A-H). Magnetic goat-anti-mouse-particles (GAM-particles) (0.1% solid particles, 1 μL) were added to each well. Then 10 μL

of a liposome stock solution were added to one column of the plate and 10 μ L of Cap03oligo (300 nM) to a second column. The mixture was incubated for 30 min at 30 °C and shaking at 750 rpm on a BioShake iQ. Then washing was conducted using a magnetic plate washer (BioTek ELx50). An Olympus Ix81 fluorescence microscope at 20x magnification was used to read out the signal intensity/particle. Four images of each well were taken and pixel analysis was automatically conducted by the software.

4.2.2.11. Imaging of Liposome Lysis

Liposomes (1:20 dilution) were hybridized with the antibody-microparticle conjugate (0.1% solid particles) as described above. One column was used as control, varying concentrations of OG (6-50 mM in the well) were applied to a second column containing the mixture. The mixture was shaken for 1 min at 750 rpm and room temperature. To check if lysis affects protein interactions this experiment was also conducted with oligoA546. Readout was conducted before and after removal of the released dye by washing with a magnetic plate washer (BioTek ELx50). An Olympus Ix81 fluorescence microscope at 20x magnification was used to read out the signal intensity/particle. Four images of each well were taken and pixel analysis was automatically conducted by the software.

4.3. Results and Discussion

4.3.1. Liposome Preparation and General Characterization

DNA-tagged liposomes were prepared via reverse phase evaporation using cholesterol to anchor the DNA onto the liposomal surface.^[10] This was done for DNA contents between 0.013 and 0.065 mol% of the phospholipid content. All liposomes were characterized with respect to their phospholipid and DNA concentration, ζ -potential and hydrodynamic diameter. The recorded DLS spectra of the obtained vesicles revealed diameters of 150-180 nm with Pdis well below 0.1 suggesting the formation of monodisperse liposome mixtures (Figure 4.1). A summary of all other characterizations can be found in Table 4.2. The ζ -potential was always negative in the range of -22 to -25 mV, which is low enough to provide colloidally stable liposome dispersions. The phospholipid concentrations were determined via ICP-OES and resulted in concentrations between 6 and 10 mM and good yields up to 22 μ mol (Table 4.2).

In order to proof the successful incorporation of the oligonucleotides and to quantify the amount of DNA on the surface a complementary strand tagged with the fluorescent dye Cy5 was used. After hybridization of the DNA-tagged liposomes with the complementary strand, centrifugation was applied for purification and the DNA concentration on the surface of the liposomes estimated using fluorescence measurements. The determined DNA concentrations for ACF#1 and ACF#2 yielded 67% and 69% of the expected DNA concentration on the liposome surface. Thus, some of the DNA molecules do not get incorporated into the vesicles and are removed during purification. The yields for

a higher initial DNA input are even lower as shown for ACF#7 and ACF#9 with only 59 and 56%, respectively. However, ACF#7, which should contain five times more DNA on the liposomal surface, reached even 7 times more DNA as ACF#1 and 2 and ACF#9 reached 23 of the expected 25 times more DNA on the surface. Thus, it is possible to incorporate such high concentrations of DNA in the liposomal membrane as proven by these measurements.

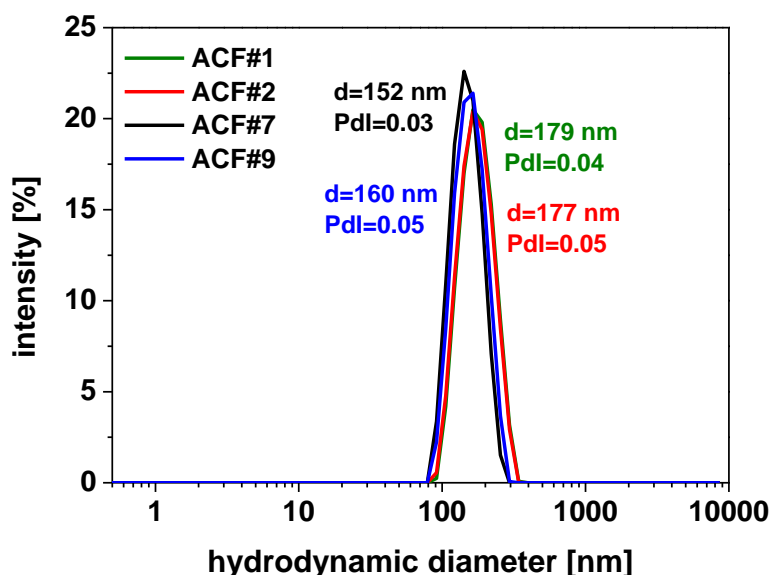


Figure 4.1. Hydrodynamic diameter of DNA-tagged liposomes encapsulating either sodium chloride (150 mM) or sodium chloride (150 mM) and sulforhodamine B (1 mM) determined by dynamic light scattering in HEPES buffer (10 mM HEPES, 200 mM NaCl, 0.01% NaN₃, pH 7.5), n=3.

Table 4.2. ζ -potentials, phospholipid and DNA concentrations of ssDNA-tagged liposomes encapsulating either sodium chloride (150 mM) or sodium chloride (150 mM) and sulforhodamine B (1 mM). ζ -potentials were determined in HEPES buffer (10 mM HEPES, 200 mM NaCl, 0.01% NaN₃, pH 7.5) using a zetasiser nano (Malvern), n=4. Phospholipid concentrations were determined using ICP-OES, n=3. DNA concentrations were determined using a hybridization assay with Cy5-tagged oligos. Fluorescence intensities were read out on a Fluostar Optima at λ_{ex} = 640 nm, λ_{em} = 675 nm and a gain of 1200, n=4.

Encapsulant/batch	ζ -potential [mV]	c(phospholipid) [mM]	Yield [μ mol]	c(DNA) [μ M]
150 mM NaCl (ACF#1)	-23 \pm 1	6.1 \pm 0.3	14.0 \pm 0.7	0.5 \pm 0.05
150 mM NaCl + 1 mM SRB (ACF#2)	-22 \pm 1	6.3 \pm 0.2	15.8 \pm 0.5	0.5 \pm 0.05
150 mM NaCl (ACF#7)	-23 \pm 2	10.0 \pm 0.2	22.0 \pm 0.4	3.6 \pm 0.2
150 mM NaCl + 1 mM SRB (ACF#9)	-25 \pm 2	6.8 \pm 0.04	17.0 \pm 0.1	11.6 \pm 0.9

4.3.2. Theoretical Calculations

In order to determine not only the concentration of DNA on the vesicle surface, but also the actual number of DNA molecules, calculations were conducted using the following equations:

$$N_{tot} = \left(\frac{\pi}{a_L}\right) * [d^2 * (d - 2t)^2] \quad (4.1)$$

with N_{tot} : number of lipids per liposome, d : hydrodynamic diameter, t : bilayer thickness and a_L : average headgroup surface area.^[20]

$$c(liposomes) = \frac{c(phospholipid)}{N_{tot}} \quad (4.2)$$

The values for the hydrodynamic diameter were determined by DLS as shown above, the bilayer thickness was estimated to be 4 nm and a headgroup surface area of 42 nm² was used. The average headgroup surface area was calculated using the molar ratios of the applied lipids (see Chapter 4.2.2.1.) and the values for the surface area of 0.71 (DPPC), 0.45 (DPPG) and 0.19 nm² (cholesterol).^[20] The small molar fraction of the DNA-tagged cholesterol was neglected. By using equation 4.1 it was possible to calculate the number of lipids per liposome. In combination with the phospholipid concentration as determined by ICP-OES a concentration of liposomes was calculated as shown in equation 4.2.^[20] This was further applied to calculate the number of ssDNA molecules per liposome, that are positioned on the outer surface of the vesicles. The results of the calculations are presented in Table 4.3.

Table 4.3. Liposome concentration and the number of external ssDNA/liposome for all batches shipped to Abbott.

Batch	N_{tot}	c(phospholipid) [mM]	c(liposomes) [nM]	c(oligos) [nM]	ssDNA/liposome
ACF#1	4.54*10 ⁵	6.1 ± 0.3	13.4 ± 0.7	502 ± 48	37 ± 4
ACF#2	4.44*10 ⁵	6.3 ± 0.2	14.2 ± 0.5	532 ± 50	37 ± 4
ACF#7	3.25*10 ⁵	10.0 ± 0.2	30.8 ± 0.6	3585 ± 185	116 ± 6
ACF#9	3.61*10 ⁵	6.8 ± 0.04	18.8 ± 0.1	11636 ± 943	618 ± 50

Also, these calculations show the successful incorporation of different concentrations of ssDNA. Here, ACF#7 reaches about three times as many DNA molecules per liposome and ACF#9 only 17 times as many DNA molecules. However, the slight deviations from the expected values may be caused by the used approximations as in case of the bilayer thickness or the headgroup surface area.

4.3.3. Control Experiments and Imaging

As the control experiments were conducted with Alexa647 tagged oligonucleotides hybridization with the liposomes was first tested also with this molecule. Finally, fluorescence spectra were recorded to quantify the amount of bound fluorescent oligonucleotides, which should directly correspond to the amount of DNA on the liposomal surface.

4.3.3.1. Estimation of the DNA Concentration on the Liposomal Surface

Figure 4.2 shows the fluorescence spectra for three different batches of liposomes, ACF#1, 2 and 7. A concentration of 7.6 nM of the pure dye-tagged oligonucleotide was used as standardization for the concentration determination.

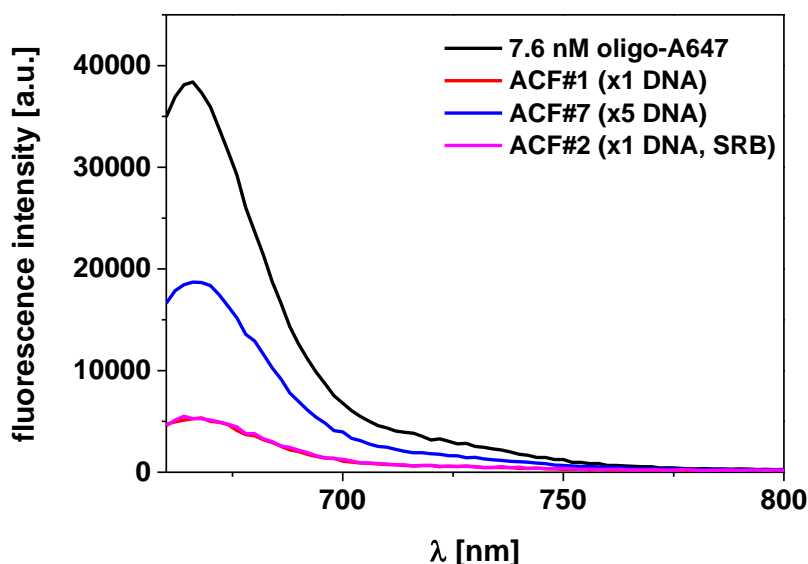


Figure 4.2. Fluorescence spectra of ACF#1, ACF#2 and ACF#7 after hybridization of oligoA647 and purification by centrifugation to determine DNA concentration on liposome surface. Spectra were recorded on a Fluorolog (Horiba Scientific) between 660 and 800 nm with $\lambda_{ex}=650$ nm.

The concentrations in the samples were estimated to be 1 μ M for the low concentrated DNA liposomes and 3.7 μ M for the liposomes with higher DNA content (Table 4.4, Chapter 4.3.3.3.). In order to investigate the efficiency of the purification by centrifugation, a control experiment was conducted to estimate the amount of liposomes that are lost during centrifugation (Figure 4.3).

Therefore, fluorescence spectra of oligonucleotide tagged SRB liposomes were recorded before and after centrifugation. The corresponding spectra are shown in Figure 4.3. The spectra clearly show that after centrifugation only about 10% of the initial signal is left. Which suggests that about 90% of the liposomes is lost during centrifugation either by insufficient pelleting of all liposomes or by disruption of the liposomes during the harsh purification.

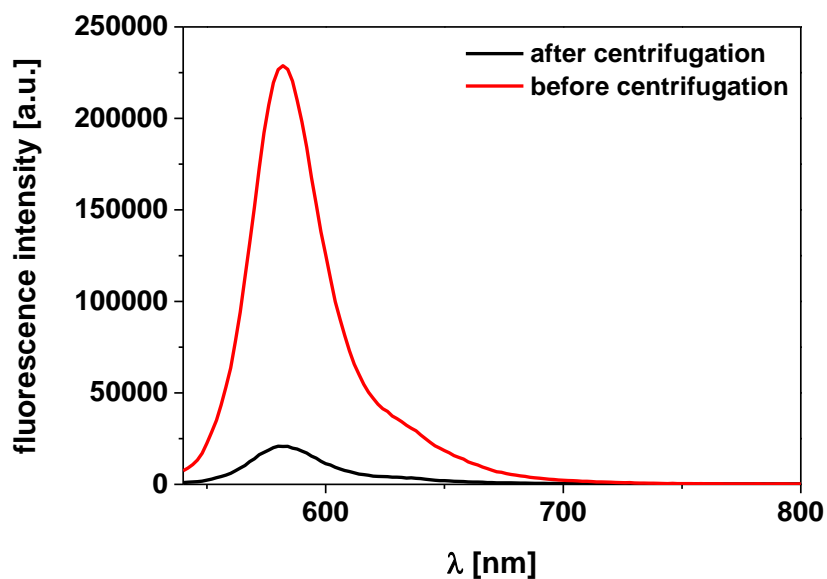


Figure 4.3. Fluorescence spectra of ACF#2 before and after hybridization of oligoA647 followed by purification by centrifugation. Spectra were recorded on a Fluorolog (Horiba Scientific) between 540 and 800 nm with $\lambda_{ex}=520$ nm.

4.3.3.2. Quenching of Oligo-A647 After Hybridization

In order to see if the fluorescence of the dye-tagged oligonucleotide is quenched during hybridization, fluorescence spectra were recorded of the free ssDNA, right after mixing with the liposomes and after a 1h hybridization. The spectra are shown in Figure 4.4.

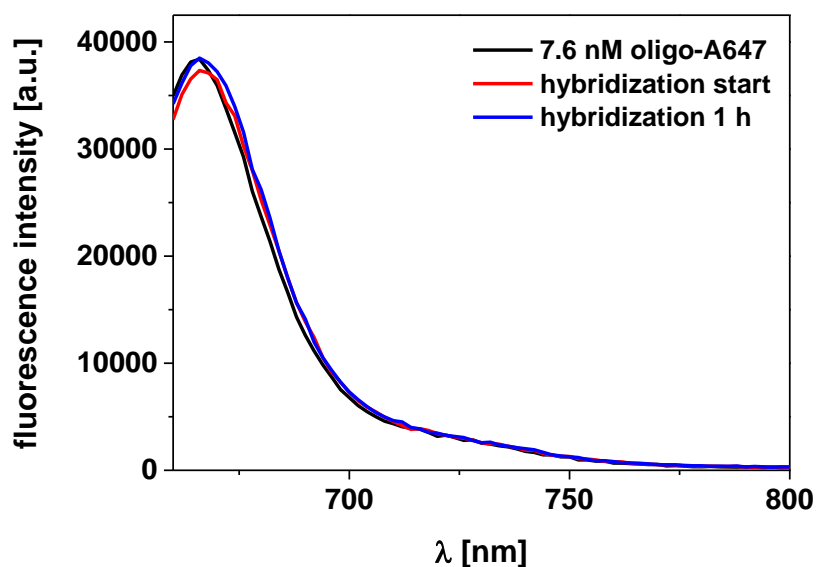


Figure 4.4. Influence of hybridization with complementary strand on fluorescence intensity of oligoA647. Spectra were recorded on a Fluorolog (Horiba Scientific) between 660 and 800 nm with $\lambda_{ex}=650$ nm.

In the beginning, most of the ssDNA is expected to be free in solution, thus no quenching is expected, which can also be seen in the fluorescence spectrum. Even after 1 h of incubation, thus after hybridization with the DNA-tagged liposomes, no quenching can be observed. Therefore, hybridization with a fluorophore-tagged oligonucleotide is well suited for quantification of the DNA concentration on the liposomal surface.

4.3.3.3. Determination of Free Oligo-A647 After Purification by Centrifugation

Another control experiment was conducted to determine the concentration of free dye-tagged ssDNA that may still be present after centrifugation. For this magnetic microparticles bearing the complementary DNA strand on their surface were mixed with the solution, which may still contain dye-tagged oligonucleotides that are not bound to the liposomes. The free oligonucleotides are then able to bind to the microparticles, which can be observed via microscopic images as shown in Figure 4.5. For quantification a calibration curve with free oligo-A647 was applied. The results of the quantification are shown in Table 4.4.

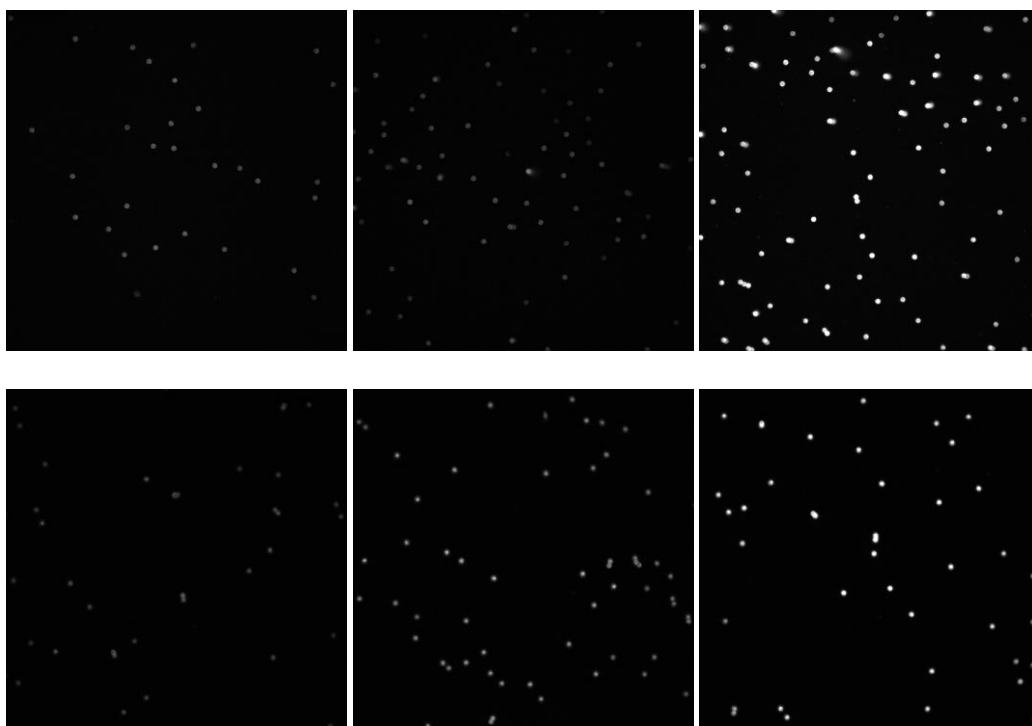


Figure 4.5. Microscopic images of residual oligoA647 bound to oligo-tagged microparticles. Top: ACF#1,2,7 (left to right), bottom: oligoA647 15,30 and 60 pM (left to right). Scale 103-2500.

After centrifugation only about 3-4% of free oligonucleotides can still be found in the sample, which is very low. However, the concentrations of the ssDNA on the liposome surface was corrected by the number of free oligonucleotides left. The concentrations of DNA in the liposome stock solution was then compared to the measurements conducted with the Cy5-tagged oligonucleotides. In both cases the quantified DNA lies in the expected range. In case of the low DNA concentrated liposomes the

Alexa647-tagged oligonucleotides yielded slightly higher concentrations. For quantification of ssDNA on the liposome surfaces only one concentration of oligo-A647 was used for standardization, not a complete calibration curve. This may have caused these slight deviations.

Table 4.4. Results of analysis of fluorescence measurements of ACF#1, ACF#2 and ACF#7 after hybridization of oligoA647 and purification by centrifugation to determine DNA concentration on liposome surface. Background correction was applied and a 7.6 nM solution of oligoA647 was measured for standardization.

	c(oligoA647)	ACF#1	ACF#7	ACF#2
c(sample) [nM]	7.6	1.0	3.7	1.0
c(oligoA647 stock after centrifugation) [nM]		50	184	51
Free oligo A647 in stock after centrifugation [nM]		2.1 ± 0.15	6.5 ± 0.31	1.4 ± 0.07
c(oligoA647 stock after centrifugation) corrected [nM]		48 ± 0.15	178 ± 0.31	49 ± 0.07
c(oligoA647 stock) estimated [μM]		0.96 ± 0.003	3.6 ± 0.006	0.98 ± 0.001
c(oligoCy5 stock) [μM]		0.50 ± 0.05	3.6 ± 0.19	0.53 ± 0.05

4.3.4. Fluorescence Correlation Spectroscopy of Liposomes

Fluorescence correlation spectroscopy is a method that is commonly used *e.g.* for the investigation of diffusion coefficients, the kinetics of chemical reactions or the quantification of fluorescent molecules or particles.^[21,22] Here, the fluorescence of particles as a function of the time is measured while Brownian motion of the particles leads to fluctuations in the fluorescence intensity.^[21] The excitation light is focused on a diluted sample using a dichroic mirror and a confocal microscope.^[22] The focal volume is very small (fl) and contains ideally only a few molecules.^[22,23] If a fluorescent particle passes this focal spot it gets excited by the laser beam and emits light that can be detected.^[21] The fluorescence fluctuations caused by diffusion of the particles can be expressed via an autocorrelation function^[21-23] as shown in Figure 4.6. The smaller the particles are, the faster is the diffusion, which results in higher fluctuations and a shift of the autocorrelation towards shorter correlation times (Figure 4.6, oligo-A647).

This also allows an estimation of the hydrodynamic radius. By fitting of the autocorrelation function the determination of diffusion coefficients and the $G(0)$ value is possible. As this value is indirectly proportional to the number of particles, it can be used for the determination of the particle concentration.^[22]

Fluorescence correlation spectroscopy was applied for the three different batches of liposomes after hybridization with an Alexa647 oligonucleotide and purification by centrifugation. In addition, a known concentration of an Alexa647-tagged oligonucleotides was analyzed for standardization. The corresponding autocorrelation functions were normalized to (0,1) and are shown in Figure 4.6.

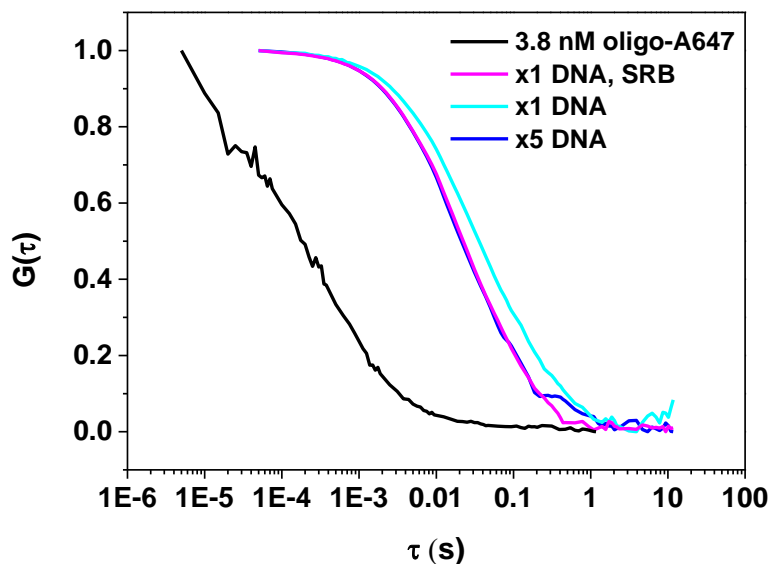


Figure 4.6. Autocorrelation function of FCS measurements of ACF#1, ACF#2 and ACF#7 after hybridization with oligoA647 and purification by centrifugation. A 3.8 nM solution of oligoA647 was used for standardization. Curves are normalized to (0;1).

$G(0)$ values were calculated by the software as listed in Table 4.5 and enable the determination of the particle number N_p :

$$N_p = \frac{1}{G(0)} \quad (4.3)$$

The liposome concentration was calculated using the number of A647-tagged oligonucleotides with a known concentration of 3.8 nM:

$$c(\text{liposomes}) = \frac{N_p(\text{liposomes}) * c(\text{oligoA647})}{N_p(\text{oligoA647})} \quad (4.4)$$

The liposome concentrations in the samples obtained via FCS range from 2-4 nM (Table 4.5). However, about 80-90% of liposomes are lost during purification via centrifugation that is done before the measurements (Figure 4.3). Therefore, the liposome concentration in the stock solution is estimated to be 5-10 times higher than the one determined by FCS. Moreover, these numbers correlate well with the theoretically calculated liposome concentrations from Chapter 4.3.2.

Thus, fluorescence correlation spectroscopy is well suited for the analysis of liposomes and enables the quantification of the actual number and concentration of liposomes and not only the lipid

concentration. As the diffusion coefficient is related to the hydrodynamic diameter of the vesicles, it can be calculated using the Stokes-Einstein equation:^[22]

$$D = \frac{k_B T}{6\pi\eta r}, \text{ so } r = \frac{k_B T}{6\pi\eta D} \quad (4.5)$$

with $k_B=1.28\text{E-}23$, $T=298$ K and $\eta=0.891$ cP. The corresponding diffusion coefficients D were determined by the software and are listed in Table 4.5 as well as all other values determined by fluorescence correlation spectroscopy.

However, the values obtained for the hydrodynamic diameter slightly differ from the DLS analysis. DLS analysis was applied before hybridization with the fluorophore-tagged oligonucleotide. Thus, a slightly higher diameter after hybridization is also expected.

Table 4.5. Results of FCS data of ACF#1, ACF#2 and ACF#7 after hybridization with oligoA647 and purification by centrifugation measured at 640 nm, 20 kHz and 25% power. $G(0)$ and D were obtained by a fit of the software. The radius was calculated using the Stokes Einstein equation.

	ACF#7 (x5 dilution)	ACF#1	ACF#2	oligoA647
G(0)	0.4	0.05	0.09	0.06
cps	119665	138375	215462	26470,7
cpp	47866	6780	18961	1482
N(particles)	2.5	20.4	11.4	17.9
c(liposomes, sample) [nM]	2.7	4.3	2.4	3.8
c(liposomes, calculated) [nM]	30.8 ± 0.6	13.4 ± 0.7	14.2 ± 0.5	
D [μm²/s]	1.8	1.2	1.9	100
r [nm]	136	204	129	2.5
d [nm]	272	408	258	5
d[nm] by DLS	123 ± 31	177 ± 46	179 ± 46	

4.3.5. Imaging of DNA-Tagged SRB Liposomes

The properties of the liposomes were not only analyzed by simple fluorescence measurements and fluorescence correlation spectroscopy but also by fluorescence imaging on a confocal microscope. For this, liposomes encapsulating 1 mM SRB and bearing 10 times as many DNA molecules as ACF#1 were applied.

4.3.5.1 Specificity of Binding

In order to see if the ssDNA-tagged liposomes bind specifically to the complementary DNA strand they were incubated with magnetic microparticles bearing the corresponding sequence. Unbound liposomes were separated magnetically. Figure 4.7 shows the imaging analysis.

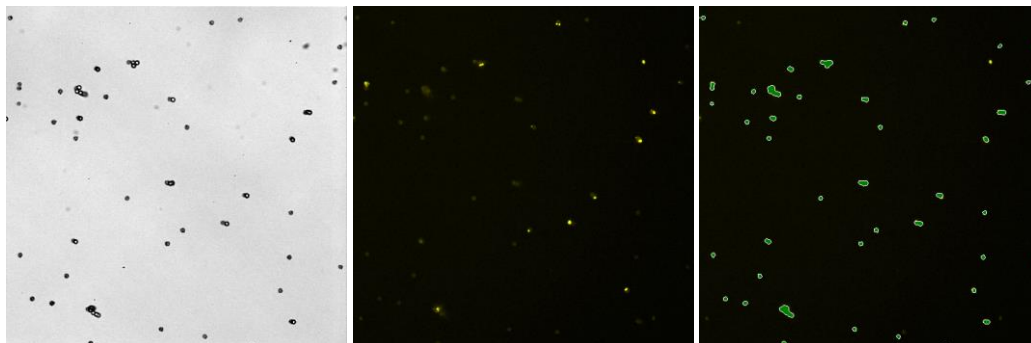


Figure 4.7. Binding of liposomes to oligo-tagged microparticle. Intensity not very high, but specific binding to the particles is observed.

On the left image only the microparticles are visible, the image in the middle shows the fluorescent liposomes. On the right image an overlay of these two images is shown, which clearly shows that the fluorescent liposomes overlap with the spots of the microparticles. This suggests a specific binding of the liposomes to the complementary strand on the microparticles. This was not only tested for one concentration of liposomes but for a series of 2-fold dilutions of liposomes as shown in Figure 4.8. The more liposomes are present, the more should be able to bind to the microparticles, which in turn leads to a higher fluorescence intensity, which is also shown in Figure 4.8.

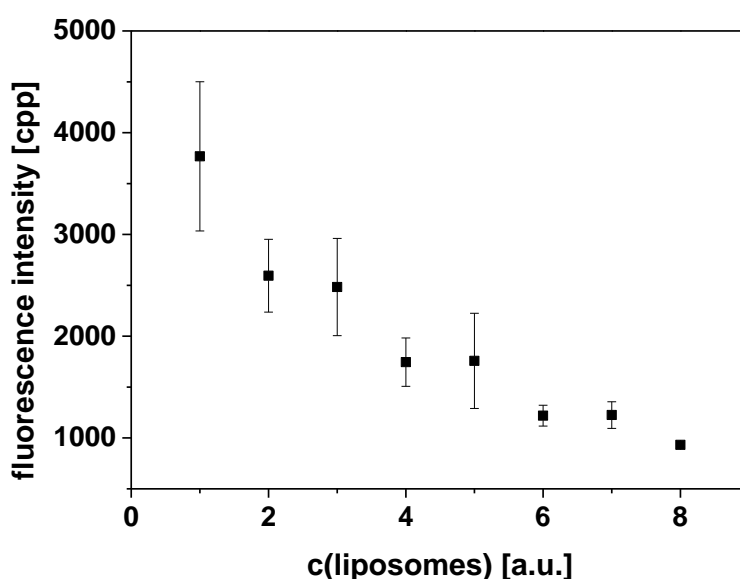


Figure 4.8. Dose response curve of liposomes binding to oligo-tagged microparticle, $n=4$. Liposome concentrations of 1-8 are arbitrary units with 1 as highest concentration followed by serial dilutions (2-fold).

4.3.5.2. Signal Enhancement Using Liposomes

The binding behavior was also compared to free dye-tagged oligonucleotides. The free oligonucleotides consist of the same sequence as the ssDNA on the liposomal surface. This time magnetic goat-anti-mouse microparticles were applied bearing the complementary DNA sequence for binding to the free oligonucleotides and the liposomes. To enable a direct comparison, concentrations were adjusted to the expected number of oligonucleotides present. The left image shows the fluorescence intensity of the free dye-tagged oligonucleotides, whereas the intensity of the liposomes is shown on the right (Figure 4.9).

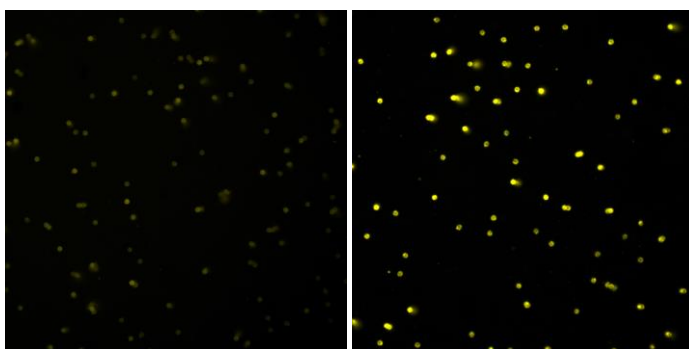


Figure 4.9. Binding of oligoA546 and SRB liposomes to antibody-particle conjugate. Scale 300-15.000.

As expected, a much higher signal is obtained in case of the liposomes. In case of the free oligonucleotides more molecules are able to bind to the particle conjugate whereas only one or two oligonucleotides on the liposomal surface probably participate in the binding due to steric hindrance. However, liposomes can entrap thousands of dye molecules in their interior, which overcomes this drawback and results in a significantly higher signal for the same amount of available ssDNA molecules. This can also be seen in Figure 4.10.

Here, a dose response curve is shown for an increasing concentration of available oligonucleotides for both, the free dye-tagged oligonucleotides and the ssDNA-tagged liposomes. In both cases the signal increases with a higher amount of ssDNA. The increase is significantly higher in case of the liposomes.

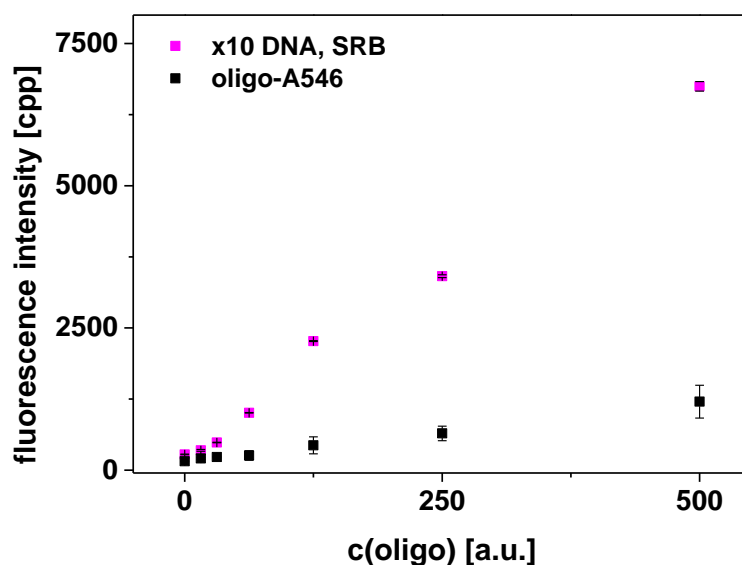


Figure 4.10. Serial 2fold dilutions of oligo-tagged SRB liposomes and oligoA546strand bound to complementary oligo-tagged-antibody-particle conjugate, $n=4$.

4.3.5.3. Lysing Conditions

The applied fluorescent liposomes entrap sulforhodamine B at a concentration of 1 mM. At this concentration part of the fluorescence is quenched due to self-quenching effects. By lysis of the liposomes the entrapped dye is released and diluted in the surrounding buffer, which can be observed via a strong increase in the fluorescence signal. This effect was investigated via fluorescence images at different concentrations of the detergent OG, which is commonly applied for liposome lysis. For this, the liposomes were again attached to magnetic microparticles to enable the analysis, which is shown in Figure 4.11.

The dispersion on the left image contains no detergent. Here, the fluorescence of the intact liposomes is still located on the particles. The image in the middle contains 17 mM OG. Here, the fluorescence intensity on the particles is already decreased, suggesting that some of the vesicles already rupture. At a detergent concentration of 22 mM as shown on the right image the fluorescence intensity drops to 0 suggesting complete lysis of the liposomes. In addition, strong background fluorescence can be observed due to the high concentration of released dye molecules.

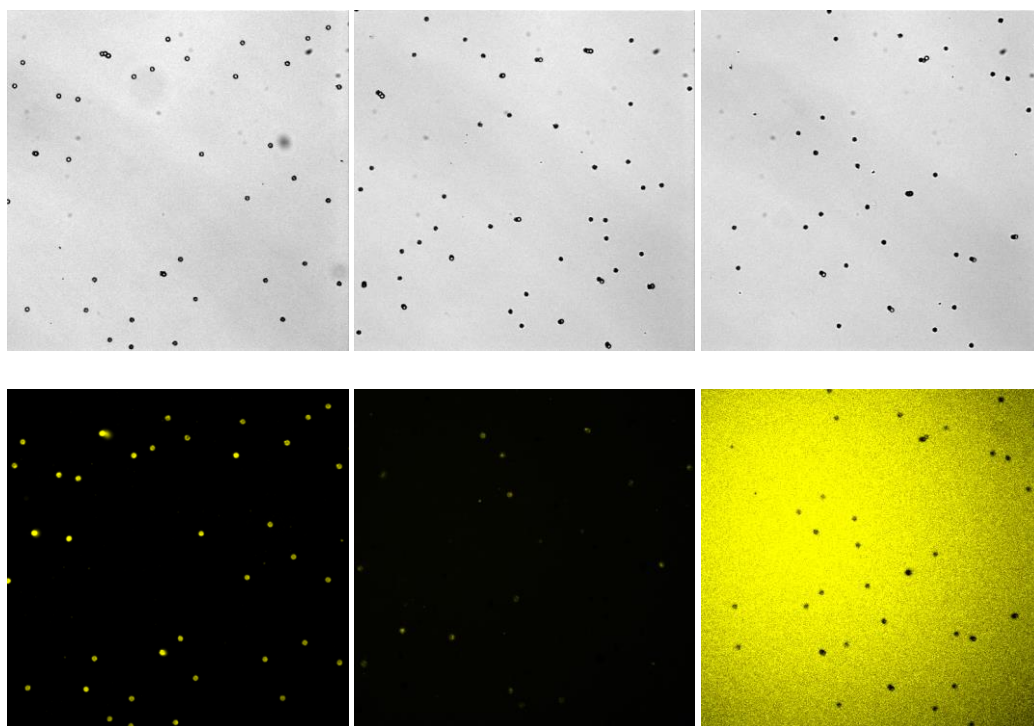


Figure 4.11. Effect of addition of OG (0, 17 and 22 mM) before removal of released dye. Scale 600-20.000 (for A,B) and 600-1000 for C.

Fluorescence analysis was again conducted after removal of the released dye molecules, which is shown in Figure 4.12 for detergent concentrations between 0 and 50 mM.

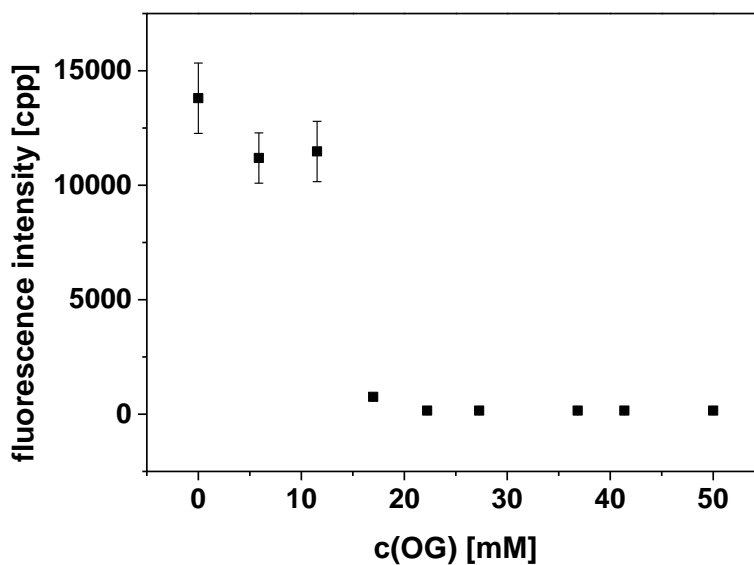


Figure 4.12. Effect of addition of OG (0-50 mM) after removal of released dye, $n=4$. At 20 mM OG intensity on particles drops to zero, suggesting complete lysis of the liposomes.

High fluorescence intensities can be measured for low detergent concentrations up to 12 mM followed by a sudden drop at 17 mM, which is reduced to 0 at detergent concentrations of 22 mM or more. At low detergent concentrations no lysis of the liposomes takes place, thus no or only a few dye molecules are released and removed, which explains the high fluorescence intensities. The more liposomes are lysed, the more dye is released, which can be removed. At detergent concentrations of 22 mM or more no residual fluorescence can be measured suggesting a complete lysis of the liposomes.

4.4. Conclusions

It was shown that the synthesis of DNA-tagged liposomes is possible up to 0.65 mol% of introduced cholesterol-tagged ssDNA, while all preparations showed similar characteristics regarding the diameter and ζ -potential. The incorporation of higher DNA concentrations may also be possible but could affect the functionality of the liposomes due to steric hindrance caused by the multiple DNA strands on the liposome surface. Moreover, quantification of the surface available ssDNA via hybridization with a fluorophore-tagged oligonucleotide was successful and revealed values in the expected range. It could also be shown that hybridization of the complementary strand doesn't affect the fluorescence signal and almost no free dye-tagged oligonucleotides could be found after centrifugation. However, the loss of 80-90% of liposomes during purification via centrifugation is extremely high. Therefore, improvements regarding the purification are essential to provide a more efficient assay. Here, chromatography-based approaches may be a good alternative. Also, FCS measurements were successfully applied to the labeled liposomes and enabled the calculation of vesicle concentrations which correlate well with theoretical calculations. Functionality of the DNA-tagged liposomes was proven by specific binding to oligo-tagged microparticles as shown by fluorescence imaging. A similar experiment also clearly shows the superior performance of DNA-tagged liposomes over simple fluorophore-tagged oligonucleotides regarding signal enhancement. Moreover, these experiments are well suited to image the ideal lysis conditions for the release of the entrapped fluorophores from the inner cavity of the liposomes and therefore provides an ideal platform for the development of liposome-based bioassays with fluorescence imaging readout.

References

- [1] B. Liu, J. Liu, *Anal. Methods* **2017**, *9*, 2633.
- [2] a) Y.-W. Lin, C.-W. Liu, H.-T. Chang, *Anal. Methods* **2009**, *1*, 14; b) J.-S. Lee, M. S. Han, C. A. Mirkin, *Angew. Chem. Int. Ed. Engl.* **2007**, *46*, 4093.
- [3] a) I.-M. Hsing, Y. Xu, W. Zhao, *Electroanalysis* **2007**, *19*, 755; b) H. Li, Z. He, *Analyst* **2009**, *134*, 800.
- [4] E. Palecek, M. Fojta, *Talanta* **2007**, *74*, 276.

- [5] B. Rittich, A. Spanová, *J. Sep. Sci.* **2013**, *36*, 2472.
- [6] E. Ruiz-Hernández, A. Baeza, M. Vallet-Regí, *ACS Nano* **2011**, *5*, 1259.
- [7] A. Bitar, N. M. Ahmad, H. Fessi, A. Elaissari, *Drug Discov. Today* **2012**, *17*, 1147.
- [8] X. Zhao, R. Tapeç-Dytioco, W. Tan, *J. Am. Chem. Soc.* **2003**, *125*, 11474.
- [9] E. Climent, L. Mondragón, R. Martínez-Mañez, F. Sancenón, M. D. Marcos, J. R. Murguía, P. Amorós, K. Rurack, E. Pérez-Payá, *Angew. Chem. Int. Ed. Engl.* **2013**, *52*, 8938.
- [10] K. A. Edwards, A. J. Baeumner, *Anal. Bioanal. Chem.* **2006**, *386*, 1613.
- [11] C. Jumeaux, O. Wahlsten, S. Block, E. Kim, R. Chandrawati, P. D. Howes, F. Höök, M. M. Stevens, *ChemBioChem* **2018**, *19*, 434.
- [12] a) K. A. Edwards, A. J. Baeumner, *Anal. Chem.* **2014**, *86*, 6610; b) M. Mayer, S. Takegami, M. Neumeier, S. Rink, A. Jacobi von Wangelin, S. Schulte, M. Vollmer, A. G. Griesbeck, A. Duerkop, A. J. Baeumner, *Angew. Chem. Int. Ed. Engl.* **2018**, *57*, 408.
- [13] C. Zylberberg, K. Gaskill, S. Pasley, S. Matosevic, *Gene Ther.* **2017**, *24*, 441.
- [14] H. Daraee, A. Etemadi, M. Kouhi, S. Alimirzalu, A. Akbarzadeh, *Artif. Cells Nanomed. Biotechnol.* **2016**, *44*, 381.
- [15] K. Qi, Q. Ma, E. E. Remsen, C. G. Clark, K. L. Wooley, *J. Am. Chem. Soc.* **2004**, *126*, 6599.
- [16] C. Hofmann, G. Roth, T. Hirsch, A. Duerkop, A. J. Baeumner, *Colloids Surf., B* **2019**, *181*, 325.
- [17] a) A. Hennig, A. Hoffmann, H. Borchering, T. Thiele, U. Schedler, U. Resch-Genger, *Anal. Chem.* **2011**, *83*, 4970; b) O. Lorenz, N. Breidenich, U. Denter, K.-H. Reinmüller, G. Rose, *Angew. Makromol. Chem.* **1982**, *103*, 159.
- [18] M. Moser, T. Behnke, C. Hamers-Allin, K. Klein-Hartwig, J. Falkenhagen, U. Resch-Genger, *Anal. Chem.* **2015**, *87*, 9376.
- [19] a) M. Gaborieau, L. Nebhani, R. Graf, L. Barner, C. Barner-Kowollik, *Macromolecules* **2010**, *43*, 3868; b) J. M. Goddard, J. H. Hotchkiss, *Prog. Polym. Sci.* **2007**, *32*, 698; c) S. Rödiger, M. Ruhland, C. Schmidt, C. Schröder, K. Grossmann, A. Böhm, J. Nitschke, I. Berger, I. Schimke, P. Schierack, *Anal. Chem.* **2011**, *83*, 3379; d) Y. Xing, N. Dementev, E. Borguet, *Curr. Opin. Solid State Mater. Sci.* **2007**, *11*, 86.
- [20] C. Fenzl, C. Genslein, C. Domonkos, K. A. Edwards, T. Hirsch, A. J. Baeumner, *Analyst* **2016**, *141*, 5265.

- [21] E. L. Elson, *Biophys. J.* **2011**, *101*, 2855.
- [22] E. Haustein, P. Schwille, *Annu. Rev. Biophys. Biomol. Struct.* **2007**, *36*, 151.
- [23] A. Ghosh, N. Karedla, J. C. Thiele, I. Gregor, J. Enderlein, *Methods* **2018**, *140-141*, 32.

5 Electrostatic Interactions of Cationic Liposomes for Pathogen Detection

Abstract

Many infections are caused by bacteria and can lead to serious diseases or even death. Thus, early detection of such infections is important. However, conventional techniques for bacteria quantification like cell culturing can be very time-consuming. Also, nanomaterial-based assays often suffer from long response times, low sensitivity or unsatisfying limits of detection. Thus, there is need for a fast and simple detection of bacteria. Therefore, highly stable cationic liposomes entrapping either sulforhodamine B or a water-soluble luminol derivative were developed to enable fluorescent or chemiluminescent analysis of bacteria. The positive surface charge of these vesicles can be exploited for electrostatic interactions with the negatively charged surface of bacteria. Successful interaction with *E.coli* as model analyte was shown by the formation of pink aggregates visible by bare eye. For quantification two different assay types were investigated and optimized. Separation of unbound material was either based on simple centrifugation or on the immobilization of the bacteria on Poly-L-Lysin coated 96 well plates. With fluorescence analysis of bound SRB encapsulating liposomes detection limits of 10^7 - 10^6 cfu ml⁻¹ were achieved depending on the assay type. The centrifugation assay in combination with chemiluminescence analysis using m-carboxy-luminol encapsulating liposomes enabled a detection of *E.coli* even down to 10^5 cfu ml⁻¹. If limitations like limited immobilization efficiency on the 96 well plates or the high blank values in case of centrifugation can be overcome, this method offers the possibility for a simple and universal detection of gram-positive and gram-negative bacteria without the need for vesicle surface functionalization.

Parts of this chapter are intended for publication.

Author contributions:

The author did most of the experimental work and wrote this chapter. Barbara Kaiser contributed with ζ -potential measurements of the *E.coli* cells and the fluorescence microtiter plate assay in different buffers as part of a research internship under the supervision of the author. Susanne Märkl contributed with measurements of the interaction of cationic liposomes and magnetic beads. Thomas Hirsch, Axel Duerkop and Antje J. Baeumner contributed with strategic discussions. Antje J. Baeumner was the leader of this project.

This chapter contains sections that were in part already described in Carola Figalist's master's thesis. This includes paragraphs within the experimental part regarding the liposome preparation and characterization. The master's thesis is entitled "Positively Charged Liposomes for Signal Enhancement via Electrostatic Interactions" and was submitted to the Faculty of Chemistry and Pharmacy at the University of Regensburg in December 2014. Sections that are identical or similar to the master's thesis are listed here in detail and are indicated in this chapter by the citation "M":

- p.104, subchapter 5.2.1., paragraph 2 (experimental)
- p.104-105, subchapter 5.2.2.1, 5.2.2.2.1., 5.2.2.2.2. (experimental)
- p.107, subchapter 5.2.2.8., paragraph 2 (experimental)

5.1. Introduction

Pathogenic bacteria like *E.coli*, *Salmonella* or *S.aureus* cause numerous infections each year which can lead to serious diseases and in some cases even to death.^[1,2] Thus, an early, fast and accurate detection of the pathogens is very important and remains a huge challenge, especially in the area of food safety and clinical diagnosis.^[1,3] Conventional techniques for pathogen detection include mainly culture and colony counting, immunological assays and polymerase chain reaction (PCR)-based methods.^[4] Although they usually provide a high specificity and sensitivity, they also suffer from several drawbacks. Quantification by culturing techniques for example often takes at least two days to obtain an initial result and is restricted to culturable bacteria.^[4] ELISAs are less time-consuming and widely applied in clinical laboratories but still require multiple incubation steps and several hours of runtime.^[4,5] Moreover, PCR-based methods require expensive specialized equipment and reagents and are prone to interferences by non-pathogenic genetic material which can cause false-positive results.^[4,5]

Therefore, various other methods for the detection of bacteria have been proposed in the last years, whereby many of them include the use of nanomaterials. Here, for example the use of gold, silica or magnetic nanoparticles or polydiacetylene (PDA) vesicles has been reported.^[4,6] However, issues regarding the detection limit, operation time and the toxicity of some materials often remain unsolved.^[3] Moreover, liposomes have been widely applied for pathogen detection. DNA-tagged liposomes have for example been reported for the picomolar detection of *C.parvum*.^[7] Cystein-loaded liposomes in combination with gold nanoparticles enabled even an attomolar detection of *Salmonella*, *Listeria* and *E.coli O157*.^[8] Usually these methods are based on specific receptor moieties on their surface, e.g. carbohydrates, antibodies, oligonucleotides or peptides, for the specific recognition of the analyte.^[3,7] However, also some biosensors based on electrostatic interactions have been reported, e.g. for amine-functionalized PDA vesicles which respond to bacteria that secrete the negatively

charged surfactin.^[9] In addition, not only released substances can be exploited for sensing, but also the surface potential of the bacteria themselves.

Bacteria usually exhibit an anionic surface charge caused by the thick negatively charged peptidoglycan layer in case of gram-positive bacteria and by the presence of lipopolysaccharides and porins on the outer membrane of gram-negative bacteria.^[5] The surface charge of liposomes can *e.g.* be tuned by the introduction of lipids or amphiphiles with charged headgroups. DOTAP, DC-chol or ethylphosphocholines are *e.g.* commonly applied for the preparation of cationic liposomes.^[10] As liposomes can be loaded with a variety of molecules they have also been studied as carriers for antibiotics.^[11] Therefore, also the electrostatic interaction between cationic liposomes and the respective bacteria is of major importance. Several studies confirm the successful interaction of cationic liposomes with bacteria like *Pseudomonas aeruginosa*, *E.coli*, *Salmonella* or *S.aureus*.^[11–13] However, these studies focus on the bactericidal action of cationic liposomes whereas only few studies have been reported that exploit this property for the direct detection of bacteria. Petaccia *et al.* for example introduced a fluorescent, surface potential sensitive probe into the lipid bilayer which responds to the presence of some bacterial strains.^[3]

This study aimed to exploit the high loading capacity of the liposomes with dye molecules to develop an assay for the detection of the model analyte *E.coli* based on simple electrostatic interactions. Therefore, the cationic liposomes were either loaded with the fluorescent dye sulforhodamine B (SRB) or the chemiluminescent dye *m*-carboxy-luminol and investigated for their suitability in different assay setups.

5.2. Experimental

5.2.1. Materials

1,2-dipalmitoyl-sn-glycero-3-phosphatidylcholine (DPPC), 1,2-dipalmitoyl-sn-glycero-3-ethylphosphocholine (EDPPC), cholesterol and the extrusion kit and membranes were purchased from Avanti Polar Lipids (avantilipids.com). The dialysis membrane spectra/por 4 with a MWCO of 12-14 kDa was purchased from spectrum labs (www.spectrumlabs.com). *E.coli* was purchased from the DSMZ (www.dsmz.de). 4-(2-Hydroxyethyl)piperazine-1-ethanesulfonic acid (HEPES), sodium azide, Sephadex-G50, phosphate buffered saline, sulforhodamine B monosodium salt (SRB), poly-L-lysine, hemin and black microtiter plates from Nunc were bought from Sigma Aldrich (www.sigmaaldrich.com). White microtiter plates were bought from Greiner Bio-One (www.gbo.com/de). Glycine and carboxylated, magnetic beads (PureProteome™) were purchased from Merck (www.merckmillipore.com) and n-Octyl-β-D-glucopyranoside (OG) was bought from Roth (www.carlroth.com). *m*-carboxy-luminol was synthesized and kindly provided by the group of Prof. Dr.

Jacobi von Wangelin (University of Hamburg). LB broth was purchased from Alfa Aesar (www.alfa.com/de/). Bacteriological agar, hydrogen peroxide, potassium hydrogen carbonate as well as all other chemicals were of analytical grade and purchased from VWR (de.vwr.com).

Millipore water ($\geq 18.2 \text{ M}\Omega \text{ cm}$) was used for the preparations of all buffers and aqueous solutions needed for liposome preparation.^[M]

5.2.2. Methods

5.2.2.1. Synthesis of Cationic Liposomes by Reverse Phase Evaporation

DPPC (17.3 mg), EDPPC (4.5 mg) and cholesterol (0.6 mg) were dissolved in chloroform (3 ml) and methanol (0.5 ml) and sonicated at 60 °C for 1 minute. 2 ml of an aqueous solution containing either sulforhodamine B (10 mM, dissolved in 210 mM NaCl, 0.02 M HEPES, pH 7.5) or *m*-carboxy-luminol (25 mM, dissolved in 0.2 M HEPES, pH 8.5) was added and the mixture sonicated at 60 °C for 4 minutes. The organic solvent was removed by using a rotary evaporator at 60 °C and a pressure of 750 mbar for 40 minutes. The solution was vortexed, and another 2 ml of the aqueous solution was added. After vortexing again the solution was rotated at 60 °C and 750 mbar for 20 minutes and then again at 60 °C and 400 mbar for 20 minutes. The dispersion was being extruded through polycarbonate membranes (1 μm and 0.4 μm) at 60 °C by pushing the syringes back and forth 21 times for each membrane. Excess of the marker molecules was removed by size exclusion chromatography with a Sephadex G-50 column followed by dialysis against HSS (10 mM HEPES, 200 mM NaCl, 200 mM sucrose, 0.01% NaN_3 , pH 7.5, in case of sulforhodamine B) or Glycin-NaOH buffer (10 mM Glycin, 200 mM NaCl, 114 mM sucrose, 0.01% NaN_3 , pH 8.6, in case of *m*-carboxy-luminol).^[M]

5.2.2.2. Characterization of Liposomes

5.2.2.2.1. Determination of Size and ζ -Potential

Dynamic light scattering (DLS) and ζ -potential measurements were carried out on a Malvern Zetasizer Nano-ZS (www.malvern.com). For all measurements the temperature was set to 25 °C. Semi-micro PMMA cuvettes were used for size determinations, disposable folded capillary cells for the ζ -potential measurements. Before the measurements the samples were diluted 1:100. As setting for liposomes, a n_D^{20} of 1.34 and an Abs of 0.000 was selected and HSS buffer ($n_D^{20} = 1.342$, viscosity = $1.1185 \text{ kg}\cdot\text{m}^{-1}\cdot\text{s}^{-1}$, dielectric constant: 78.5) was used as dispersant. An equilibration time of 60 s was applied before each measurement.^[M]

5.2.2.2.2. Determination of Phospholipid Concentration

The phospholipid concentration was determined by using a Flame-EOP inductively coupled plasma optical emission spectrometer (ICP-OES) from Spectro (www.spectro.com). Therefore, 20 μl of the liposome sample was diluted in 2980 μl 0.5 M HNO_3 and could then be used for the measurement.

0.5 M HNO₃ and a solution of 100 μM of PO₄³⁻ in 0.5 M HNO₃ were used for calibration before each measurement.^[M]

5.2.2.3. Preparation of *E.coli* Culture

E.coli was cultivated in LB-medium (10 ml) over night at 37 °C under continuous shaking. 1 ml of the bacteria solution was then centrifuged for 5 min at 1500 rcf and the pellet resuspended in PBS buffer. For colony counting this stock solution was diluted 1:10⁶ and 50 μl of this solution spread onto an Agar plate and incubated overnight at 37 °C. This was done for 3 different plates and the grown colonies were counted the next morning.

5.2.2.4. Bactericidal Effect of Cationic Liposomes

The *E.coli* stock solution was diluted 1:10⁶ in LB-medium and subsequently mixed with different concentrations of cationic liposomes (0-200 μM in the final mixture). The dispersion was incubated for 1 h at room temperature followed by plating on Agar plates (50 μl/plate, 2 plates/concentration). The plates were incubated overnight at 37 °C and the grown colonies counted the next morning.

5.2.2.5. Bead Experiments

Liposomes (0-200 μM) were diluted in phosphate buffer (10 mM, pH 6) and added to the wells of a 96 well plate (100 μl/well). Then a 1:10 dilution of carboxy-magnetic beads was added (10 μl/well, 10 mg ml⁻¹ stock solution). After incubation at 23 °C, 500 rpm for 30 min, the bead-liposome aggregates were separated using a magnetic plate. The supernatant was removed, and the residual aggregates washed twice with HEPES buffer (200 μl/well). The fluorescence signal was read out with a FLUOStar OPTIMA microplate reader at wavelengths of λ_{ex}=544 nm and λ_{em}=575 nm and a gain of 1500 before (in 100 μl HSS) and after lysis with 30 mM n-octyl-β-D-glucopyranoside (OG, 100 μl). Three individual measurements of each dilution were made.

5.2.2.6. Microtiter Plate Coating with Poly-L-Lysin

Poly-L-Lysin (200 μl/well, 50 μg ml⁻¹ in PBS) was added to the wells of a white (for chemiluminescence analysis) or black MaxiSorp microtiterplate (for fluorescence analysis) and incubated overnight at 4 °C. Before using the plate, the Poly-L-Lysin solution was removed and the wells washed twice with PBS buffer.

5.2.2.7. Bacteria Assay

5.2.2.7.1. Bacteria Assay on Poly-L-Lysin Coated Microtiter Plates

The *E.coli* stock solution was transferred into PBS buffer and diluted to concentrations between 0 and 10⁸ cfu ml⁻¹. The dispersions were then incubated in the wells of a Poly-L-Lysin coated microtiterplate at room temperature for 1 h. After washing twice with PBS buffer cationic liposomes (50 μM in PBS) were added and incubated for 1 h at room temperature. The wells were then washed twice with PBS

buffer (200 $\mu\text{l}/\text{well}$). For fluorescence analysis PBS buffer (100 $\mu\text{l}/\text{well}$) was added and the fluorescence read out before and after lysis of the liposomes with n-Octyl- β -D-glucopyranoside solution (OG, 300 mM, 10 $\mu\text{l}/\text{well}$). Three individual measurements of each dilution were made. For chemiluminescence analysis carbonate buffer (0.1 M, 100 mM NaCl, pH 10.5, 186 $\mu\text{l}/\text{well}$), OG (300 mM, 10 $\mu\text{l}/\text{well}$) and Hemin (10 μM , 2 $\mu\text{l}/\text{well}$) were added after washing with PBS. H_2O_2 (2 mM, 4 $\mu\text{l}/\text{well}$) was added right before the measurement. Four individual measurements of each dilution were made.

5.2.2.7.2. Bacteria Assay with Centrifugation

5.2.2.7.2.1. Fluorescence Analysis

The *E.coli* stock solution was transferred into PBS buffer. Six different dilutions (1 ml each; 1:10, 1:100, 1:1000, 1:10⁴, 1:10⁵, and 1:10⁶) of the *E.coli* solutions were made in phosphate buffer (10 mM, pH 6) and cationic liposomes were added to them (50 μM). The mixture was centrifuged at 1500 rcf for 10 min). After removal of the supernatant the pellet was redispersed in 1 ml n-Octyl- β -D-glucopyranoside solution (30 mM). Fluorescence spectra were recorded between 560 and 654 nm with $\lambda_{\text{ex}}=544$ nm, $\lambda_{\text{em}}=575$ nm and a detector voltage of 550 V. Three individual measurements of each dilution were made.

5.2.2.7.2.2. Chemiluminescence Analysis

The *E.coli* stock solution was transferred into PBS buffer and diluted to concentrations between 0 and 10⁸ cfu ml⁻¹. The dispersions were then incubated with cationic liposomes (50 μM) for 4 h at room temperature. Then the mixture was centrifuged for 30 min at 1500 rcf, the supernatant removed, and the residuum resuspended in PBS buffer (500 μl). This step was repeated twice, after the last centrifugation the residuum was resuspended in carbonate buffer (0.1 M, 100 mM NaCl, pH 10.5, 500 μl) containing 30 mM OG. For the measurement the mixture was added to the wells of a white microtiter plate (100 $\mu\text{l}/\text{well}$). Hemin (10 μM , 1 $\mu\text{l}/\text{well}$) was added as catalyst for chemiluminescence analysis. H_2O_2 (2 mM, 2 $\mu\text{l}/\text{well}$) was added right before the measurement. Three individual measurements of each dilution were made.

5.2.2.7.3. Bacteria Assay with Magnetic Beads

The *E.coli* stock solution was transferred into PBS buffer and diluted to concentrations between 0 and 10⁸ cfu ml⁻¹. The dispersions were then incubated with magnetic beads (50 $\mu\text{g ml}^{-1}$) for 2 h at room temperature. After magnetic separation, the supernatant was removed, and the residuum was washed twice with PBS buffer (500 μl). After the second washing step the pellet was resuspended in PBS buffer containing the cationic m-carboxy-luminol liposomes (50 μM) and the mixtures incubated for 2 h at room temperature. Then unbound liposomes were removed by magnetic separation, the supernatant was removed, and the residuum washed twice with PBS buffer (500 μl). After the last

washing step, the pellet was resuspended in carbonate buffer (0.1 M, 100 mM NaCl, pH 10.5, 500 μ l) containing 30 mM OG. For the measurement the mixture was added to the wells of a white microtiter plate (100 μ l/well). Hemin (10 μ M, 1 μ l/well) was added as catalyst for chemiluminescence analysis. H₂O₂ (2 mM, 2 μ l/well) was added right before the measurement. Three individual measurements of each dilution were made.

5.2.2.8. Fluorescence Measurements

Fluorescence spectra of SRB encapsulating liposomes were recorded with an Aminco Bowman 2 spectrofluorometer between 560 and 650 nm with $\lambda_{\text{ex}}=544$ nm, $\lambda_{\text{em}}=575$ nm and a detector voltage of 550 V.

A FLUOStar OPTIMA microplate reader from BMG LABTECH (www.bmg-labtech.com) was used for the fluorescence measurements of SRB encapsulating liposomes. The emission was read out at wavelengths of $\lambda_{\text{ex}}=544$ nm and $\lambda_{\text{em}}=575$ nm.^[M] The gain was adjusted before each measurement and was always between 1200 and 1500.

5.2.2.9. Chemiluminescence Measurements

A BioTek microplate reader was used for the chemiluminescence measurements with *m*-carboxyluminol containing liposomes. Before chemiluminescence analysis Hemin (10 μ M, 1 μ l/well) was added to the lysed liposome dispersions. H₂O₂ (2 mM, 2 μ l/well) was added right before the measurement, the read height was adjusted to 6 mm. The gain was adjusted before each measurement and was always between 60 and 80.

5.3. Results and Discussion

5.3.1. Liposome Preparation and Characterization

The cationic liposomes used in this work were synthesized by reverse phase evaporation. Preparation parameters and lipid composition have been optimized with respect to vesicle diameter, colloidal stability and minimized dye leakage in a previous study.^[14] The optimized lipid composition is shown in Figure 5.1. The membrane is mainly composed of DPPC, which is a common zwitterionic phospholipid applied in liposome formulations. The addition of cholesterol helps to prevent leakage of entrapped molecules as this lipid is able to influence the membrane fluidity. EDPPC is a synthetic cationic phospholipid with an ethylated phosphate group. This lipid gives the vesicles an overall positive surface charge.

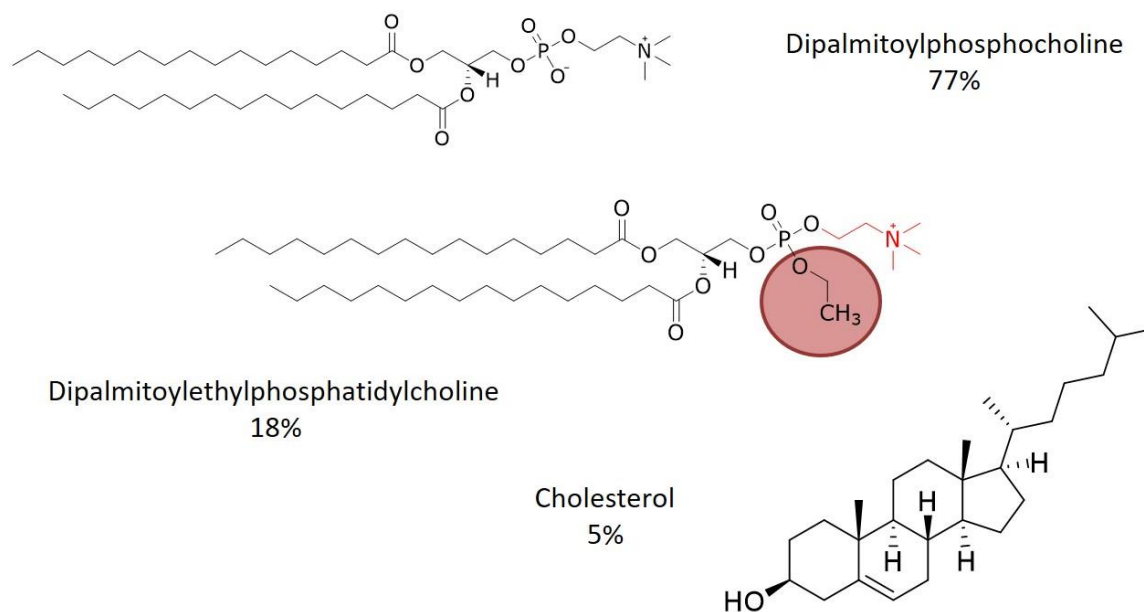


Figure 5.1. Optimized lipid composition for the preparation of cationic liposomes.

Liposomes prepared with this composition are between 160 and 250 nm in size with Pdl's usually below 0.2 which suggests a mostly monodisperse vesicle mixture (Figure 5.2). ζ -potentials recorded in HSS buffer are usually above +15 mV which guarantees the colloidal stability of the liposome dispersions.

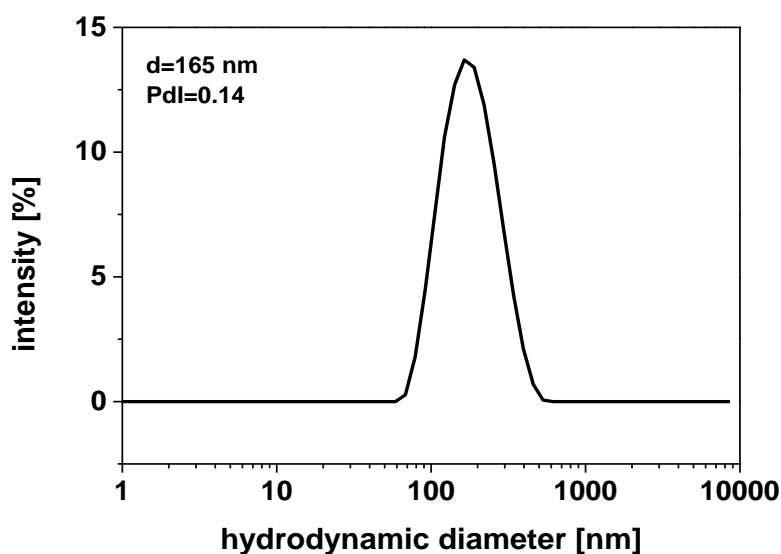


Figure 5.2. Hydrodynamic diameter of cationic SRB-encapsulating liposomes in HSS buffer determined by DLS.

5.3.2. Electrostatic Interaction with Magnetic Beads

Moreover, these vesicles have been demonstrated to be able to bind electrostatically to negatively charged surfaces and liposomes of similar size as shown by DLS, SPR, electrochemical and fluorescence measurements.^[14] Due to the fact that most bacteria, gram-positive and gram-negative, exhibit a negative surface charge, the liposomes should be able to bind to the cells and enable a simple detection method for bacteria. At first 1 μm big magnetic beads bearing carboxy groups on their

surface were applied as model for bacteria cells. For this, different concentrations of cationic liposomes entrapping the fluorescent dye sulforhodamine B were simply mixed with the beads in a microtiter plate and unbound material separated magnetically after an incubation of 30 minutes at room temperature. As negative control, the same was done for liposomes only without the addition of magnetic beads. Then, the fluorescence intensity of the bound liposomes was analyzed after lysis of the vesicles, which is shown in Figure 5.3.

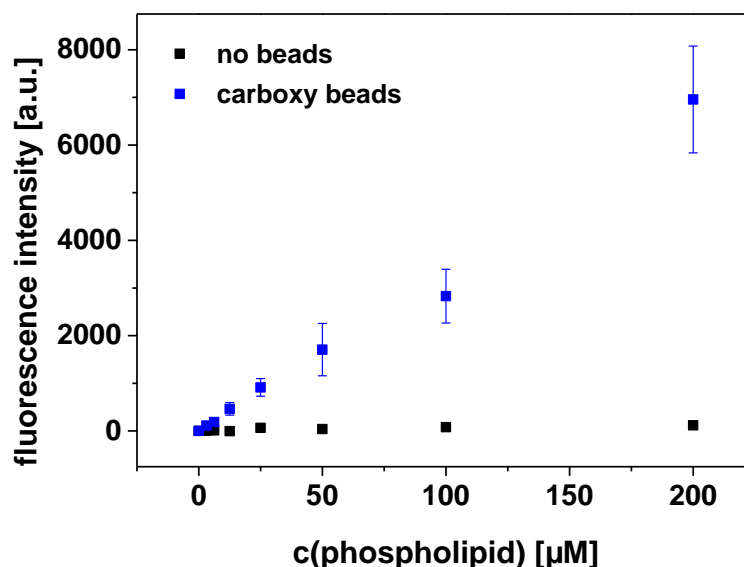


Figure 5.3. Different concentrations of liposomes bound to magnetic carboxy beads. Fluorescence intensities were read out on a FluostarOPTIMA microplate reader at $\lambda_{ex}=544$ nm and $\lambda_{em}=575$ nm and a gain of 1500, $n=3$.

As expected, no signal was obtained in case of the negative control experiment but a significant increase in the fluorescence intensity was observed with an increasing concentration of initially supplied liposomes. Thus, the more liposomes are present in the beginning, the more are able to bind to the negatively charged magnetic beads. This proves that these cationic liposomes are not only able to bind to similarly sized vesicles but also to bigger particles with negative surface charge, which exhibit a similar size as *e.g.* an *E.coli* cell. Thus, also a successful interaction with the anionic bacteria surface should be possible.

5.3.3. Bacteria Quantification via Fluorescence Readout

To proof the negative surface charge of the applied *E.coli* cells, ζ -potential measurements were conducted in phosphate buffer for a pH range from 4-9. Cationic liposomes were investigated in the same range to find the optimum pH for all further measurements. The results are shown in Figure 5.4.

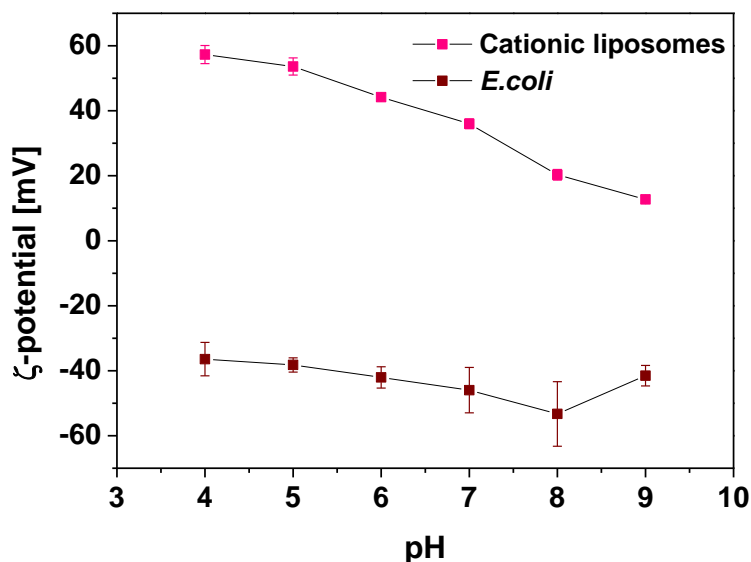


Figure 5.4. ζ -potentials of *E.coli* cells and cationic liposomes dispersed in phosphate buffer in a pH range of 4-9, $n=4$.

The ζ -potential values for the *E.coli* cells are always in the range of -40 to -50 mV with no significant influence of the pH. In contrast, the ζ -potential of the cationic liposomes decreases with increasing pH from +55 to +20 mV. However, as too acidic conditions may affect the stability of the liposomes and the *E.coli* cells during incubation, pH values between 6 and 7 were used for all further experiments.

Moreover, these opposite surface potentials suggest that an electrostatic interaction between the vesicles and the *E.coli* cells is possible and a resulting agglomeration may be exploited for detection of the bacteria. Therefore, different concentrations of *E.coli* cells were mixed with cationic liposomes in a cuvette. After a 2 h incubation the formation of pink agglomerates was observed on the bottom of the cuvette for a bacteria concentration of 10^8 cfu ml⁻¹ (Figure 5.5, left). For lower concentrations (10^5 cfu ml⁻¹, Figure 5.5, right) this agglomeration was not visible by bare eye anymore.

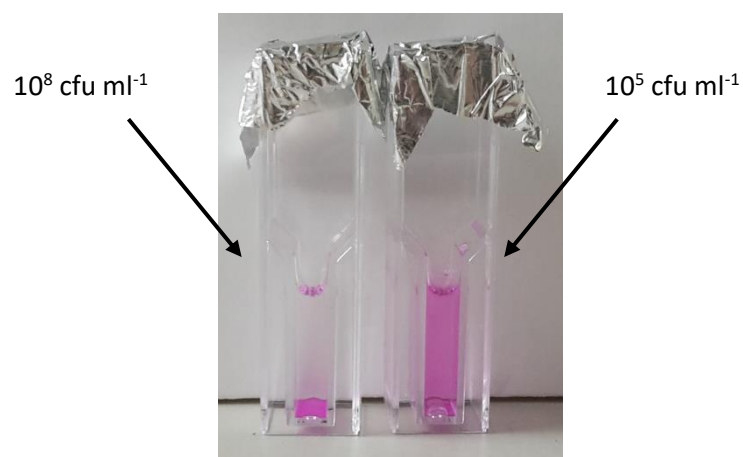


Figure 5.5. Mixtures of cationic liposomes and different concentrations of *E.coli* after a 2 h incubation at room temperature.

5.3.3.1. Centrifugation Assay

For separation of the vesicle-bacteria agglomerates from unbound liposomes centrifugation was applied. This resulted in the formation of pink pellets, which were washed and finally redispersed in OG. A decrease in color intensity was already observed by bare eye as shown in Figure 5.6.



Figure 5.6. Left: formation of pink pellet after centrifugation. Right: liposome-*E.coli* agglomerates after centrifugation and redispersion in 30 mM OG.

Then, also the fluorescence intensity of the lysed liposomes was determined. The more *E.coli* cells are present, the more liposomes should be able to bind and stronger agglomeration should take place. Thus, it was expected to see an increase in the fluorescence intensity with an increasing number of bacteria. Above *E.coli* concentrations of 10^6 cfu ml^{-1} the peak maxima can clearly be distinguished as shown in Figure 5.7. However, for lower concentrations the signals lie closely together and cannot be distinguished from each other anymore. Moreover, the formed pellets in case of the lower *E.coli* concentrations are much smaller and also less stable, which makes a reliable and complete removal of the supernatant almost impossible.

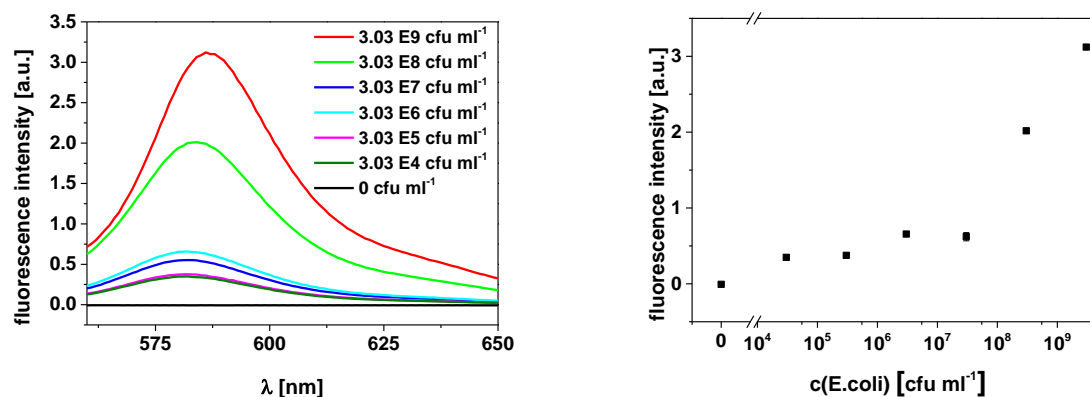


Figure 5.7. Fluorescence spectra and the corresponding intensities at the peak maximum of lysed liposomes after incubation with *E.coli* cells and separation via centrifugation. Fluorescence spectra were recorded between 560 and 650 nm using an Aminco Bowman 2 spectrofluorometer at $\lambda_{ex}=544$ nm and $\lambda_{em}=575$ nm and a detector voltage of 550 V, $n=3$.

5.3.3.2. Microtiter Plate Assay

Therefore, a different way for separation was tested. Here, black microtiterplates were coated with Poly-L-Lysin first. This polymer is positively charged, thus *E.coli* cells should be able to attach to the coated plate and at the same time it prevents the cationic liposomes from binding to the plate when no bacteria are present. After coating, different concentrations of *E.coli* were incubated in the wells and after removal of unbound cells, cationic liposomes were added to bind to the captured bacteria. Unbound liposomes were also removed by washing and the fluorescence intensity of the lysed liposomes was used for analysis. First, this was tested for different buffer systems, LB-medium and water as shown in Figure 5.8.

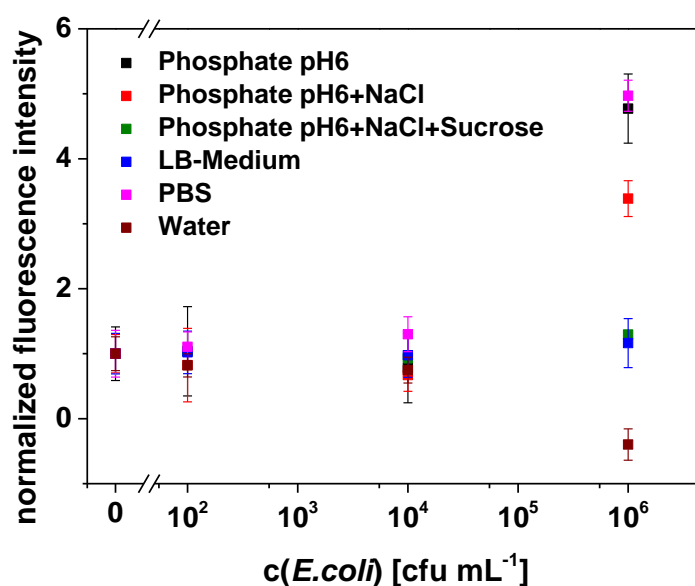


Figure 5.8. Microtiterplate assay in different solvents. Fluorescence was read out on a FluostarOPTIMA microplate reader at $\lambda_{ex}=544$ nm and $\lambda_{em}=575$ nm and a gain of 1500, $n=3$. Fluorescence intensities were normalized to the blank value.

The best results were obtained for standard PBS buffer and a 10 mM phosphate buffer at pH 6 without any additives. Here, the fluorescence signal significantly increases above concentrations of 10^4 cfu ml⁻¹. The addition of 200 mM sodium chloride shows a weaker increase in fluorescence intensity. A reason for this may be that high salt concentrations also affect the electrostatic interactions. It is assumed that the electrostatic attraction is reduced at higher salt concentrations. The salt concentration, which is present in the PBS buffer still seems to be low enough to enable strong interactions. The presence of LB-medium however, seems to disturb the electrostatic interaction between the liposomes and the *E.coli* cells probably due to interferences by tryptone or yeast extract, which are both present in the medium. Here, no signal increase for higher bacteria concentrations was observed. The same holds for the presence of sucrose. Incubation in water leads to disruption of the vesicles, thus no fluorescence signal can be detected anymore. Therefore, PBS buffer was chosen as buffer for all further experiments.

In order to see if the liposome concentration influences the assay sensitivity three different concentrations between 10 and 100 μ M were tested. The results are shown in Figure 5.9. For a liposome concentration of only 10 μ M almost no fluorescence can be detected, even for very high bacteria concentrations. In case of 100 μ M liposomes an increase in intensity can be observed for 10^6 cfu ml⁻¹ or more. However, the obtained standard deviations are very high. The significant increase in signal can also be observed for 50 μ M liposomes. In this case only low standard deviations are observed, suggesting that this vesicle concentration is completely sufficient for the microtiter plate assay. In addition, some cationic liposomes have also been reported for their bactericidal action which is based on the neutralization of the bacteria surface charge via the positively charged vesicles.^[13] Therefore, also the cationic liposomes in this study were tested for bactericidal effect. After an 1 h incubation of different concentrations of cationic liposomes between 0 and 200 μ M with *E.coli* cells, the mixture was plated onto agar plates. Table 5.1 presents the colonies grown after incubation at 37 °C overnight.

Table 5.1. Colonies of *E.coli* grown overnight after a 1 h incubation with cationic liposomes.

c (cationic liposomes) [μ M]	Counted colonies
0	121 \pm 18
10	115 \pm 19
50	108 \pm 20
100	91 \pm 14
200	96 \pm 1

As only viable bacteria are able to multiply, these results indicate the viability of the *E.coli* cells after incubation with the cationic liposomes. Up to a concentration of 50 μM no significant decrease in the counted colonies were observed. Higher concentrations, however, seem to be able to kill some of the cells. This also explains the observed higher standard deviations for 100 μM liposomes in the microtiter plate assay in Figure 5.9. Thus, no more than 50 μM of liposomes were applied for all further investigations.

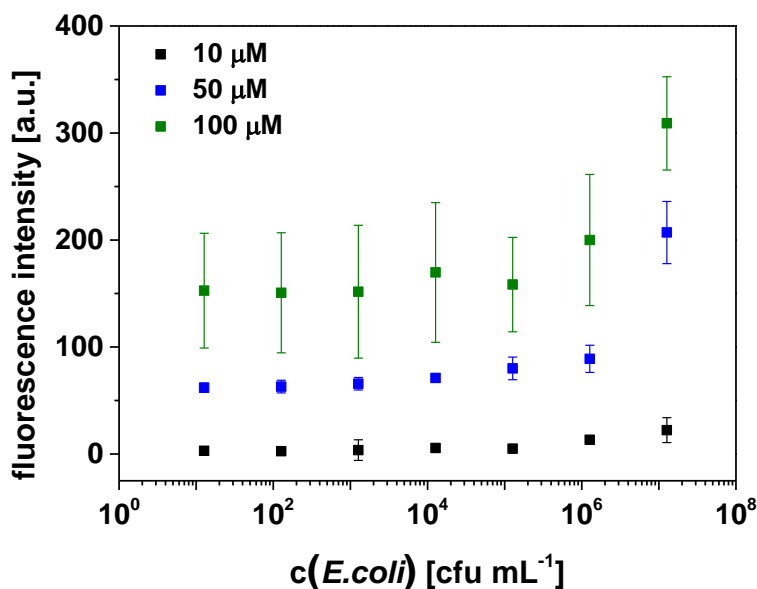


Figure 5.9. Microtiterplate assay for different liposomes concentrations in PBS buffer. Fluorescence was read out on a FluostarOPTIMA microplate reader at $\lambda_{\text{ex}}=544$ nm and $\lambda_{\text{em}}=575$ nm and a gain of 1200, $n=3$.

The obtained detection limit of about 10^6 cfu mL^{-1} as achieved with 50 μM liposomes in the microtiter plate assay does still not meet the expectations. Also, variations of other parameters like incubation time, temperature or shaking did not lead to an improvement. Therefore, changes in the lipid composition were investigated, *i.e.* the EDPPC content of the vesicle membrane was increased to yield a higher positive charge on the liposome surface. This may be able to enhance the interaction with the bacteria and may thus result in lower limits of detection.

Figure 5.10 shows the ζ -potential measurements of the freshly synthesized liposomes. 18 mol% is the standard amount of EDPPC, which had been applied for the previous experiments. In addition, 30, 40 and 50 mol% of EDPPC were mixed with DPPC. It is clearly visible that the surface potential increases from +15 mV to +25 mV with increasing amount of the cationic phospholipid. It was possible to increase the ζ -potential even more, above 30 mV, when creating a 50:50 mixture with cholesterol and no DPPC at all. Both of the 50 mol% variations were then applied to the centrifugation assay for bacteria detection.

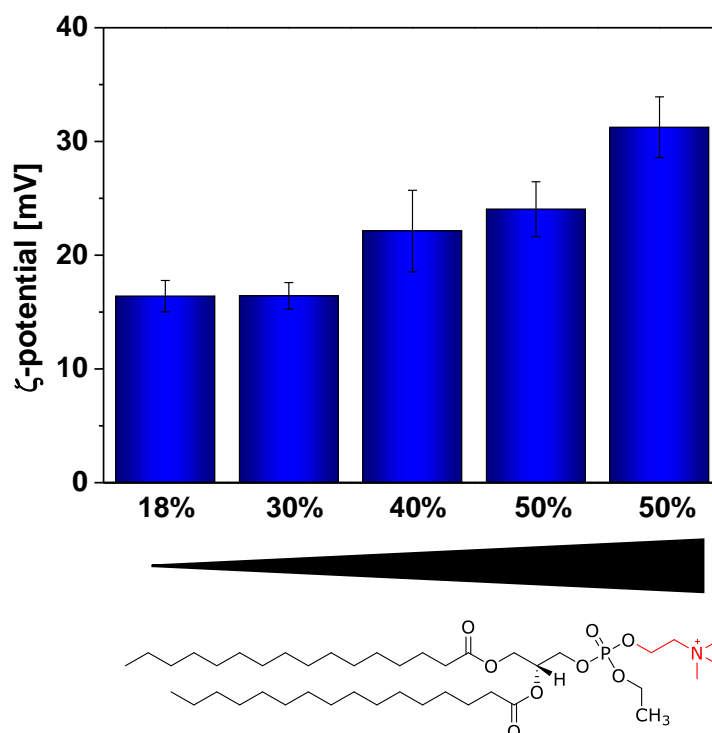


Figure 5.10. ζ -potentials of SRB containing liposomes with different mixtures of EDPPC and DPPC and EDPPC and cholesterol, $n=4$.

Figure 5.11 shows the dose response curve for both types of liposomes. In both cases no improvement in the assay sensitivity was observed. Thus, the higher positive surface charge did not improve the interaction but may have led to an increase colloidal stability of the vesicles that rather prevents

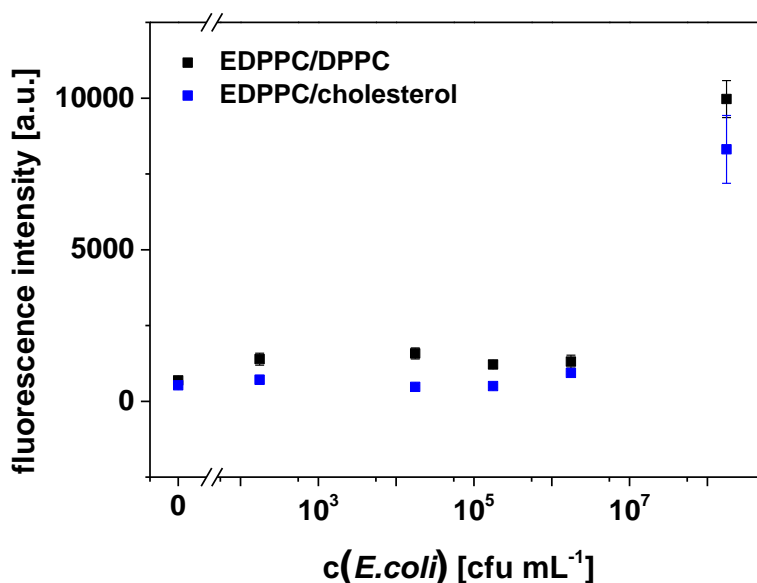


Figure 5.11. Centrifugation assay with SRB encapsulating liposomes either composed of EDPPC/DPPC (1:1) or EDPPC/cholesterol (1:1). Fluorescence was read out on a FluostarOPTIMA microplate reader at $\lambda_{ex}=544$ nm and $\lambda_{em}=575$ nm and a gain of 1200, $n=4$.

agglomeration with other particles. Therefore, the standard cationic liposomes seem to be the better choice.

5.3.4. Bacteria Quantification via Chemiluminescence Readout

As none of the optimizations resulted in a significant improvement in sensitivity the reason may be the detection method. A recent project in our group showed that anionic liposomes loaded with *m*-carboxy-luminol instead of SRB were able to lower the LOD in a sandwich hybridization assay by the factor of 150. Here, ECL readout was applied.^[7] Moreover, this dye shows excellent chemiluminescence properties.^[15] Due to the simpler handling of CL measurements in comparison with ECL, the bacteria assay was modified to enable chemiluminescence readout instead of fluorescence. Therefore, new cationic liposomes were synthesized with *m*-carboxy-luminol as encapsulant. As shown in Figure 5.12a the DLS spectrum of the new liposomes revealed a diameter of 142 nm with a low Pdl of only 0.13 and the ζ -potential of the vesicles was positive with +15 mV.

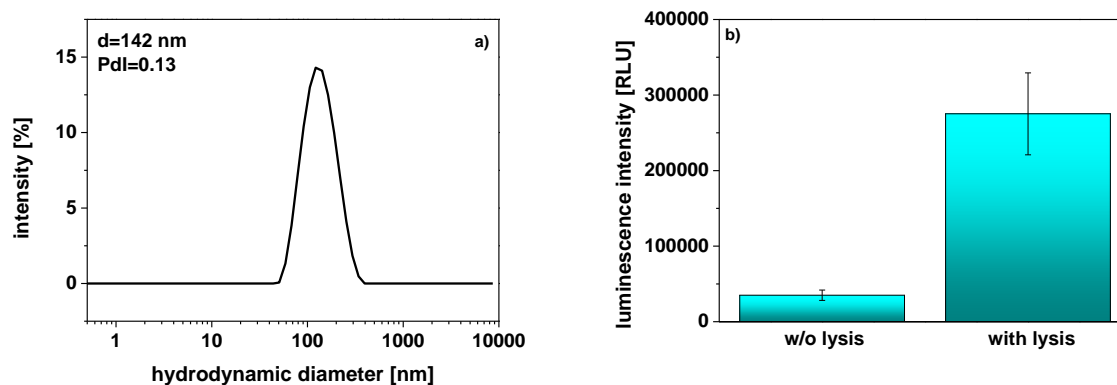


Figure 5.12. Left: DLS spectrum of cationic *m*-carboxy-luminol containing liposomes in HSS buffer, $n=3$. Right: Chemiluminescence intensities of intact and lysed cationic *m*-carboxy-luminol liposomes in carbonate buffer (0.1 M, pH 10.5). Chemiluminescence measurements were conducted on a BioTek microplate reader with Hemin and H_2O_2 as co-reagents, a read height of 6 mm and a gain of 60, $n=4$.

In order to proof the successful incorporation of *m*-carboxy luminol, chemiluminescence measurements of the intact and lysed liposomes were conducted. Hemin and H_2O_2 were used as co-reagents. As shown in Figure 5.12b only a low chemiluminescence intensity could be observed before lysis of the liposomes. After addition of a detergent a strong increase in chemiluminescence was observed, which shows that the incorporation of the dye was successful.

5.3.4.1. Magnetic Bead-Based Assay

As both assay types that have been tested so far are restricted either by insufficient capturing of bacteria on the 96 well plate or by insufficient separation as in case of centrifugation a third assay type was tested to further improve the sensitivity. Here, cationic magnetic beads serve as separators. For this, the beads were first incubated with the *E.coli* cells and afterwards unbound bacteria were separated magnetically. Then, the cationic liposomes were applied, and unbound liposomes also removed by magnetic separation. Chemiluminescence readout was used for analysis. Here, a similar dose response curve as in case of the fluorescence-based assays was obtained (Figure 5.13). A significant signal increase can only be observed above bacteria concentrations of 10^6 cfu ml⁻¹. A reason for this may be the presence of the magnetic beads. After incubation with the cells they already cover part of the bacteria surface and may even form agglomerates with other bacteria. This not only limits the space on the surface of the cells for the liposomes to bind to but also causes steric hindrance, which explains the high limit of detection.

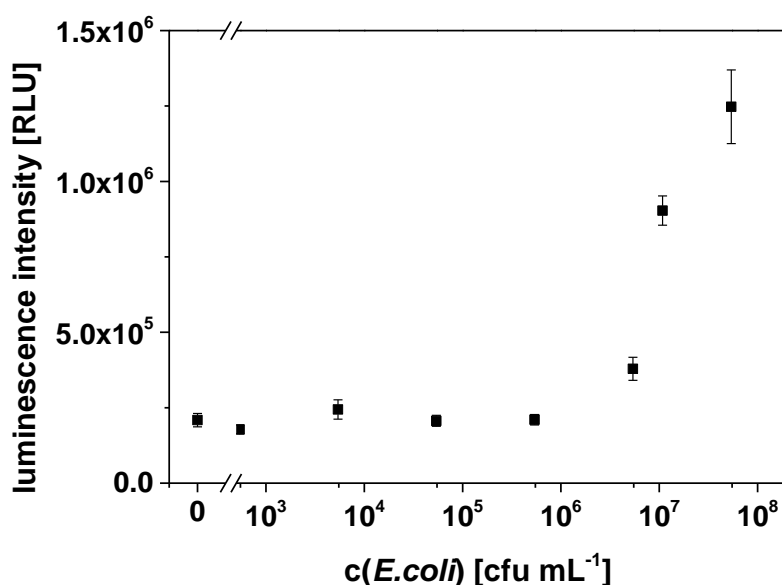


Figure 5.13. Magnetic bead assay with cationic *m*-carboxy-luminol containing liposomes. Chemiluminescence measurements were conducted in 30 mM OG in carbonate buffer (0.1 M, pH 10.5) on a BioTek microplate reader with Hemin and H₂O₂ as co-reagents, a read height of 6 mm and a gain of 80, $n=4$.

5.3.4.2. Microtiter Plate Assay

The new liposomes were then also applied to the microtiter plate and the centrifugation assay that was already tested for fluorescence analysis. The result for the microtiterplate assay is shown in Figure 5.14. The dose response curve is again very similar to the assay with fluorescence readout. Also here, the expected decrease in the LOD was not achieved. In this case, the limiting factor does not seem to be the detection method but rather the insufficient capturing of the *E.coli* cells on the Poly-L-Lysin coated wells of the microtiter plate.

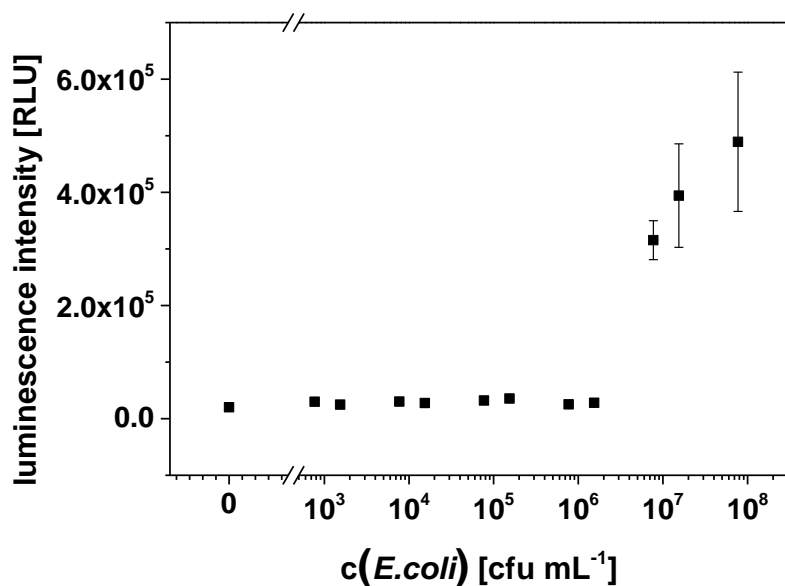


Figure 5.14. Microtiterplate assay with cationic *m*-carboxy-luminol containing liposomes. Chemiluminescence measurements were conducted in 30 mM OG in carbonate buffer (0.1 M, pH 10.5) on a BioTek microplate reader with Hemin and H₂O₂ as co-reagents, a read height of 6 mm and a gain of 80, n=4.

5.3.4.3. Centrifugation Assay

In contrast, an improvement in the LOD was observed in case of the centrifugation assay. Here, the LOD could be lowered to $\sim 10^5$ cfu ml⁻¹, which is almost 100 times lower as achieved with fluorescence readout (Figure 5.15).

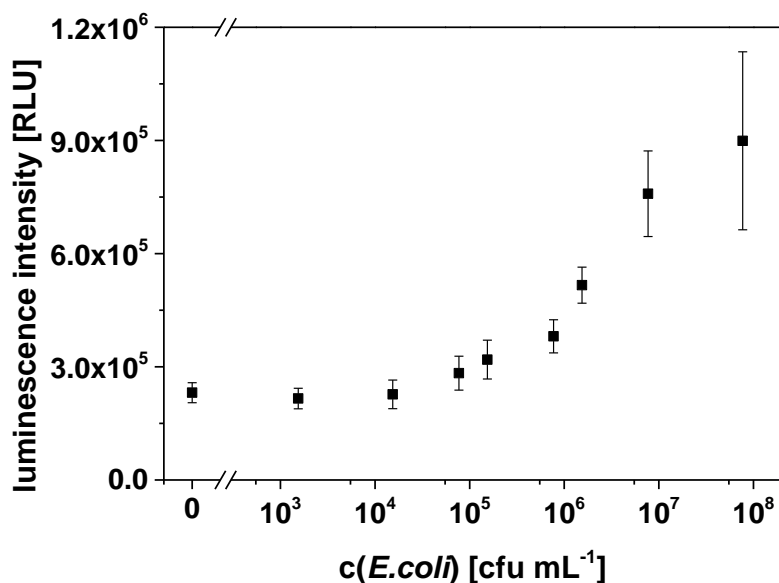


Figure 5.15. Centrifugation assay with cationic *m*-carboxy-luminol containing liposomes. Chemiluminescence measurements were conducted in 30 mM OG in carbonate buffer (0.1 M, pH 10.5) on a BioTek microplate reader with Hemin and H₂O₂ as co-reagents, a read height of 6 mm and a gain of 80, n=4.

However, careful handling is indispensable in case of separation via centrifugation to obtain reliable results. Therefore, a complete removal of the supernatant without destroying the relatively unstable liposome-bacteria pellet must be ensured.

5.4. Conclusions

Interactions between cationic liposomes and *E.coli* cells were successfully demonstrated by agglomeration visible by bare eye, fluorescence and chemiluminescence measurements. Quantification of *E.coli* cells using fluorescence readout resulted in detection limits of 10^6 - 10^7 cfu ml⁻¹ dependent on the assay type. The detection limit could be further reduced to 10^5 cfu ml⁻¹ using chemiluminescence readout, here a centrifugation-based assay showed the most promising results. However, the LOD seems to be limited by the investigated assay types. Either by insufficient bacteria immobilization on the microtiterplate surface, by steric hindrance using magnetic beads or by reliable separation using centrifugation. Thus, for the future the capturing of *E.coli* cells on other surfaces may be interesting to yield a more efficient immobilization and separation. Moreover, the use of a cationic lipid consisting of a linker may enable better availability for the bacteria and may thus increase the binding efficiency of the liposomes to the cells. Also preculturing of low concentrated bacteria samples may help to decrease the detection limit for *E.coli* quantification. If these challenges and limitations can be overcome direct detection of *E.coli* cells based on electrostatic interactions using dye loaded cationic liposomes offers a fast and simple alternative for the quantification of bacteria.

References

- [1] Y. Liu, H. Zhou, Z. Hu, G. Yu, D. Yang, J. Zhao, *Biosens. Bioelectron.* **2017**, *94*, 131.
- [2] A. Loutfi, S. Coradeschi, G. K. Mani, P. Shankar, J. B. B. Rayappan, *J. Food Eng.* **2015**, *144*, 103.
- [3] M. Petaccia, C. Bombelli, F. Paroni Sterbini, M. Papi, L. Giansanti, F. Bugli, M. Sanguinetti, G. Mancini, *Sens. Actuators, B* **2017**, *248*, 247.
- [4] M. S. Verma, J. L. Rogowski, L. Jones, F. X. Gu, *Biotechnol. Adv.* **2015**, *33*, 666.
- [5] A. Ahmed, J. V. Rushworth, N. A. Hirst, P. A. Millner, *Clin. Microbiol. Rev.* **2014**, *27*, 631.
- [6] a) P. Tuitemwong, N. Songvorawit, K. Tuitemwong, *J. Nanomater.* **2013**, *2013*, 1; b) J. D. Driskell, C. A. Jones, S. M. Tompkins, R. A. Tripp, *Analyst* **2011**, *136*, 3083; c) H. Lin, Q. Lu, S. Ge, Q. Cai, C. A. Grimes, *Sens. Actuators, B* **2010**, *147*, 343; d) M. Rangin, A. Basu, *J. Am. Chem. Soc.* **2004**, *126*, 5038.
- [7] M. Mayer, S. Takegami, M. Neumeier, S. Rink, A. Jacobi von Wangelin, S. Schulte, M. Vollmer, A. G. Griesbeck, A. Duerkop, A. J. Baeumner, *Angew. Chem. Int. Ed. Engl.* **2018**, *57*, 408.

- [8] M.-P. N. Bui, S. Ahmed, A. Abbas, *Nano Lett.* **2015**, *15*, 6239.
- [9] J. Park, S. K. Ku, D. Seo, K. Hur, H. Jeon, D. Shvartsman, H.-K. Seok, D. J. Mooney, K. Lee, *Chem. Commun.* **2016**, *52*, 10346.
- [10] a) P. P. Karmali, A. Chaudhuri, *Med. Res. Rev.* **2007**, *27*, 696; b) C. Montis, S. Sostegni, S. Milani, P. Baglioni, D. Berti, *Soft Matter* **2014**, *10*, 4287.
- [11] Z. Drulis-Kawa, A. Dorotkiewicz-Jach, J. Gubernator, G. Gula, T. Bocer, W. Doroszkiewicz, *Int. J. Pharm.* **2009**, *367*, 211.
- [12] G. N. Tapias, S. M. Sicchierolli, E. M. Mamizuka, A. M. Carmona-Ribeiro, *Langmuir* **1994**, *10*, 3461.
- [13] M. T. Campanhã, E. M. Mamizuka, A. M. Carmona-Ribeiro, *J. Lipid Res.* **1999**, *40*, 1495.
- [14] C. Figalist, *Master's Thesis*, University of Regensburg, Regensburg, **2014**.
- [15] S. Rink, *Master's Thesis*, University of Regensburg, Regensburg, **2018**.

6 Cationic Liposomes for DNA Preconcentration

Abstract

Common methods for the extraction, purification and concentration of genomic DNA include solid phase extraction, end point PCR or the use of magnetic silica beads. These techniques are *e.g.* time-consuming, prone to impurities, or require the use of organic solvents or chaotropic salts, which often causes interferences during DNA quantification *e.g.* by qPCR. Here, cationic liposomes were tested for their ability to preconcentrate genomic DNA extracted from *E.coli*. The DNA can simply be captured via electrostatic interactions with the phospholipid vesicles and purified via centrifugation. Quantification of the concentrated DNA was done via picogreen analysis. Short incubation times of only 5 min at room temperature followed by a 15 min centrifugation at 15.000 g resulted in good DNA recoveries up to 75%. Thus, cationic liposomes in combination with centrifugation enables a fast and efficient method for the concentration of genomic DNA without the need for high temperatures or organic solvents.

Parts of this chapter are intended for publication.

Author contributions:

The author did most of the experimental work and wrote this chapter. Cornelia Hermann contributed with the synthesis and characterization of one of the liposome batches. Vanessa Tomanek and Clemens Spitzenberg repeated and optimized some of the experiments under the supervision of the author. Antje J. Baeumner contributed with strategic discussions and was the leader of this project.

This chapter contains paragraphs that were in part already described in Carola Figalist's master's thesis. This includes paragraphs within the experimental part regarding the liposome preparation and characterization. The master's thesis is entitled "Positively Charged Liposomes for Signal Enhancement via Electrostatic Interactions" and was submitted to the Faculty of Chemistry and Pharmacy at the University of Regensburg in December 2014. Sections that are identical or similar to the master's thesis are listed here in detail and are indicated in this chapter by the citation "M":

- p.125, subchapter 6.2.1., paragraph 2 (experimental)

- p.125-126, subchapter 6.2.2.4., 6.2.2.5.1. (experimental)

6.1. Introduction

One of the simplest methods for the quantification of double stranded DNA is the use of UV/vis spectroscopy. DNA shows a specific peak at 260 nm which can be used for quantification.^[1] Typically, 1 OD corresponds to 50 $\mu\text{g ml}^{-1}$ DNA.^[2] The absorbance ratio A_{260}/A_{280} can also give information on the purity of the DNA sample and should lie between 1.7 and 2.0.^[1] Unfortunately, impurities caused by ssDNA or RNA cannot be detected by absorbance measurements as they also absorb at 260 nm.^[1,2] Moreover, analysis via UV/vis spectroscopy is limited to DNA samples between 5-50 mg ml^{-1} .^[2] Another possibility is the use of polymerase chain reaction (PCR) techniques. PCR can selectively amplify DNA. While end point PCR can only provide semi-quantitative information, qPCR allows real time analysis of the samples and quantification down to low DNA levels.^[3] Here, a fluorescent dye, *e.g.* SYBR Green I or EvaGreen, binds to the dsDNA and PCR cycles are conducted until enough DNA is present to be detected via fluorescence during the extension phase of the PCR cycle.^[3,4] However, PCR-based methods are expensive and extremely sensitive towards impurities. Thus, only very pure DNA samples can provide reliable data.^[2] Ideally, other methods for the quantification of DNA stocks should be conducted beforehand to serve as template for PCR analysis.^[1] Here, fluorescence techniques have been proposed as they enable a more sensitive quantification of dsDNA than absorbance measurements. Fluorescent dyes like Hoechst 33258 or picogreen are the most prominent examples.^[1,5] A calibration curve using a DNA standard enables the quantification of dsDNA from 1 $\mu\text{g ml}^{-1}$ down to 25 pg ml^{-1} .^[2] In case of the Hoechst dye selectivity towards dsDNA can be influenced via high or low salt concentrations.^[2] In contrast, picogreen is highly selective towards dsDNA but sensitive to interferences by some detergents and salts.^[1,2]

One of the mostly applied techniques for DNA isolation includes the phenol-chlorophorm extraction, where hydrophobic cell components in the organic phase are separated from the extracted DNA in the aqueous phase.^[6] However, the use of organic solvents cannot only be hazardous to health and the environment but also a thorough removal of the solvents is necessary to enable the suitability for

further DNA analysis.^[2,7] Another common technique relies on solid phase extraction. After disruption of the cell, DNA is adsorbed *e.g.* onto spin columns consisting of a silica matrix, glass particles or anion exchange carriers and eluted after several washing steps which can become very time-consuming.^[7,8] Here, no toxic organic solvents are necessary, however, often the addition of high salt concentrations or chaotropic salts is necessary which interfere *e.g.* with picogreen or qPCR analysis if not sufficiently removed.^[2,9]

For the concentration of DNA after isolation simple methods like the precipitation with alcohol can be applied. However, this can lead to shearing of the DNA, especially in case of high molecular weight DNA.^[10] DNA extraction and concentration using magnetic beads offer a fast and simple alternative. These beads usually consist of a magnetic core surrounded by polymer or silica shells which can either be applied without or with specific surface receptors.^[6] The DNA can be adsorbed onto the bead surface and separated from other components via magnetic forces.^[3] However, sedimentation or aggregation of the microparticles often result in lower extraction efficiencies.^[3] Moreover, magnetic bead-based approaches often require the use of chaotropic salts like guanidine HCl or organic solvents that need to be efficiently removed before further DNA analysis.^[2,8] Recently, also the use of magnetic ionic liquids has been reported which overcome some of the problems using magnetic beads like sedimentation or aggregation.^[3,9]

Another material that is known to interact well with DNA are cationic liposomes. Here, usually the formation of lipoplexes is exploited for applications in gene therapy or DNA vaccination.^[11] This study investigates the applicability of cationic liposomes for DNA preconcentration via electrostatic adsorption to the surface of the vesicles without the need for chaotropic salts or organic solvents.

6.2. Experimental

6.2.1. Materials

1,2-dipalmitoyl-sn-glycero-3-phosphatidylcholine (DPPC), 1,2-dipalmitoyl-sn-glycero-3-ethylphosphocholine (EDPPC), cholesterol and the extrusion kit and membranes were purchased from Avanti Polar Lipids (avantilipids.com). The dialysis membrane spectra/por 4 with a MWCO of 12-14 kDa was purchased from spectrum labs (www.spectrumlabs.com). *E.coli* was purchased from the DSMZ (www.dsmz.de). 4-(2-Hydroxyethyl)piperazine-1-ethanesulfonic acid (HEPES), sodium azide, phosphate buffered saline and black microtiter plates from Nunc were bought from Sigma Aldrich (www.sigmaaldrich.com) as well as the GenElute™ Genomic DNA kit for DNA extraction. The Invitrogen™ Quant-iT™ PicoGreen™ assay kit containing the picogreen reagent, DNA standard and a 10xTE buffer was purchased from fisher scientific (www.fishersci.de). The phosphorus standard for ICP-MS measurements was bought from Perkin Elmer (www.perkinelmer.com). LB broth was

purchased from Alfa Aesar (www.alfa.com/de/). Bacteriological agar as well as all other chemicals were of analytical grade and purchased from VWR (de.vwr.com).

Millipore water ($\geq 18.2 \text{ M}\Omega \text{ cm}$) was used for the preparations of all buffers and aqueous solutions needed for liposome preparation.^[M]

DNase free water was applied for the preparation of all aqueous solutions needed for DNA extraction, preconcentration or picogreen analysis.

6.2.2. Methods

6.2.2.1. Cultivation of *E.coli*

Two *E.coli* colonies grown on Agar plates were suspended in LB-medium (10 mL) and used for cultivation of *E.coli* for 4-5 h at 37 °C under continuous shaking. The obtained stock solution was then applied for the extraction of genomic DNA. For colony counting this stock solution was diluted 1:10⁶ and 50 μL of this solution spread onto an Agar plate and incubated overnight at 37 °C. This was done for 2 different plates and the grown colonies were counted the next morning. Usually *E.coli* cultures of $\sim 10^9 \text{ cfu ml}^{-1}$ were obtained.

6.2.2.2. Extraction of Genomic DNA

The GenElute kit by Sigma Aldrich was applied for the extraction of genomic DNA from *E.coli* following the instructions of the kit. 1.5 ml of the *E.coli* stock solution were applied for extraction and two elution steps in TE buffer were applied to increase the yield. The extracted genomic DNA was stored in aliquots at -18 °C.

6.2.2.3. Characterization of Genomic DNA

For characterization absorbance spectra were recorded between 200-400 nm on a Cary spectrophotometer. Background correction was conducted using TE buffer as blank solution. The peaks at 260 and 280 nm were analyzed to obtain information on the quality of the extracted DNA and to estimate its concentration.

Moreover, picogreen analysis was applied to determine the concentration of double-stranded DNA in the solution. For this the stock solution was diluted 1:25 in TE buffer. 10 μl of this dilution were then mixed with 490 μl of TE buffer and 500 μL of the picogreen reagent. A calibration curve between 0 and 250 ng ml^{-1} was used for analysis.

6.2.2.4. Preparation of Liposomes

DPPE (17.3 mg), EDPPC (4.5 mg) and cholesterol (0.6 mg) were dissolved in Chloroform (3 mL) and Methanol (0.5 mL) and sonicated at 60 °C for 1 minute. 2 mL of a sodium chloride solution (300 mM, dissolved in 0.2 M HEPES, pH 8.5) was added and the mixture sonicated at 60 °C for 4 minutes. The

organic solvent was removed by using a rotary evaporator at 60 °C and a pressure of 750 mbar for 40 minutes. The solution was vortexed, and another 2 mL of the sodium chloride solution was added. After vortexing again the solution was rotated at 60 °C and 750 mbar for 20 minutes and then again at 60 °C and 400 mbar for 20 minutes. The solution was being extruded through polycarbonate membranes (1µm and 0.4 µm) at 60 °C by pushing the syringes back and forth 21 times for each membrane. Excess of sodium chloride was removed by size exclusion chromatography with a Sephadex G-50 column followed by dialysis against HSS buffer (10 mM HEPES, 200 mM NaCl, 200 mM sucrose, 0.01% NaN₃, pH 7.5).^[M]

6.2.2.5. Characterization of Liposomes

6.2.2.5.1. Determination of Size and ζ-potential

Dynamic light scattering (DLS) and ζ-potential measurements were carried out on a Malvern Zetasizer Nano-ZS (www.malvern.com). For all measurements the temperature was set to 25 °C. Semi-micro PMMA cuvettes were used for size determinations, disposable folded capillary cells for the ζ-potential measurements. Before the measurements the samples were diluted 1:100. As setting for liposomes a n_D^{20} of 1.34 and an Abs of 0.000 was selected and HSS buffer ($n_D^{20} = 1.342$, viscosity = 1.1185 kg·m⁻¹·s⁻¹, dielectric constant: 78.5) was used as dispersant. An equilibration time of 60 s was applied before each measurement.^[M]

6.2.2.5.2. Determination of Phospholipid Concentration

The phospholipid concentration was determined by using the ELAN 9000 inductively coupled plasma mass spectrometer (ICP-MS) from Perkin Elmer (www.perkinelmer.com). For this, the liposome samples were diluted 1:600 in 5% HNO₃ (15 ml) and could then be used for the measurement. For calibration a standard curve between 0 and 500 ppb was measured using dilutions of a phosphorus standard in 5% HNO₃. Scandium was added to the calibration solutions and the samples as internal standard.

6.2.2.6. DNA Preconcentration Using Magnetic Beads

10 µl of a liposome stock solution were added to 990 µl of genomic DNA (diluted 1:250 in 1x TE buffer). The mixture was incubated at room temperature for 15 min under continuous shaking at 300 rpm. Then, 1 µl of a 1:1000 dilution of magnetic beads (1 µM, carboxy functionalized, 1 µm) was added and the mixture incubated for another 15 min at room temperature under continuous shaking at 300 rpm. Separation of unbound DNA was done magnetically. After complete removal of the supernatant the pellet was resuspended in 10 µl 1xTE buffer and vortexed vigorously. The 10 µL was used completely for DNA quantification via picogreen analysis. As negative control samples containing only DNA and only liposomes were treated the same way.

6.2.2.7. DNA Preconcentration Using Centrifugation

10 μ l of a liposome stock solution were added to 990 μ l of genomic DNA (diluted 1:250 in 1x TE buffer). The mixture was incubated at room temperature for 15 min under continuous shaking at 300 rpm. Separation of unbound DNA was done via centrifugation at 15.000 g for 15 min. After complete removal of the supernatant the pellet was resuspended in 10 μ l 1xTE buffer and vortexed vigorously. The 10 μ l was used completely for DNA quantification via picogreen analysis. As negative control samples containing only DNA and only liposomes were treated the same way.

Experiments were either conducted in standard Eppendorf tubes or in DNA LoBind Eppendorf tubes. The following incubation parameters were varied for optimization experiments (Table 6.1):

Table 6.1. Incubation parameters for optimization experiments. Only one parameter was varied in each experiment. The others were kept constant at incubation for 15 min at 25 °C in TE buffer with a liposome concentration of 80 μ M and a centrifugation speed of 15.000 g for 15 min.

Incubation [min]	time	Incubation [°C]	temperature	c(liposomes) [μ M]	Centrifugation [g]	speed	Buffer
5		25		8	2.500		HSS
15		30		80	5.000		TE
30		40		400	7.500		SSC
60		50		800	10.000		HSS+guanidin HCl
					15.000		TE+guanidin HCl
							SSC+guanidin HCl

6.2.2.8. Picogreen Analysis

After mixing 10 μ l of the sample with 490 μ l TE buffer, 500 μ l of the picogreen reagent (1:200 dilution in TE buffer) are added vortexed vigorously. The mixture is incubated for 5 min and then transferred to the wells of a black microtiter plate (200 μ l/well). The fluorescence intensity was read out on a BioTek microplate reader at λ_{ex} =480 nm and λ_{em} =520 nm. The gain was adjusted before each measurement and was usually between 90 and 121. Three replicates of each sample are measured.

For calibration the DNA standard (100 μ g ml⁻¹) was diluted to a concentration of 500 ng ml⁻¹ in TE buffer. The diluted standard was then applied for preparation of the standard solutions according to the protocol in Table 6.2.

Before the measurement the DNA dilutions were mixed with 500 μ l of the picogreen reagent and then treated the same way as the samples as described above. The standard solutions were used to create a calibration curve, which was then applied for quantitative analysis of the samples.

Table 6.2. Volumes of TE buffer and DNA standard to create the calibration curve.

V(TE) [μL]	V (500 ng ml ⁻¹ DNA) [μl]	c(DNA) in assay [ng ml ⁻¹] (after addition of picogreen reagent)
0	500	250
450	50	25
495	5	2.5
499,5	0,5	0.25
500	0	blank

6.3. Results and Discussion

6.3.1. Liposome Preparation and DNA Extraction

Cationic liposomes were prepared via reverse phase evaporation using DPPC, cholesterol and the cationic phospholipid EDPPC. This resulted in the formation of colloiddally stable vesicles with diameters of ~ 300 nm and a positive ζ -potential of +14 mV (Figure 6.1). The hydrophilic inner cavity of the liposomes entrapped a solution of 300 mM sodium chloride to yield colorless liposome dispersions that do not interfere with any optical characterization of genomic DNA as for example with the picogreen dye which was used for DNA quantification in this chapter.

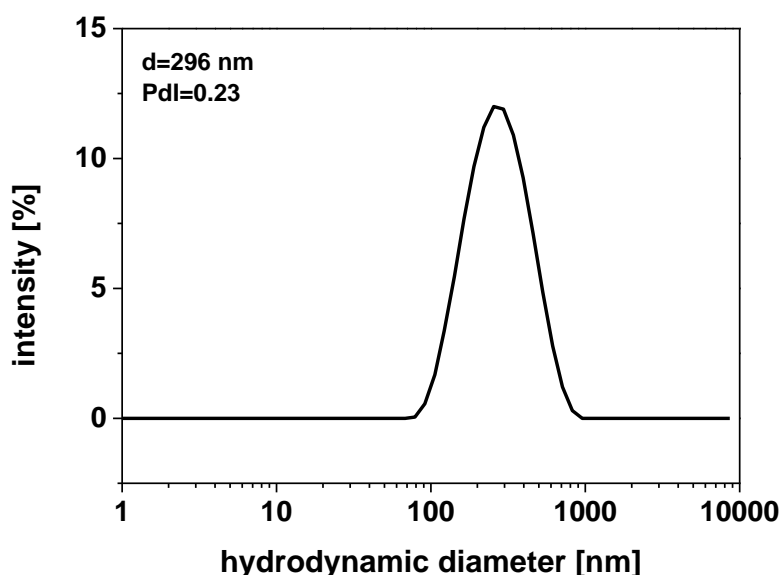


Figure 6.1. Hydrodynamic diameter of cationic liposomes encapsulating sodium chloride (300 mM) determined by dynamic light scattering in HSS buffer.

Genomic DNA was extracted from *E.coli* cells using the commercially available GenElute Kit from Sigma Aldrich. The DNA was eluted in TE buffer and stored at -18 °C. Absorbance spectra of the extracted DNA show a broad peak at 260 nm which is typical for genomic DNA (Figure 6.2).^[12] Ideally, the ratio

of A_{260}/A_{280} should be between 1.7 and 2.0.^[1] Here, values of 1.4 were obtained. Therefore, the extracted DNA still suffers from some impurities like proteins. The intensity at 260 nm also allows an estimation of the DNA concentration. However, absorbance is not very precise and prone to interferences by impurities that also absorb at 260 nm. This may falsify these results. Therefore, quantification of genomic DNA was done via a picogreen assay. The picogreen dye interacts specifically with double-stranded DNA while interferences by single-stranded DNA or RNA are minimized. A calibration curve using a DNA standard between 0 and 250 ng ml⁻¹ enables a more precise quantification of the extracted genomic DNA and usually resulted in concentrations in the range of 5-17 μ M.

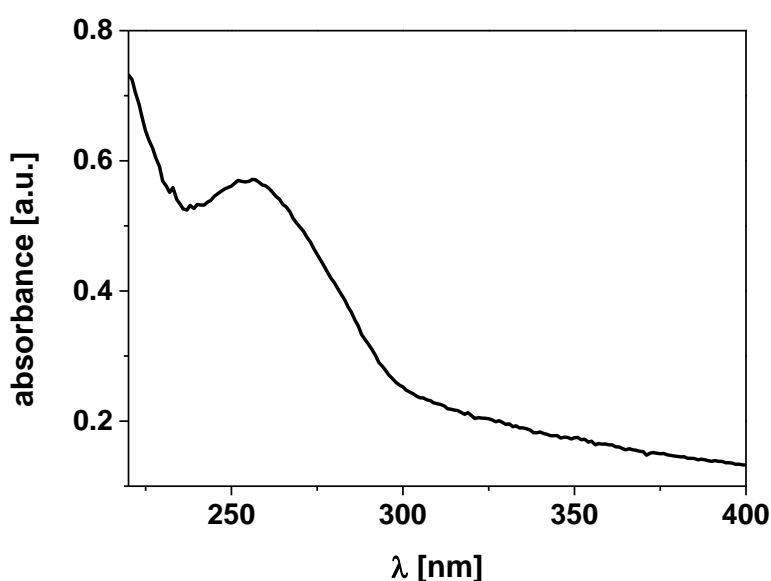


Figure 6.2. Absorbance spectrum between 220 and 400 nm of the extracted genomic DNA recorded on a Cary spectrophotometer.

6.3.2. Concepts for DNA Preconcentration with Cationic Liposomes

Two different concepts were investigated for preconcentration of genomic DNA via cationic liposomes. In both cases the cationic surface charge of the liposomes is used to electrostatically bind the DNA to the vesicles. In a next step unbound DNA must be separated from the DNA-liposome complexes. In the first concept, magnetic beads are applied to bind to these complexes. This enables a simple magnetic separation from unbound DNA. The second concept uses centrifugation of the DNA-liposome complexes for separation. In both cases picogreen analysis was used for quantification of the genomic DNA after preconcentration.

6.3.2.1. Separation via Magnetic Beads

In combination with DNA, buffer plays an important role. EDTA containing buffers like TE buffer have a stabilizing effect regarding the long-term storage of DNA as EDTA chelated Mg^{2+} -ions and therefore

serves as DNase inhibitor.^[10] For hybridization purposes, specific hybridization buffers are developed that provide the correct stringent conditions for a successful hybridization.^[10] The commercially available magnetic beads that have been widely applied for DNA preconcentration usually need chaotropic salts like guanidine HCl in their buffer composition to achieve a successful concentration.^[13] Therefore, also different buffers were investigated for preconcentration using cationic liposomes for both strategies. The osmolality of the HSS buffer is adjusted to the encapsulant of the liposomes. Ideally, it should be 50-100 mOsmol kg⁻¹ higher than the osmolality of the encapsulant.^[14] This provides excellent stability for the liposomes as shown in earlier studies.^[15] TE buffer stabilizes the DNA and SSC buffer is a hybridization buffer commonly used in liposome-based hybridization assays.^[10,16] These three buffers were once investigated with and once without the addition of the chaotropic salt guanidine HCl. Samples containing only DNA or only liposomes were treated alongside as negative control. Figure 6.2 shows the enrichment factors for preconcentration using cationic liposomes and magnetic beads. Enrichment factors were determined using equation 6.1.

$$\text{enrichment factor (EF)} = \frac{c(\text{DNA})_{\text{after preconcentration}}}{c(\text{DNA})_{\text{before preconcentration}}} \quad (6.1)$$

It can be seen that DNA preconcentration using cationic liposomes and magnetic beads for separation works in principle (Figure 6.3).

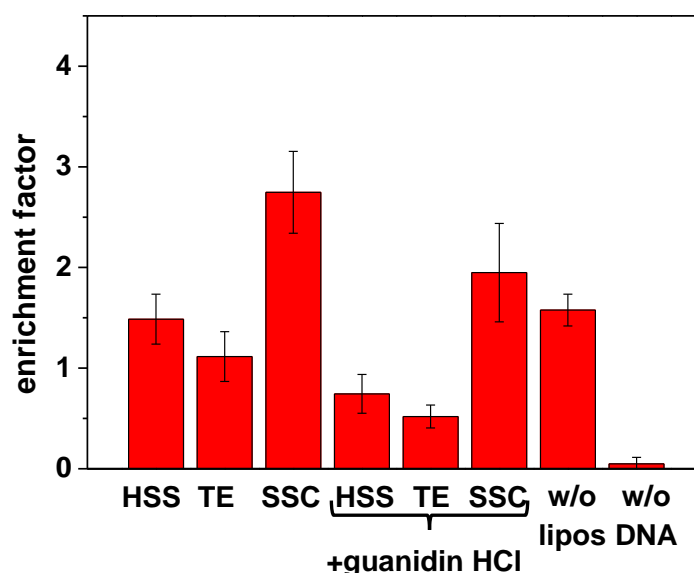


Figure 6.3. Enrichment factors for DNA preconcentration in different buffers using magnetic beads for separation. The DNA stock solution was diluted 1:250 before mixing with the liposomes. DNA concentrations were determined using a picogreen assay kit, the fluorescence was read out at a BioTek microplate reader at $\lambda_{ex}=480$ nm and $\lambda_{em}=520$ nm and a gain of 121, $n=3$.

However, only enrichment factors up to 3 can be reached which is not very efficient. Incubation in hybridization buffer seems to work best while almost no enrichment can be observed for HSS and TE

buffer. SSC buffer may have an influence on the 3D structure (folding) of the DNA which favors the attachment to the liposomal surface. The addition of the chaotropic salt guanidine HCl even decreases the efficiency of preconcentration. In case of the commercially available kits based on magnetic beads these salts are necessary to overcome the electrostatic repulsion between anionic beads and DNA.^[13] This is not necessary here. Moreover, the negative control sample, which doesn't contain any cationic liposomes or beads also yielded enrichment factors of around 2. Thus, a high amount of DNA does not seem to be concentrated by the liposomes but by unwanted binding to the walls of the Eppendorf tubes.

6.3.2.2. Separation via Centrifugation

The same experiment was conducted using cationic liposomes and centrifugation for the concentration of DNA (Figure 6.4). Here, overall higher enrichment factors of 20-25 were achieved. Surprisingly, the hybridization buffer gave the lowest DNA recovery in this case, whereas TE buffer worked best. Again, the addition of guanidine HCl showed no improvement. However, also in this case similar or only slightly lower enrichment factors were also obtained although no liposomes were present for capturing the DNA. Thus, the DNA molecules seem to stick to the walls of the Eppendorf cups. In this case also the centrifugation speed of 21.000 g for separation may have been too fast.

As separation by centrifugation seems to be the more promising concept all further optimizations were only conducted for this method.

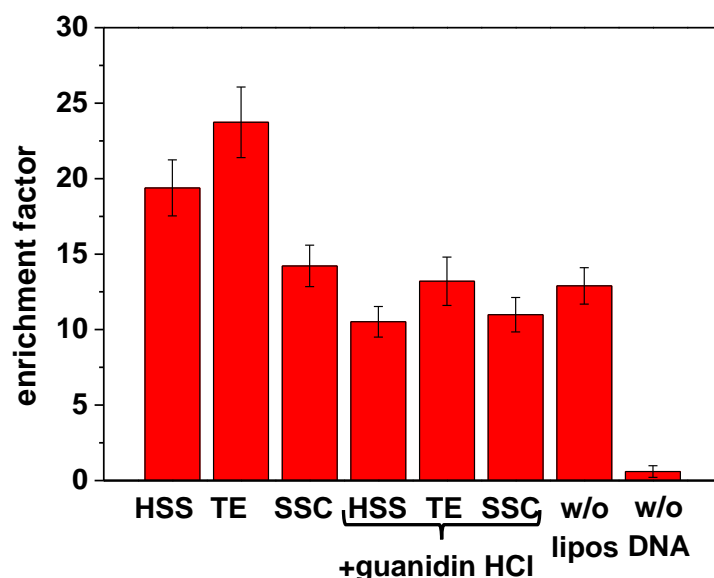


Figure 6.4. Enrichment factors for DNA preconcentration in different buffers using centrifugation at 21.000 g for separation. The DNA stock solution was diluted 1:250 before mixing with the liposomes. DNA concentrations were determined using a picogreen assay kit, the fluorescence was read out at a BioTek microplate reader at $\lambda_{ex}=480$ nm and $\lambda_{em}=520$ nm and a gain of 121, $n=3$.

6.3.3. Optimization of DNA Preconcentration Using Centrifugation

As 21.000 g results in high DNA recoveries for the negative control samples slower centrifugation speeds between 2.500 and 15.000 g were investigated to see if this value can be minimized. It was found that 7.500 g results already in a good enrichment factor of ~35 with only low interference by unbound DNA molecules (Figure 6.5). A similar result was achieved using 15.000 g. Below 7.500 g a significant decrease in the enrichment factors was observed. However, these lower centrifugation speeds showed no improvement regarding the samples without liposomes and are therefore not ideal for DNA preconcentration. Moreover, the same experiment was conducted using a lower DNA concentration (1:25.000 dilution) for mixing with the liposomes. Unfortunately, the obtained signals were below the detection limit of the picogreen assay which was applied for quantification of the DNA. Here, the use of a more sensitive method for DNA quantification of DNA, like qPCR, will be necessary.

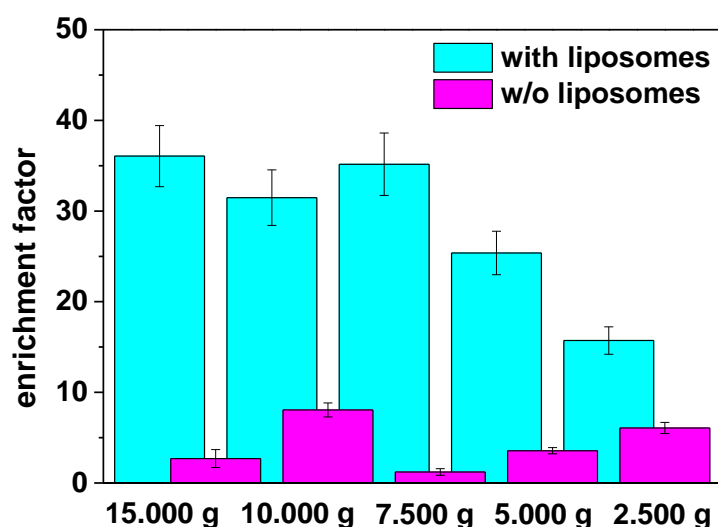


Figure 6.5. Enrichment factors for DNA preconcentration using centrifugation at different speeds. The DNA stock solution was diluted 1:250 before mixing with the liposomes. DNA concentrations were determined using a picogreen assay kit, the fluorescence was read out at a BioTek microplate reader at $\lambda_{ex}=480$ nm and $\lambda_{em}=520$ nm and a gain of 90, $n=3$.

The experiment was also conducted for three different batches of liposomes containing different concentrations of phospholipid in their stock solution (3-9 mM, Table 6.3 Figure 6.6a).

Again, a centrifugation speed of 7.500 g and 15.000 g resulted in similar enrichment factors. The assay worked with all liposome batches and the batches of liposomes did not have a definite effect as expected. They only slightly differ in the phospholipid concentration but are identical regarding the lipid composition, preparation and surface charge. Overall, the values for the negative control vary significantly from measurement to measurement and may not be a consequence of the centrifugation speed alone but may also be caused by differences in the handling of the samples.

Table 6.3. Characterization of cationic liposomes encapsulation 300 mM sodium chloride via ICP-MS analysis, n=3.

	c(phospholipid) [mM]
"old lipos" M	3.1 ± 0.3
"old lipos" H	6.5 ± 0.06
"new lipos" H	8.8 ± 0.3

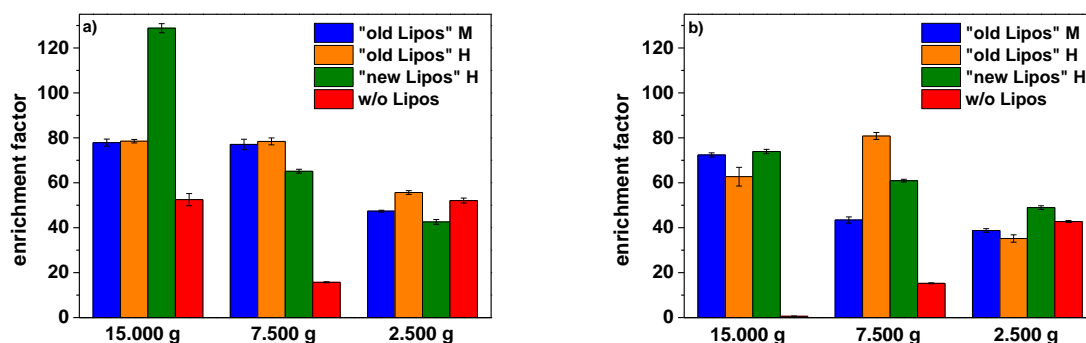


Figure 6.6. Enrichment factors for DNA preconcentration using centrifugation at different speeds. The DNA stock solution was diluted 1:250 before mixing with the liposomes. The assay was conducted either in a) standard 2 mL Eppendorf Cups or in b) DNA LoBind 2 mL Eppendorf Cups. DNA concentrations were determined using a picogreen assay kit, the fluorescence was read out at a BioTek microplate reader at $\lambda_{ex}=480$ nm and $\lambda_{em}=520$ nm and a gain of 90, n=3.

The experiments so far have all been conducted in standard Eppendorf tubes. Due to the large values in case of the samples without liposomes it was assumed that a large amount of DNA is also able to stick to the walls of these Eppendorf tubes and can therefore not be separated sufficiently.

In order to see, if the standard Eppendorf tubes do really have an effect on the negative control values, the same experiment was conducted in DNA LoBind cups (Figure 6.6b). Here, binding of free DNA to the walls of the tubes should be minimized and enable a more sufficient separation. Surprisingly, similar results were obtained for a centrifugation speed of 2.500 and 7.500 g. However, in case of 15.000 g interference by free DNA is significantly lower. Thus, a centrifugation speed of 15.000 g and DNA LoBind cups were applied for all further experiments.

Apart from the centrifugation speed, also other factors may influence the efficiency of the DNA preconcentration. Therefore, DNA preconcentration was performed under different conditions by varying the incubation time, temperature and the liposome concentration. Variations in the incubation temperature showed that 25 or 50 °C work best, whereas in case of 40 °C a loss in the efficiency can be observed (Figure 6.7a). Also the phase transition temperature of the lipid bilayer is supposedly at

~40 °C and may be responsible for this effect. Variations in the liposome concentration show similar enrichment factors for all tested liposome concentrations (0.8 mM, Figure 6.7b).

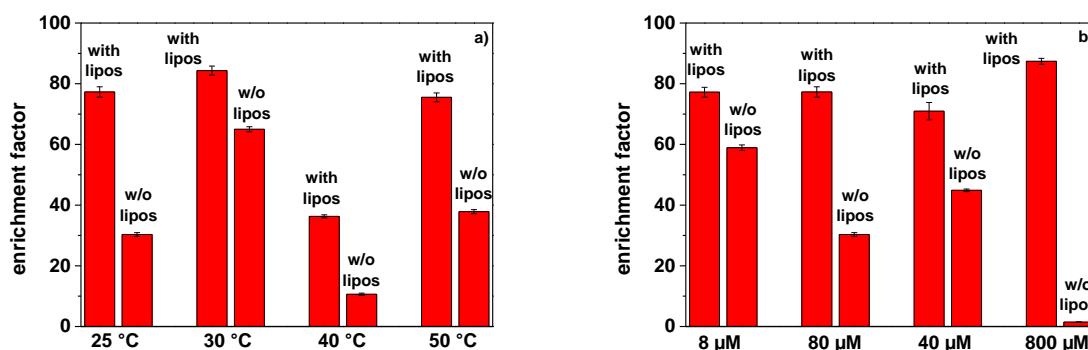


Figure 6.7. a) Enrichment factors for DNA preconcentration using centrifugation at 15.000 g. Incubation was done at different temperatures between 25 and 50 °C. The DNA stock solution was diluted 1:250 before mixing with the liposomes. The assay was conducted in DNA LoBind 2 mL Eppendorf Cups. DNA concentrations were determined using a picogreen assay kit, the fluorescence was read out at a BioTek microplate reader at $\lambda_{ex}=480$ nm and $\lambda_{em}=520$ nm and a gain of 90, $n=3$. b) Enrichment factors for DNA preconcentration using centrifugation at 15.000 g. Incubation was done with different liposome concentrations between 8 and 800 μ M. The DNA stock solution was diluted 1:250 before mixing with the liposomes. The assay was conducted in DNA LoBind 2 mL Eppendorf Cups. DNA concentrations were determined using a picogreen assay kit, the fluorescence was read out at a BioTek microplate reader at $\lambda_{ex}=480$ nm and $\lambda_{em}=520$ nm and a gain of 90, $n=3$.

As also low liposome concentrations are sufficient for preconcentration this assay is not only fast but also requires only a low amount of material which also reduces the costs of the assay. However, huge differences in the negative control values can be observed (factors between 5 and 60%).

Moreover, an increase in the incubation time does not have a significant effect on the efficiency of the DNA concentration (Figure 6.8). As already observed in the measurements before, high variations for the negative control samples were obtained, e.g. a 15 min incubation results in a significantly higher negative control. This may however not be caused by the incubation time but for example by insufficient removal of the supernatant after centrifugation or other handling effects. Here, more studies will be necessary to find the cause of this phenomenon. However, 5 min seem to be completely sufficient to obtain good DNA recoveries, which enables DNA preconcentration based on cationic liposomes and centrifugation in a very short time.

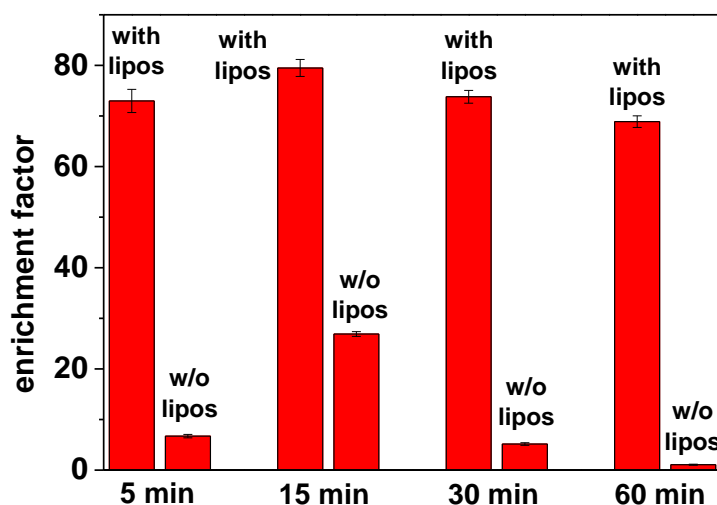


Figure 6.8. Enrichment factors for DNA preconcentration using centrifugation at 15,000 g. Incubation was done for different times between 5 and 60 minutes. The DNA stock solution was diluted 1:250 before mixing with the liposomes. The assay was conducted in DNA LoBind 2 mL Eppendorf Cups. DNA concentrations were determined using a picogreen assay kit, the fluorescence was read out at a BioTek microplate reader at $\lambda_{ex}=480$ nm and $\lambda_{em}=520$ nm and a gain of 90, $n=3$.

6.4. Conclusions

The two investigated concepts for DNA preconcentration revealed that magnetic separation results in limited DNA recoveries whereas separation by centrifugation results in good DNA recoveries up to 80%. The use of different buffers had a significant effect on the efficiency in both cases. Optimizations of the assay parameters in case of centrifugation revealed that short incubation and centrifugation times of only 5 and 15 minutes, respectively, are already sufficient for an effective preconcentration. Moreover, only low concentrations of liposomes are necessary. The developed assay is therefore not only very simple and fast, but also economical regarding the required materials. However, quantification via picogreen is only possible for high starting concentrations of DNA. The signal intensity of the picogreen assay is prone to interferences by several components like some salts, organic solvents, detergents or proteins which can impact the sensitivity of this assay significantly. Therefore, real-time PCR experiments will be necessary to verify the results obtained by picogreen quantification and to enable the detection of lower DNA concentrations. In addition, more experiments are necessary to understand the high differences in the negative control samples between the measurements and to reduce the effects caused by differences in the handling of the samples. Moreover, the development of magnetic, cationic liposomes will be interesting to avoid the rather harsh separation via centrifugation.

References

- [1] S. J. Ahn, J. Costa, J. R. Emanuel, *Nucleic Acids Res.* **1996**, *24*, 2623.
- [2] T. Demeke, G. R. Jenkins, *Anal. Bioanal. Chem.* **2010**, *396*, 1977.
- [3] M. N. Emaus, K. D. Clark, P. Hinners, J. L. Anderson, *Anal. Bioanal. Chem.* **2018**, *410*, 4135.
- [4] E. Navarro, G. Serrano-Heras, M. J. Castaño, J. Solera, *Clin. Chim. Acta* **2015**, *439*, 231.
- [5] a) A. I. Dragan, J. R. Casas-Finet, E. S. Bishop, R. J. Strouse, M. A. Schenerman, C. D. Geddes, *Biophys. J.* **2010**, *99*, 3010; b) C. Labarca, K. Paigen, *Anal. Biochem.* **1980**, *102*, 344.
- [6] F. M. Carpi, F. Di Pietro, S. Vincenzetti, F. Mignini, V. Napolioni, *Recent Pat. DNA Gene Seq.* **2011**, *5*, 1.
- [7] L. Griffiths, D. Chacon-Cortes, *BSAM* **2014**, 1.
- [8] J. Prodělalová, B. Rittich, A. Španová, K. Petrová, M. J. Beneš, *Journal of Chromatography A* **2004**, *1056*, 43.
- [9] K. D. Clark, O. Nacham, H. Yu, T. Li, M. M. Yamsek, D. R. Ronning, J. L. Anderson, *Anal. Chem.* **2015**, *87*, 1552.
- [10] S. Surzycki, *Basic Techniques in Molecular Biology*, Springer, Berlin Heidelberg, **2000**.
- [11] a) H. Daraee, A. Etemadi, M. Kouhi, S. Alimirzalu, A. Akbarzadeh, *Artif. Cells Nanomed. Biotechnol.* **2016**, *44*, 381; b) C. Zylberberg, K. Gaskill, S. Pasley, S. Matosevic, *Gene Ther.* **2017**, *24*, 441.
- [12] D. A. Guzmán-Embús, M. Orrego Cardozo, C. Vargas-Hernández, *J. Appl. Phys.* **2013**, *114*, 194704.
- [13] B. Rittich, A. Spanová, *J. Sep. Sci.* **2013**, *36*, 2472.
- [14] M. B. Esch, A. J. Baeumner, R. A. Durst, *Anal. Chem.* **2001**, *73*, 3162.
- [15] a) C. Figalist, *Master's Thesis*, University of Regensburg, Regensburg, **2014**; b) K. A. Edwards, K. J. Meyers, B. Leonard, A. J. Baeumner, *Anal. Bioanal. Chem.* **2013**, *405*, 4017.
- [16] H. A. Hartley, A. J. Baeumner, *Anal. Bioanal. Chem.* **2003**, *376*, 319.

7 Conclusions and Future Perspectives

The government as well as health organizations like the WHO recommend and demand very low limits of hazardous substances in food, drinking water or the environment. The quantification of such low concentrations of hazardous substances requires sensitive analytical techniques which includes efficient signal amplification strategies. In addition, the demand for point-of-care devices that can be used on-site is strongly increasing, especially in 3rd world regions.^[1,2] This complicates the use of standard analytical techniques like ICP, GC or HPLC-based methods that require expensive and often large equipment. Thus, there is an increasing need for the development of chemical sensors and bioassays that meet these new requirements. Here, mainly simple assay setups, short analysis times, low cost, a possible miniaturization and integration into chips as well as long-term stability and robustness of the used materials are crucial and can often be accomplished using nanomaterials.^[2,6] The applicability of a variety of nanocontainers, including liposomes, as efficient signal amplification tool in (bio)analysis was demonstrated in this thesis. While still major improvements are necessary regarding the sensitivity of nanocages and -containers for chemosensors, their unique characteristics render them ideal for being used as signal amplification tools in several bioassays or imaging applications. Some of them are even capable to outperform gold standard techniques like ELISAs that are based on enzymatic signal amplification and offer promising approaches regarding multimodal and theranostic strategies for imaging applications. Thus, nanocontainers will hold an important role for the development of sensitive detection techniques and point-of-care devices in the area of food safety and environmental analysis as well as in the field of clinical diagnosis and therapy. For almost all of these applications, the surface design and signal amplification via loading of marker molecules into the nanocontainer are indispensable. This was also demonstrated by the other results of this thesis, which focus on liposomes. Here, the importance of the surface design of liposomes to render them suitable for versatile applications in the field of bioanalysis is shown. This includes solutions regarding the tunability of the surface charge, the controlled introduction of specific surface tags and the quantification of the membrane-bound receptors. The developed liposomes have been shown to be promising tools as signal enhancers for the detection of bacteria, for imaging applications as well as for the preconcentration of DNA. This is not only achieved via a controlled surface design but also by the loading of small molecules into the inner cavity of the vesicles. In this thesis, the fluorescent dye sulforhodamine B, the chemiluminescent dye *m*-carboxyluminol and high concentrated sodium chloride solutions were successfully entrapped and adapted to their application.

Anionic liposomes loaded with marker molecules have been reported as signal amplification tools in a variety of bioassays while cationic liposomes have been intensively studied for drug delivery

applications.^[3,4] The positively charged surface of the lipid vesicles can however also be beneficial for analytical applications as shown in this thesis for the direct detection of *E.coli* without the use of a receptor unit. Here, the electrostatic interaction between dye-loaded, cationic liposomes and *E.coli* was successfully demonstrated and applied for the quantitative analysis of the analyte via different assay setups. However, limitations caused by these assay setups as well as unsatisfying detection limits require further optimizations. This includes the investigation of other surface coatings for a more efficient immobilization of the bacteria as well as the investigation of other cationic lipids or amphiphiles to achieve an enhanced interaction with the cell surface. Here, a linker unit between the hydrophobic anchor and the cationic headgroup may be advantageous to enable a better availability and more efficient binding to the bacteria. One important aspect in the development of all analytical assays is selectivity.^[5] In case of liposomes, this is usually achieved by the attachment of receptors to the vesicle surface that are able to specifically bind to the analyte of interest.^[4] For sensitivity reasons, also the reduction of non-specific binding is crucial. The non-specific-binding of anionic liposomes to surfaces has for example been intensively studied via SPR.^[7] However, due to the fact that cationic liposomes have barely been applied in bioanalysis, further investigations towards their non-specific binding will be necessary. Selectivity as well as non-specific binding will also play an important role for the direct detection of bacteria from real samples. As most bacteria and other biological molecules like proteins exhibit a negative surface charge,^[7] the cationic liposomes will not be able to differ between the species but enable a quantification of the overall bacterial contamination. To introduce specificity, the capturing of bacteria via specific antibodies may be a possibility. Alternatively, purification of the sample before analysis needs to be conducted to prevent non-specific binding to other interfering bacteria or proteins. Another possibility is the use of a strongly diluted sample solution. Under ideal growth conditions only bacteria are multiplied and can thus be detected via the liposomes while interferences by proteins and other substances can be neglected. Other concepts rely on the specific rupture of the vesicle membrane caused by bacteria. Here, *e.g.* bacteria that secrete sphingomyelinase or phospholipase are of great interest,^[8] but also some *Listeria* strains have been reported to successfully cause dye leakage from liposomes.^[9] This enables the specific quantification of bacteria classes and may also be a promising concept regarding the detection via cationic liposomes. Here, the ability of different bacteria towards their ability to lyse these vesicles needs to be studied. Due to the close proximity after mixing the cationic liposomes with the *E.coli* cells, also energy-transfer related assays may be an elegant alternative. This would however require the labeling of the bacteria cells prior to mixing with the vesicles, *e.g.* via membrane staining dyes.^[10] The cationic liposomes can be loaded with the suitable FRET donor or receptor either in the membrane or the inner cavity of the vesicle to enable the development of a FRET-based bioassay. If limitations caused by the selectivity can be overcome, dye loaded cationic liposomes will also have great potential for the imaging of bacteria.

This is commonly achieved using gram-staining or nucleic acid binding dyes for the visualization of all bacterial cells.^[10] The advantage of liposomes for imaging applications is their strong signal enhancement compared to single dye molecules which provides a much better contrast.^[11] This was also supported by the results in this thesis. Here, DNA-tagged liposomes clearly outperformed the corresponding fluorophore-tagged oligonucleotide. In addition, liposomes have been proven to be ideal for tools for multimodal imaging.^[11] By simultaneous loading of dye molecules and an antimicrobial agent this feature could also be applied for the quantification of bacteria via cationic liposomes as proposed in this thesis followed by an instantaneous killing of the cells.

Besides their use as signal amplification tool for bacteria detection, also the applicability of cationic liposomes for the preconcentration of genomic DNA has been demonstrated in this thesis. In order to avoid optical interferences with other dyes used for analysis, cationic, colorless sodium chloride liposomes have been prepared for the development of an assay for the preconcentration of genomic DNA. Preliminary studies for the preconcentration of genomic DNA via cationic liposomes proved the general capability of the lipid vesicles in this area. DNA quantification via picogreen allowed first optimizations regarding assay parameters like different buffers, incubation times or temperatures. However, the limited sensitivity of the picogreen assay as well as interferences by detergents or high salt concentrations requires a more precise analysis via qPCR which is commonly used for DNA quantification.^[12,13] As also qPCR is sensitive to many interfering substances, detailed studies will be necessary to find the ideal conditions.^[12] One question is *e.g.* if the intact liposomes interfere with this method. In this case, lysis conditions must be optimized regarding interferences by applied detergents. Finally, a dose-response curve and the direct comparison to other DNA preconcentration methods like commercially available magnetic beads or alcohol precipitation will be necessary to enable a statement on the performance of the liposome-based assay. Another big challenge will be the preconcentration of DNA from real samples. As this assay relies on the electrostatic interaction of the genomic DNA with cationic liposomes, interferences via other negatively charged substances like proteins or RNA will be hard to avoid. Thus, an efficient purification of the samples will be crucial for this type of assay.

In general, the optimization of assay parameters is usually a very time-consuming process. In case of liposomes for example, a completely new batch of liposomes needs to be synthesized, if different conditions like the type or concentration of surface tag needs to be varied. At the same time, it cannot be guaranteed that all of the synthesized vesicles exhibit the same analytical characteristics with respect to size, number of surface tags or dye-loading. Here, the insertion of the biotinylated lipopeptide has been shown to be a fast and simple alternative. It not only provides a concentration-controlled functionalization of liposome surfaces but also the production of vesicles that only differ by the surface tag and otherwise exhibit exactly the same analytical characteristics. This feature may also

be of great interest for multi-analyte detection and can be expanded to other lipid bilayer-based nanomaterials. In addition, the insertion of such anchor molecules can serve a useful tool for the development of asymmetric liposomes which is often achieved by reverse emulsification via droplet emulsion transfer techniques.^[14] Asymmetric liposomes are intensively studied to provide *e.g.* more realistic cell membrane models or to improve the biocompatibility and delivery capacity in case of drug delivery vehicles.^[15] But also analytical applications can be envisioned, like *e.g.* FRET-based sensor approaches across the lipid bilayer.

To ensure however a wide applicability of the lipopeptide, also the design with other functional groups than biotin is crucial. A carboxyl-tagged lipopeptide could for example be exploited for the attachment of various biological molecules like proteins or DNA before insertion into the liposomes. Also other functionalities like -NH₂ or -SH can provide this feature. Surface functionalization via the direct method revealed dramatic batch-to-batch differences regarding the yield and signaling power. In addition, the incorporation of DPPE-biotin seems to be limited to 4 mol%. Here, further studies will be necessary to find the cause of this phenomenon. The formation of liposomes is mainly influenced by the operation temperature, hydration medium and miscibility of the lipids in the lipid composition.^[16,17] Thus, variations in the composition, *e.g.* a reduction in the cholesterol content or the use of other phospholipids to increase the miscibility may be a promising approach. As DPPE belongs to the poorly hydrating phospholipids also the investigation of other hydration solutions should be considered. Here, especially the ionic strength influences *e.g.* the tendency for the formation of a hexagonal phase.^[16] Moreover, studies regarding the quantification of the surface functional groups will be necessary to enable a better interpretation of the obtained data. Commonly, a HABA/avidin assay is applied for the quantification of biotin moieties on protein surfaces.^[18] The HABA dye forms a weak complex with streptavidin which absorbs light at 500 nm. Biotinylated samples are able to displace the dye which leads to a decreased absorbance proportional to the amount of sample.^[19] Unfortunately, it was found to be unsuitable for the quantification of biotin on the liposomes used in this thesis. Crosslinking and limited sensitivity resulted in unreliable data. HPLC-based approaches have been reported to enable the quantitative analysis of some lipid compositions.^[20] This may also be an interesting approach to obtain information on the exact membrane composition of the liposomes used in this study. However, this method will give information on the total biotin content and not on the outer surface content only. A promising alternative may be the use of a fluorophore-labeled, monomeric streptavidin. This could provide information on the surface bound biotin only, without the drawbacks of crosslinking caused by normal streptavidin. Here, the challenge will be to find an appropriate way for separation. For fluorescently labeled liposomes also the use of fluorescence correlation spectroscopy may offer the possibility for a quantification of the surface ligands. The results of this thesis already show the suitability of this method for the quantitative analysis of the vesicle number, concentration and

diffusion coefficients. In combination with liposomes, this FCS has moreover been reported to study membrane dynamics like fluidity or the lipid phase.^[21] Recently, also the release of molecules, such as drugs has been analyzed.^[22] But also interactions with molecules like proteins or peptides can be studied due to the large changes in the diffusion correlation times.^[23] This may also be a promising approach for mechanistic studies regarding the insertion of fluorophore-tagged anchors into liposomes. Moreover, several studies describe the quantification of some proteins as well as the quantification of receptor densities on live cells.^[24] Thus, it should also be possible to adapt these information and apply FCS for the quantification of any type of fluorescent ligand attached to liposomes.

In case of DNA-tagged liposomes a possibility for the quantification of surface tags was shown in this thesis by using fluorophore-tagged oligonucleotides. Several control experiments and theoretical calculations confirmed the suitability of this assay. However, challenges regarding the purification and separation from the unbound oligonucleotides remains. While in general, the separation from unwanted material via centrifugation worked well in case of the quantification of ssDNA on the vesicle surface, it was found that up to 90% of the liposomes are lost either due to membrane disruption or insufficient pelleting. Also in other assays developed in this thesis, a sufficient purification and separation was found to be a common challenge. In case of *E.coli* quantification via cationic liposomes, the separation was limited by insufficient bacteria immobilization, steric hindrance caused by magnetic beads or sometimes irregular and unreliable separation via centrifugation. Moreover, the high variations in the negative control values in case of DNA preconcentration can in part be ascribed to an irregular and insufficient pelleting of the liposomes. One possible strategy to overcome this problem is the development of magnetic liposomes that are magnetic enough to enable a sufficient separation similar to magnetic beads. For this, an efficient incorporation of magnetic nanoparticles into liposomes is crucial. So far, magnetic liposomes have mainly been reported for drug delivery applications, where a magnetic field is used to trigger the controlled release from liposomes.^[25] In the field of bioanalysis, the focus lies on the improvement of diffusion-controlled assays.^[26] For these applications mainly the encapsulation of magnetite nanoparticles has been reported either in the lipid bilayer or the large inner cavity of the vesicles.^[25] However, also the incorporation of other magnetic nanoparticles can be envisioned. The main challenge will be to render the liposomes strongly magnetic, which is in turn affected by the type, size and number of the entrapped nanoparticles. Thus, there is still need for detailed investigations regarding the development of magnetic liposomes that are suitable for magnetic separation means while properties like their analytical performance and their colloidal long-term stability are not affected.

Nevertheless, advantages like the strong signaling power and biocompatibility of liposomes outweigh the remaining problems and challenges and will thus hold a promising future for liposomes as versatile tool in bioanalysis. As demonstrated by the discussed strategies as well as the findings obtained within this thesis, the relatively simple tunability of the surface via charges or ligands and the variety of molecules that can be entrapped render these vesicles suitable for numerous possible applications.

References

- [1] a) V. Gubala, L. F. Harris, A. J. Ricco, M. X. Tan, D. E. Williams, *Anal. Chem.* **2012**, *84*, 487; b) P. Yager, G. J. Domingo, J. Gerdes, *Annu. Rev. Biomed. Eng.* **2008**, *10*, 107.
- [2] D. Quesada-González, A. Merkoçi, *Chem. Soc. Rev.* **2018**, *47*, 4697.
- [3] A. Akbarzadeh, R. Rezaei-Sadabady, S. Davaran, S. W. Joo, N. Zarghami, Y. Hanifehpour, M. Samiei, M. Kouhi, K. Nejati-Koshki, *Nanoscale Res. Lett.* **2013**, *8*, 102.
- [4] Q. Liu, B. J. Boyd, *Analyst* **2013**, *138*, 391.
- [5] J. Vessman, R. I. Stefan, J. F. van Staden, K. Danzer, W. Lindner, D. T. Burns, A. Fajgelj, H. Müller, *Pure Appl. Chem.* **2001**, *73*, 1381.
- [6] a) N. Wongkaew, M. Simsek, C. Griesche, A. J. Baeumner, *Chem. Rev.* **2019**, *119*, 120; b) C. A. Hermann, A. Duerkop, A. J. Baeumner, *Anal. Chem.* **2019**, *91*, 569.
- [7] C. Fenzl, C. Genslein, C. Domonkos, K. A. Edwards, T. Hirsch, A. J. Baeumner, *Analyst* **2016**, *141*, 5265.
- [8] a) D. H. Schmiel, V. L. Miller, *Microbes and Infection* **1999**, *1*, 1103; b) H. Xing, C. L. Zhang, G. Ruan, J. Zhang, K. Hwang, Y. Lu, *Anal. Chem.* **2016**, *88*, 1506; c) M. N. Holme, S. Rana, H. M. G. Barriga, U. Kauscher, N. J. Brooks, M. M. Stevens, *ACS Nano* **2018**, *12*, 8197.
- [9] H. Goldfine, C. Knob, D. Alford, J. Bentz, *Proc. Natl. Acad. Sci. USA* **1995**, *92*, 2979.
- [10] I. Johnson, *The molecular probes handbook. A guide to fluorescent probes and labeling technologies*, Life Technologies, Carlsbad, Calif., **2010**.
- [11] B. R. Smith, S. S. Gambhir, *Chem. Rev.* **2017**, *117*, 901.
- [12] T. Demeke, G. R. Jenkins, *Anal. Bioanal. Chem.* **2010**, *396*, 1977.
- [13] S. J. Ahn, J. Costa, J. R. Emanuel, *Nucleic Acids Res.* **1996**, *24*, 2623.

- [14] a) M. Yanagisawa, M. Iwamoto, A. Kato, K. Yoshikawa, S. Oiki, *J. Am. Chem. Soc.* **2011**, *133*, 11774; b) T. Hamada, Y. Miura, Y. Komatsu, Y. Kishimoto, M. Vestergaard, M. Takagi, *J. Phys. Chem. B* **2008**, *112*, 14678.
- [15] a) J. Whittenton, R. Pitchumani, S. Thevananther, K. Mohanty, *J. Microencapsul.* **2013**, *30*, 55; b) M. B. C. de Matos, B. S. Miranda, Y. Rizky Nuari, G. Storm, G. Leneweit, R. M. Schiffelers, R. J. Kok, *J. Drug Target.* **2019**, *27*, 681; c) D. Marquardt, B. Geier, G. Pabst, *Membranes* **2015**, *5*, 180.
- [16] J. Li, X. Wang, T. Zhang, C. Wang, Z. Huang, X. Luo, Y. Deng, *Asian Journal of Pharmaceutical Sciences* **2015**, *10*, 81.
- [17] F. Szoka, D. Papahadjopoulos, *Ann. Rev. Biophys. Bioeng.* **1980**, *9*, 467.
- [18] N. M. Green, *Methods in Enzymology* **1970**, *18*, 418.
- [19] E. González, L. M. Shepherd, L. Saunders, M. W. Frey, *Materials* **2016**, *9*.
- [20] a) M. Oswald, M. Platscher, S. Geissler, A. Goepferich, *Int. J. Pharm.* **2016**, *497*, 293; b) M. Oswald, S. Geissler, A. Goepferich, *Int. J. Pharm.* **2016**, *514*, 93.
- [21] A. J. García-Sáez, D. C. Carrer, P. Schwille, *Methods Mol. Biol.* **2010**, *606*, 493.
- [22] R. Bouchaala, L. Richert, N. Anton, T. F. Vandamme, S. Djabi, Y. Mély, A. S. Klymchenko, *ACS Omega* **2018**, *3*, 14333.
- [23] S. T. Hess, S. Huang, A. A. Heikal, W. W. Webb, *Biochemistry* **2002**, *41*, 697.
- [24] a) Y. Tian, M. M. Martinez, D. Pappas, *Appl. Spectrosc.* **2011**, *65*, 115A-124A; b) Y. Chen, A. C. Munteanu, Y.-F. Huang, J. Phillips, Z. Zhu, M. Mavros, W. Tan, *Chemistry* **2009**, *15*, 5327.
- [25] O. A. Inozemtseva, S. V. German, N. A. Navolokin, A. B. Bucharskaya, G. N. Maslyakova, D. A. Gorin in *Micro and Nano Technologies Ser* (Eds.: D. P. Nikolelis, G. Paraskevi Nikoleli), Elsevier, San Diego, **2018**, pp. 175–192.
- [26] K. A. Edwards, A. J. Baeumner, *Anal. Chem.* **2014**, *86*, 6610.

Curriculum Vitae

Persönliche Daten

Name	Carola Hofmann, geb. Figalist
Geburtsdatum	16.10.1988
Geburtsort	München
Staatsangehörigkeit	Deutsch

Ausbildung

03/2015-07/2019	Promotionsstudium Chemie , Universität Regensburg <i>„Synthesis and Characterization of Liposomes with Controlled Surface Design for Analytical Applications“</i> Institut für Analytische Chemie, Chemo- und Biosensorik (Prof. Dr. Antje J. Baeumner)
10/2012-01/2015	Masterstudium Chemie , Universität Regensburg Masterarbeit: <i>„Positively Charged Liposomes for Signal Enhancement via Electrostatic Interactions“</i> Institut für Analytische Chemie, Chemo- und Biosensorik (Prof. Dr. Antje J. Baeumner, Dr. Thomas Hirsch)
10/2009-09/2012	Bachelorstudium Molecular Life Science , Friedrich-Alexander-Universität Erlangen-Nürnberg Bachelorarbeit: <i>„O,O-Chelatliganden als HIF-α stabilisierende Substanzen“</i> Institut für Anorganische und Analytische Chemie (Prof. Dr. Nicolai Burzlaff)
06/2008	Allgemeine Hochschulreife , Emil-von-Behring-Gymnasium, Spardorf

Auszeichnungen

- 2016 Vortragspreis
10. Interdisziplinäres Doktorandenseminar, Berlin
- 2015 „ASCOS Award“
9th Advanced Study Course on Optical Chemical Sensors -
Nanotechnology for (Bio)chemical Sensors, Porto, Portugal

Sonstiges

- 2016 Fortbildung “Qualitätssicherung in der Analytischen Chemie“
GdCh und Bundesanstalt für Materialforschung, Berlin
- 2015 Teilnahme am 9th Advanced Study Course on Optical Chemical
Sensors - Nanotechnology for (Bio)chemical Sensors, Porto, Portugal

Publications

1. C. Hofmann, G. Roth, T. Hirsch, A. Duerkop, A. J. Baeumner, Tethering functionality to lipid interfaces by a fast, simple and controllable post synthesis method, *Colloids Surf., B* **2019**, *181*, 325-332, 10.1016/j.colsurfb.2019.05.049.
2. C. Hofmann, A. Duerkop, A. J. Baeumner, Nanocontainers for analytical applications, *Angew. Chem. Int. Ed.* **2019**, 10.1002/anie.201811821.

Presentations

Oral Presentations

2017 12th Workshop on Biosensor & Bioanalytical Microtechniques in Environmental, Food & Chemical Analysis, Rom, Italien

Rapid and Simple Surface Functionalization Strategy for Lipid-Based Membranes

2016 10. Interdisziplinäres Doktorandenseminar, Berlin

Surface Modification of Liposomes – A Comparative Study

2015 11th Workshop on Biosensor & Bioanalytical Microtechniques in Environmental, Food & Chemical Analysis, Regensburg

Novel Surface Modification for Liposomes and Application as Signal Enhancers in Bioassays

Poster Presentations

2016 39th International Conference on Environmental and Food Monitoring, Hamburg

Surface Modification of Liposomes for Analytical Applications

2015 11th Workshop on Biosensor & Bioanalytical Microtechniques in Environmental, Food & Chemical Analysis, Regensburg

Novel Surface Modification for Liposomes and Application as Signal Enhancers in Bioassays

2015 Deutsches BioSensor Symposium, München

Cationic Liposomes for Signal Enhancement in Bioanalytical Sensors

2015 Anakon, Graz, Österreich

Cationic Liposomes for Secondary Signal Enhancement in Bioassays

Eidesstattliche Erklärung

Ich erkläre hiermit an Eides statt, dass ich die vorliegende Arbeit ohne unzulässige Hilfe Dritter und ohne Benutzung anderer als der angegebenen Hilfsmittel angefertigt habe; die aus anderen Quellen direkt oder indirekt übernommenen Daten und Konzepte sind unter Angabe des Literaturzitats gekennzeichnet.

Weitere Personen waren an der inhaltlich-materiellen Herstellung der vorliegenden Arbeit nicht beteiligt. Insbesondere habe ich hierfür nicht die entgeltliche Hilfe eines Promotionsberaters oder anderer Personen in Anspruch genommen. Niemand hat von mir weder unmittelbar noch mittelbar geldwerte Leistungen für Arbeiten erhalten, die im Zusammenhang mit dem Inhalt der vorgelegten Dissertation stehen.

Die Arbeit wurde bisher weder im In- noch im Ausland in gleicher oder ähnlicher Form einer anderen Prüfungsbehörde vorgelegt.

Ort, Datum

Unterschrift